February 5, 2008

X-ray and IR Point Source Identification and Characteristics In the Embedded, Massive Star-Forming Region RCW 38

Scott J. Wolk, Bradley D. Spitzbart, Tyler L. Bourke

Harvard–Smithsonian Center for Astrophysics, 60 Garden Street, Cambridge, MA 02138

and

João Alves [1]

European Southern Observatory, Karl-Schwarzschild Strasse 2, D-85748 Garching bei München, Germany

ABSTRACT

We report on results of a 96.7 ks *Chandra* observation of one of the youngest, most embedded and massive young stellar clusters studied in X-rays – RCW 38. We detect 460 sources in the field of which 360 are confirmed to be associated with the RCW 38 cluster. The cluster members range in luminosity from 10^{30} ergs s^{-1} to $10^{33.5}$ ergs s^{-1}. Over ten percent of the cluster members with over 100 counts exhibit flares while about 15% of cluster members with over 30 counts are variable. Of the sources identified as cluster members, 160 have near-infrared (NIR) counterparts either in the 2MASS database or detected via VLT observations. Of these about 20% appear to have optically thick disks. An additional 353 members are identified through NIR observations of which at least 50% possess optically thick disks. We fit over 100 X-ray sources as absorbed Raymond-Smith type plasmas and find the column to the cluster members varies from $10^{21.5}$ to 10^{23} cm^{-2}. We compare the gas to dust absorption signatures in these stars and find $N_{\rm H}$= A$_V \times 2 \times 10^{21}$cm^{-2}. We find that the cluster contains 31 candidate OB stars and is centered about 10″ (0.1 pc) west of the primary source of the ionization, the O5 star IRS 2. The cluster has a peak central density of about 400 X-ray sources pc $^{-2}$. We estimate that the total cluster membership exceeds 2000 stars.

Subject headings: H II regions – ISM; individual (RCW 38) – stars; formation – X-rays; point sources – X-rays; stars

---

[1]Current Address: Calar Alto Observatory, Centro Astronómico Hispano Alemán C/Jesús Durbn Remón 2-2 E-04004 Almera, Spain

1. Introduction

The evolution of high mass clustered star forming regions is complex and poorly understood. Only the nearby (0.5 kpc), optically revealed, Orion Nebular Cluster (ONC) is well studied. Yet, a wide variety of high mass embedded clusters are found within 2 kpc of the Sun (Lada & Lada 2003). Within this limit, the young cluster RCW 38 (l=268^o, b=-1^o) is unique as the only region other than the ONC to contain over 1300 members. RCW 38 is significantly more embedded and spatially denser that the ONC (Smith et al. 1999) and other regions that have been studied recently with *Spitzer* and *Chandra* (e.g., Trifid (Rho et al. 2006), M17 and the Rosette Nebula (Townsley et al. 2003), RCW 49 (Whitney et al. 2004, Churchwell et al. 2004)). RCW 38 provides a unique opportunity to study the evolution of a rich cluster during the phase where its most massive member (O5) has just completed its ultracompact HII region (UCHII) phase and is now greatly influencing its natal environment and the evolution of its low mass members.

At a distance of 1.7 kpc, RCW 38 (Rodgers, Campbell & Whiteoak 1960) is one of the brightest H II regions at radio wavelengths (e.g., Wilson et al. 1970). It is a uniquely young (<1 Myr), embedded ($A_V \sim 10$) stellar cluster surrounding an early O star, IRS 2 (∼O5; Frogel & Persson 1974; Smith et al. 1999), *Chandra* and deep near infrared observations reveal a dense cluster embedded in a diffuse hot plasma (Wolk et al. 2002). The O star has evacuated its immediate surroundings of dust, creating a wind bubble ∼0.1 pc in radius (Smith et al. 1999, Vigil et al. in prep.) which is confined by the surrounding molecular cloud, as traced by mm continuum and molecular line emission (Bourke et al. 2004). This bubble is filled with diffuse thermal and synchrotron X-ray emission (Wolk et al. 2002), and diffuse emission can be traced outside of the bubble, showing a similar structure to the diffuse infrared emission in the region. At the interface between the bubble and cloud is a region of warm dust and ionized gas, which shows evidence for ongoing star formation, particularly along its western edge (Smith et al. 1999, Vigil et al. in prep.). Extended warm dust is found throughout the 2–3 pc region at mid-infrared wavelengths, and coincides with the extended X-ray plasma. This is evidence that the influence of the massive stars reaches beyond the confines of the O star bubble. RCW 38 appears similar in structure to RCW 49 and M 20 which have been studied with IRAC and MIPS on *Spitzer* (Whitney et al. 2004, Churchwell et al. 2004 and Rho et al. 2006) but it is not as evolved. RCW 38 appears to be a blister compact H II region lying just inside the edge of a giant molecular cloud.

In this paper we discuss the X-ray point sources observed in our recent *Chandra* and near-infrared observations. Section 2 describes the basic observational setup and data reduction, §3 assesses cluster membership via quartile (X-ray color) analysis, §4 examines X-ray source variability while §5 models the X-ray spectra. Both of these results are used to evaluate the effectiveness of using X-ray color as a membership criterion. In §6 we fold in ground based infrared data for a variety of purposes. We estimate disk parameters for the X-ray sources as well as evaluating the full stellar content of the cluster. We further evaluate the relationship between the inferred gas and dust columns along the line of sight and examine the effect of X-ray biases in source selection. We also estimate the total size of the cluster with special focus on the O and B stars. In §7 we pay

special attention to some extreme objects in the field and their implications for the 3 dimensional structure of the region. We summarize our results in §8.

2. Observation and Data Reduction

Chandra observed RCW 38 on 2001 December 10-11 for 96.7 ks (ObsID 2556), using Advanced CCD Imaging Spectrometer (ACIS) chips 0, 1, 2, 3, 6 and 7 in very faint mode. The ACIS combines the ability to image X-rays at a $0\farcs492$ plate scale with moderate spectral resolution (R$\sim 30-50$) and time tagging every 3.2 seconds. The combined field of view (FOV) of the 4 chips in the imaging array is $16\farcm9 \times 16\farcm9$. The aimpoint of the array was 8h59m19.20s $-47^{\rm o}30'22\farcs0$ (J2000.0), and the satellite roll angle (i.e., orientation of the CCD array relative to the north–south direction) was 51°. The roll angle was selected so that photons from the H II region Bran 213A would strike the ACIS spectroscopic array where upon chips 6 and 7 were also turned on. While the H II region was clearly detected these data will not be discussed here since the mirror point-spread function (PSF) is considerably degraded far off-axis. The focal plane temperature was -119.7°C. The radiation environment was benign.

2.1. Data Preparation

The raw data was originally processed under the *Chandra* X-ray Center's standard processing version 6.4.0. We reprocessed the observation using the latest version 6.13.2. Using acis_process_events on the level 1 events files, a gain correction is applied from CALDB 2.21. The CTI correction and VFAINT background cleaning, available since version 6.12, were also applied. An energy filter was applied to remove photons above 8 keV and below 300 eV. We found that the VFAINT correction removed good events from bright sources and did not reveal any new faint sources. So the VFAINT correction was backed out leaving only the CTI correction. Following standard processing, bad grade and bad status (grades 1, 5 and 7, status >0) events and bad time intervals were filtered using the CIAO tool *dmcopy*.

Time-dependent gain corrections were applied and acis_process_events rerun. While there were over 3×10^6 level 1 events, our "cleaned" data file used for analysis contained 171,973 events. The central portion of these data is shown in Figure 1.

An exposure map was created using *merge_all*, accurately representing the effective exposure time for a 1.7 keV photon. We chose this single energy for the exposure map since it is intermediate between the maximum of the effective area of the HRMA/ACIS system and an estimated mean source energy of ~ 2.0 keV. The exposure map corrects for the changes in the effective area of the mirror as a function of off-axis distance and telescope dithering. The exposure map is later applied automatically by CIAO tools extracting count rates and spectra.

2.2. Source Detection

PWDetect[1] was used for source detection on our cleaned events list to identify sources across the entire I array. Threshold significance was set to detect sources between 4 and 5.31 equivalent Gaussian sigmas and the data are searched on scales of 0.5 to 16″. With these settings, a false detection rate of $< 1\%$ is expected. We did not change any PWDetect settings. Source detection was done on the whole field at once. The program did not seem to be confused by faint sources embedded in diffuse emission.

PWDetect produces a regions file defining the source extent for extracting photons. These regions were adapted to more meaningful regions based on the actual *Chandra* PSF and chip position for each source. *mk_psf* was used to obtain images of the PSF at various off-axis angles θ (arcmin), and rotation angles ϕ (degrees), around the ACIS array. At each source location an ellipse was generated to enclose 95% of the total X-ray energy. This lead to the following derived parameterization applied to our sources for elliptical regions around PWDetect's returned source locations:

$$major \;\; axis = 1.97 - 0.22\theta + 0.15\theta^2$$

$$minor \;\; axis = 2.03 - 0.13\theta + 0.08\theta^2$$

$$angle = 95.4 + 0.47\phi$$

This formulation was used, except as noted below, to define the extraction region for each source.

Several spurious and overlapping sources were visually edited. To aid in editing unresolved and confused sources a near-infrared K_S image with X-ray contours over-plotted proved helpful (Figure 2). The near-infrared data are discussed in detail in §6.

In most cases, background subtraction was made via background regions centered on each source. The background regions were elliptical annuli centered on the source with inner axes 2.7 times the length of the axes for source region and the outer axes 4.1 times the source region axes. The inner edge of this annulus was chosen to make certain no energy from the extended wings was included in the background. The outer axis of the background annulus was chosen to be 4.1 times the source axis to allow the maximum background area which would not generally need to be adjusted for other sources. Background regions were manually adjusted in cases where chip edges or other sources interfered. For areas near the center of the cluster, with several nearby sources, a common background region was created from a suitable region nearby. Sources in the central arcminute of the cluster were divided into two sectors, northwest and southeast. In each half a common two part background was used since the diffuse emission is present in the region which changes spectrally from northwest to southeast. The two background regions are indicated by the ellipses in Figure 1.

[1]http://cxc.harvard.edu/cont-soft/software/pwdetect.1.0.html

A total of 460 sources were found on the ACIS-I array, including 31 sources with more than 200 net counts, 49 sources with 100-200 net counts, 71 sources with 50-100 net counts, and 78 sources with 20-50 net counts. Sources 95 and 228 were removed from the list as duplicates late in the analysis process, hence they are skipped in the enumeration. All X-ray sources are listed in Table 1. The first column of Table 1 gives the internal identification of each source while column 2 gives the official IAU/CXC designation. Columns 3 and 4 list the right ascension and declination (J2000). Columns 5 and 6 list the off–axis distance in arcminutes and the net counts background subtracted and corrected for the aperture size respectively while columns 7 and 8 lists the number of intervals of constant flux at 95% and 99% significance requirements. While details of this last column are discussed in §4, the key point is that more than one interval indicates a variable source.

3. Cluster Membership

As stars progress from Class 0 to Class III (Lada & Shu 1990), it is only with an unbiased sample of cluster membership that the evolution of the star+disk system can be understood. Since optical spectroscopic follow up is not possible for such an absorbed/obscured cluster we develop here a method of using the X–ray color and spatial properties of each source to assess the probability that it is a cluster member independent of its infrared properties. The typical method of model independent spectral analysis is to use X-ray colors in the form of hardness ratios, HR=(Cts_h-Cts_s)/(Cts_h+Cts_s) where "h" and "s" refer to the hard and soft bands respectively. Hardness ratios are of inherently limited value because of biases in the selection of bandpasses which lead to very non-uniform errors and limited dynamic range. Sources with low counts tend to be driven toward the center of the distribution and there is a fundamental difficulty in breaking the degeneracy between temperature and absorption. Instead, we use a quartile analysis technique for model free analysis of X-ray data explored by Hong et al. (2004). Quartile analysis avoids some biases inherent in the selection of bandpasses needed to calculate hardness ratios. In this form of quartile analysis, one starts with the full ACIS band pass of E_{lo}= 0.3 keV and E_{up} =8.0 keV. $E_{x\%}$ is defined as the photon energy below which x% of the photon counts are found and $Q_x = \frac{(E_{x\%}-E_{lo})}{(E_{up}-E_{lo})}$ is defined to be the normalized quartile. The ratio of the bottom to top quartile (x= 25 and 75respectively) is representative of a two-point slope of the spectrum. For the case of a single temperature, the median, $m(= Q_{50})$, is a function of the absorption. The quartiles are not independent, as the absorption changes the quartile ratio for a given temperature. Hong et al. (2004) plot the data by normalizing the quartile ratio axis as $3\times Q_{25}/Q_{75}$ while the median is compressed as $\log(m/(1-m))$. On such a plot one can distinguish changes in temperature from extinction and can even distinguish thermal and non-thermal changes.

To determine if cluster members occupy a common region in such a quartile diagram we study the most probable cluster members, those source that lie within $200''$ of IRS 2. By calculating the number of X-ray sources within $1'$ of each X-ray source we find the distribution of X-ray sources is sharply peaked with a full width at half maximum of about $200''$. Plotting all such X-ray sources

in the diagram shown at the top of Figure 3 shows there is a clustering of the data in color space. The bottom panel of Figure 3 shows the same axes but now for sources *more* than 200″off axis. The difference is striking. Of the 63 sources with over 100 counts and less than 200″ off-axis, 62 lie between $-0.65 < \log(m/1-m)) < 0.25$. $\log(m/1-m)) = -0.65$ is the vertical line in Figure 3. We fitted the distribution of the data between those two points using a two-variable linear regression first order equation $3\times Q_{25}/Q_{75} = 1.2\times\log(m/(1-m))+1.8$ with a mean absolute deviation (MAD; Beers et al. 1990) of 0.15. The diagonal lines in Figure 3 are 3 deviations above and below this fit. Sixty-one of the bright sources near the cluster center could be found within three deviations of the fit. One point was clearly not a cluster member (Source 39) and the other point was on the fringe. This is indicative of a group of sources with similar extinctions and spectral signatures.

There are 209 X-rays sources within 200″ of the IRS 2 and with less than 100 counts. Of these, 36 have between 50 and 100 counts and all lie within 3 MAD of the best fit line. An additional 54 have between 30 and 50 counts. Two of these (Source 34 and Source 175) are clearly too unabsorbed (too low a value in the X-axis) to be considered cluster members. Three others lie just below the -3σ deviation demarcation but we *do not exclude* these are candidate members since the measurement errors can account for this small difference. The remaining 119 sources have less than 30 counts, four of these are discrepant by having too low of value along the X-axis and we exclude these sources from cluster membership. Fifteen lie just below the -3σ deviation demarcation. This is more than twice the rate of such sources seen with 30-50 counts. Again we do not exclude these sources, we instead conclude that the measurement errors associated with the quartiles is biased such that sources with low counts have systematically lower values of Q_{25}/Q_{75} and that the errors are twice as high for sources with least than 30 counts compare to those with 30-50 counts. This last point is consistent with the results from Hong et al. (2004). Overall we exclude seven X-ray sources within 200″ of IRS 2 from cluster membership based on the quartile analysis. We consider the 202 remaining X-ray sources to be probable cluster members.

There are 183 X-ray sources more than 200″ from IRS 2. One hundred and ten of these lie within the $\pm 3\sigma$ deviation limits described above. We chose these limits to be somewhat inclusive and to error on the side of membership. We exclude from probable cluster membership 94 sources which are outside of these limits and more than 200″ from IRS 2. Along with the seven sources nearer to IRS 2, the identification of 101 sources in the field as background (or foreground) field objects is consistent with expectations derived from the Champlane survey (Hong et al. 2005). Our observations reached a mean flux limit of about 2×10^{-14} ergs $s^{-1}cm^{-2}$ (2-10 keV) averaged across the field. Preliminary results from the Champlane survey for *Chandra* fields in the plane of the Galaxy away from the galactic core indicate that we can expect to find about 70 background AGN, cataclysmic variables, neutron stars, black holes, and other non–PMS star point sources in the ACIS-I field. Some examples include sources 14, 18 and 113 which are quite hard and absorbed in X–rays and yet appear unabsorbed at near-IR wavelengths (see §6). The Champlane effort excludes soft X-ray sources such as dMe stars and white dwarfs and thus should be taken as a lower limit.

The probable cluster members are noted in Table 2. Probable non-members are noted in

Table 3. In these tables the first column is the source number, followed by the quartile values, Q_{25}, m and Q_{75}, with errors interleaved. The plot values are calculated for convenience and listed in the final two columns.

3.1. Cluster Density

We plot the positions of the members and non–members in Figure 4. It is clear that the members are clustered while the non–members have a more uniform distribution. A density analysis was performed by calculating the number of cluster members within 15″ of each cluster member. Asymmetries in a plot cluster density as a function of the distance from the dominant ionizing source IRS 2 indicate that it is not the center of the cluster. The geometric centroid was calculated in terms of stellar (X–ray source) density, *not* mass density, using cluster members within 100″ of IRS 2, and is located at: 08h59d04.64s, −47°30′44.″00. This is displaced 10.4″ to the west southwest of IRS 2 and aligned roughly with the 10 μm dust ridge reported by Smith et al. (1999). Varying the inclusion radius by 50″ can change this centroid location by 6″, this is mostly controlled by the initial guess that the center was near IRS 2.

The results of the full density analysis are shown in Figure 5. The cluster density drops to half the peak density of about 100 X-ray sources per arcminute at about 15″ (∼0.12 pc) from the cluster center. We find the cluster is very sharply peaked with broad wings relative to a Gaussian profile – hence, this is not a relaxed system. We fitted the data in Figure 5 as an exponential of the number of sources per parsec^2 $\sim exp(-5.0d)$ where d is the distance from the cluster center in parsec. The peak cluster density, as measured via this fit, is about 400±20 X-ray sources per parsec^2 (=100±10 X-ray sources per square arcminute). The density of the non-members is 2.3 per square arcminute ±1.1. A plot of the density profile of these sources shows a slight enhancement about 100″ from the cluster centroid indicating that as many as 8 of the candidate non–members have been misidentified as such. While the quartile system as applied here is not a perfect system for determining cluster membership based on X-ray colors, it appears highly effective.

We can use these data to estimate the total cluster size. Recent work on mass stratification in the ONC by Feigelson et al. (2005) indicates that at our sensitivity limit of log $L_x \sim 30.0$ one detects about 16 percent of the stars in a cluster that is similar to the ONC. Comparisons to measurements of the ONC are quite appropriate to RCW 38 as both clusters have mid to early O stars. Since our sensitivity was a little below this limit we expect that we are detecting at most 15% of the cluster members. This should include half of all stars above 0.5 $M_\odot$. Scaling from the 360 members detected we estimate that the total cluster size could be as high as 2400 members with a peak density of about 1000 sources in the central parsec^2.

4. Variability

In this section, we examine the variability of the X-ray source population. Variability studies allow us to begin to assess the plausibility of X-ray generation mechanisms. These can be constrained by the timescales and flux changes observed in the variability. Variability also offers corroborating evidence that a source is stellar in nature and hence a possible cluster member. Unlike other X-ray sources almost all coronal sources vary given a long enough observation (see Getman et al. 2005). These variations can either be stochastic or impulsive deviations from constancy.

Various methods can be employed to investigate variability. This topic has been reviewed briefly by Wolk et al. (2005) and more thoroughly by Güdel (2004) and Favata & Micela (2003). One rigorous technique commonly used is a one–sample Kolmogorov-Smirnov (KS) test to identify if the photon arrival times are consistent with a constant rate. The KS test does not give any information on the nature of the variability in objects. We identify X-ray sources as variable if they have a KS statistic less than 0.001. That is, the cumulative event arrival time distribution deviates from a linear distribution at a confidence greater than 99.9%. Amongst the brightest 31 sources (those with over 200 net counts), 7 (23%) were variable at $> 99.9\%$ confidence. That rate is maintained among the 80 sources with over 100 net counts, of which 19 (23%) were variable at $> 99.9\%$ confidence.

4.1. Flaring

About 25% of the bright sources are detected as variable in 100ks, but the KS test tells us nothing about flaring. As demonstrated in Wolk et al. (2005), the use of Bayesian Blocks (BBs; Scargle 1998) provides a method of flare detection without the biases inherent in binning the data. In some senses the BB method is similar to the KS test; the existence of more than one block indicates that the flux has changed at a certain confidence level. However, while the KS test reports very little about the nature of the change, the number of BBs and measurements of the mean rate, σ and duration of those blocks allow quantitative analysis. The BB method is explicitly designed to avoid binning the observation into equally spaced time intervals. Bayesian Blocks conform to complex X-ray lightcurves remarkably well (see Getman et al. 2005). We tested each lightcurve with a "prior ratios" set to approximate both 95% and 99% confidence that a flux change has occurred.

Using the BB technique, 7 of the 31 sources (22.5%) with over 200 counts and 21 of the brightest 80 (26%) could not be fitted with one block at a constant level with over 99% confidence. This number is very similar to the 23% which varied at similar confidence as measured by the KS test. Overall 37 sources required more than one BB. These results are tabulated as part of Table 1.

The BB method converts the lightcurve to temporal periods of constant flux, thus, one can measure the amount of rise between the blocks and estimate the rate of change between blocks. In

their study of the extremely deep COUP data set, Wolk et al. (2005) find that most stellar sources have a characteristic rate, R_{char} and found sources were at their characteristic levels for about 75% of the time. They further found that a normalized rate of rise $\Delta \equiv 1/R_{char} \times dR/dt > 10^{-4}s^{-1}$ was indicative of a flare. Following Wolk et al. we define dR as the difference between the rates of adjacent blocks and dt as the shorter of the two blocks. We choose the value of the minimum block as the characteristic rate since we do not have the long observation time to define a true characteristic level.

Twenty-four sources have this form of impulsive variability (see Figures 6, 7). Wolk et al. (2005) further use a criterion that each flare be bright. To do this they use the error on the BB count rate as σ and define "bright" in the sense that the rate in the flaring block is 2.5 σ brighter than the characteristic block.

$$R_{flare} - 2.5\sigma > R_{char} * 1.2$$

All 24 flares met this criterion. No star was seen to flare twice. Figure 8 shows lightcurves of ten sources which varied in X-rays but were not seen to flare.

4.2. Flare Rates

We can use these data to assess flare rates. Since the fraction of stars seen to vary (via either the Bayesian blocks of KS method) does not decrease as we limit the total counts from 200 to 100, we assume that the test is fully valid at this count rate. There are 103 stars with over 75 counts, of which 23 vary (30%). This fraction exceeds the variability rate seen at higher fluxes so we do not appear to be missing any true variable. However, of 48 sources with between 50 and 75 counts, only 5 (10%) vary. Of the 87 sources with between 30 and 50 counts, 7 (8%) vary. Clearly there is a roll-off in the sensitivity to variability below 75 counts. To prevent biases in the data we constrain the following analysis to sources with over 100 counts.

Nine of 72 (12.5%) probable cluster members with over 100 counts flared in 96.7 ks. This represents a little less than half of the bright cluster members which are detected as variables. Non-member Source 404 flared, none of the 6 other bright non-members varied. Assuming that all stars are the same and that there are no stars more prone to flare than others then we conclude there are about 775 ks between flares. This is in between the values obtained for Solar mass stars in the ONC (one flare per 640 ks; Wolk et al. 2005) and all stars in the much older cluster – NGC 2516 (About 1 per megasecond; Wolk et al. 2004).

Finally, variability analysis can be used to assess the veracity of the quartile approach to cluster member selection. We expect stars to vary more than other X–ray sources. Of the 35 stars seen to vary with 99% confidence, 34 of them are identified as cluster members by the quartile approach. This gives us great confidence among the bright sources. Further, variability was detected on sources down to 30 counts. In the field there are 202 cluster members with between 30 and 100 counts, 16.8% of those vary. In contrast, only one of the 22 non-cluster members varies. The lone

non-member to flare was Source 404. From spectral analysis we find that it is one of the most unobscured sources in the field and hence likely a foreground dMe star.

5. Spectral Analysis

Analysis of the X-ray spectra of each source was performed to determine the bulk temperature of the corona and the intervening column of hydrogen. Source and background pulse height distributions in the total band (0.3-8.0 keV) were constructed for each X-ray source. Model fitting of spectra was performed using *Sherpa* (Freeman et al. 2001). The final fits were done with CIAO version 3.1.0.1. The CIAO script *psextract* was used to extract source spectra and to create an Ancillary Response Function (ARF) and Redistribution Matrix Function (RMF) files. For sources with over 30 counts, data for each source were grouped into energy bins which required a minimum of 8 counts per bin and background subtracted. The optimization method set to Levenberg-Marquardt and χ–Gehrels statistics were employed. For sources with under 30 counts, models were fitted unbinned using cstat statistics (Cash 1979) and Powell optimization.

5.1. Choosing a Spectral Fitting Model

For uniformity it is desirable to settle on a single model spectrum for all sources. To find the most appropriate model for our sources, we ran a series of test fits on the brightest 80 sources, those with over 100 counts. In these tests, the 80 sources were successively fitted with various absorbed thermal plasma models. These included the model from Raymond–Smith (1977), the "mekal" model (Mewe et al. 1985, Mewe et al. 1986, Kaastra 1992, Liedahl et al. 1995), APEC[2], thermal bremsstrahlung (Kellogg, Baldwin & Koch 1975) plus blackbody and single power law models. The fitting was done using *Sherpa*, the absorption law was assumed to be $abs(E) = e^{-N_{\rm H}\ \sigma(E)}$ in which the photo-electric absorption cross-sections ($\sigma(E)$) are taken from Morris & McCammon (1983). Absorption and temperature or the power law index (Γ) were left as fitted parameters. A two temperature absorbed Raymond–Smith model was also tested. To evaluate the results of the test, we used The mean was calculated after trimming away outliers more than 2 MADs from the median (similar results were obtained with a 3 MAD cut). The results are summarized in Table 4. In this table, the columns represent the various models, Raymond-Smith plasma, two–temperature Raymond-Smith plasma, APEC, mekal, thermal bremsstrahlung, blackbody and power–law. The rows represent the mean χ^2 per degree of freedom, the MAD and the number of outlying measurements rejected in the MAD determination process. This last row indicates the stability of the model relative to the data. From the data in the table it is clear that the blackbody and power–law fits are poor for the bulk of the sources. Among the single temperature fits, the

[2]An emission spectrum from collisionally-ionized diffuse gas calculated using the APEC code v1.10. More information can be found at http://hea-www.harvard.edu/APEC.

Raymond-Smith and APEC fits are clearly superior to mekal and thermal bremsstrahlung for these data. The reduced χ^2 tend to be slightly higher for both thermal bremsstrahlung and mekal, and the fraction of rejected fits is very high for the mekal models.

It was difficult to determine superiority between the APEC and Raymond–Smith models. APEC had a slightly lower mean χ^2 per degree of freedom (d.o.f.), but more scatter than Raymond-Smith fits. APEC performed marginally better for the brightest sources, but Raymond-Smith performed better at the faint end. We compared luminosities determined by the two models and found the standard deviation between the two models was about 20%. This difference is dominated by outliers, removing the 10 outliers lowered the deviation between the two models to 3%. When we compared the $N_{\rm H}$ fit to the outliers to the visual extinction (calculated in §6) we found that the $N_{\rm H}$ calculated using the Raymond–Smith model was more consistent with the independently derived A_V and the independently derived $N_{\rm H}$ to A_V relation. For these reasons we chose the Raymond-Smith model for our main spectral fitting model.

A few sources are fitted very well by a single power law, these are probably background AGN. Still, in most cases a thermal model (e.g. APEC or Raymond-Smith) is better even for non–cluster members. Similarly some very cool sources, probably white dwarfs, are best fitted as blackbodies (see §7.2). Finally, some sources simply defy fitting by any one model.

5.2. Global Fitting of X-ray Spectra

When performing bulk processing on the catalog of $\approx$ 460 X-ray sources we found it was advantageous to perform a preliminary fit to the data with a simple blackbody and use the result of this fit as the initial guess for the Raymond–Smith fit. This ensured that the local minimum found by Levenberg-Marquardt optimization was realistic. From the experiments above, we see that the two-temperature models were no better than the one-temperature fits. This is expected in a high extinction environment as we have here. Any cool component which may exist is overwhelmed by soft absorption due to the large hydrogen column. We attempted detailed two-temperature fits for all sources with over 100 counts. Of the 80 fits only 35 of them had more than 10% of the flux contributed by each component and had temperatures of the two–components separated by more than 5%. Two issues show up throughout the fitting process. 1) There is a fundamental degeneracy in the fits between $N_{\rm H}$ and kT, fits of similar quality can be obtained by increasing $N_{\rm H}$ and then correspondingly changing the temperature. This is especially true in regions of high absorption such as RCW 38. 2) Since there is little sensitivity to X-rays above 10 keV, model fits are not very reliable much above this energy range. Because of this, if the fitted temperatures exceed 15 keV we simply label them "$>$ 15" in the tables.

The fit results for the two–temperature fits are tabulated in Table 5 including results for three non-cluster members. In Table 5, Column 1 gives the source name from Table 1, Column 2 gives the goodness of fit to an absorbed two–temperature Raymond–Smith plasma in terms of χ^2/d.o.f.

Columns 3–8 give the fit parameters $N_{\rm H}$, kT_1,kT_2 and the associated errors. Column 9 lists the log of unabsorbed flux from 0.3-8.0 keV, while column 10 lists the ratio of the flux of the two components kT_1/kT_2. For the cluster members, the luminosity from 0.3-8.0 keV of each source is calculated based on the derived unabsorbed flux and the cluster distance of 1.7 kpc and listed in column 11. These are the brightest and best fitted cluster members and can be used to derive the basic cluster parameters. The mean $N_{\rm H}$ of these stars is $2.6\times10^{22}{\rm cm}^{-2}$ with a MAD of 0.2, a mean $kT_1 \sim 700$ eV (MAD =80 eV) and the mean $kT_2 \sim 4.7$ keV (MAD =190 eV). The mean kT_1 is very similar to the average value of about 800 eV seen in several other clusters (Sanz-Forcada et al. 2003).

For the remaining cluster members we performed absorbed one–temperature fits using a two step fitting procedure. Initial conditions were set so that $N_{\rm H}$=1.0 $\times10^{21}$ cm^{-2} and kT=1.0 keV. Then an initial fit was made with an absorbed thermal blackbody model. These fit results were then used as initial conditions for an absorbed Raymond–Smith plasma model. The results of the fits to the Raymond–Smith models are tabulated in Table 6. In Table 6, Column 1 gives the source name from Table 1, Column 2 gives the goodness of fit to an absorbed one–temperature Raymond–Smith plasma in terms of χ^2/d.o.f. Columns 3–7 give the fit parameters $N_{\rm H}$, kT, associated errors and unabsorbed flux. The luminosity of each source is calculated based on the derived unabsorbed flux and the cluster distance of 1.7 kpc and listed in column 8. The median $N_{\rm H}$ of these stars is $2.6\times10^{22}{\rm cm}^{-2}$ while the median kT is ~ 2.55 keV.

We separately tabulated fits for sources with less than 30 counts. Cstat statistics and Powell optimization were used, appropriate for faint sources. These fits have large, though non–systematic, errors (Table 7). The columns in this table are identical to the columns of Table 6. The median $N_{\rm H}$ of these stars is $3.2\times10^{22}{\rm cm}^{-2}$ while the median kT_1 is ~ 2.1 keV. Note that change to higher $N_{\rm H}$ would lead to a high kT as well *if the sources were similar.* It is easy to understand that the fainter sources are preferentially more absorbed, but it appears that they are also cooler.

Finally, we performed fits on the non-cluster members. Only 29 of these have over 30 counts. Three were fitted as two-temperature plasmas, although the fits to sources 39 and 447 will be revisited later. Most of the 26 remaining sources were well fitted by the Raymond–Smith model with reduced $\chi^2 < 1.71$ for all and reduced χ^2 between 1.3 and 0.3 for all but three others. The median kT for these sources was about 1.25 keV and the mean $N_{\rm H}$ was about $0.5\times10^{21}{\rm cm}^{-2}$. As a group, they are cooler and less absorbed than the cluster members. For completeness we tabulated fits for non cluster members with under 30 counts. These results are tabulated in Tables 8 and 9. The columns in this table are identical to the first 8 columns of Table 6. Thermal spectra of the brighter non–cluster members range from 140 eV to over 15 keV. The softer sources may be foreground dMe stars or white dwarfs (see §7). In Table 9 the temperatures of 30% of the sources exceed 15 keV (compared to 7.5% in Table 7), indicating these are probably power law sources and most likely background AGN.

We summarize all the spectral data in Figures 9, 10 and 11 which show the histograms of the

derived plasma temperature, source extinction and X-ray luminosity function (XLF) respectively. Focusing first on the cluster member sources with 30 counts or greater, the typical plasma temperature is similar to that of stars in the ONC (Getman et al. 2005). We derive a mean (rejecting outliers[3] plasma temperature of 2.9 keV (MAD= 0.15). The bulk of the sources are between 1 and 4 keV with a tail off to higher temperatures. The $N_{\rm H}$ column is symmetrically distributed among the sources with an outlier resistant mean of 2.8×10^{22} cm^{-2} and a MAD of 0.10. If we include the fainter members, we find that these tend to be more absorbed with $N_{\rm H}$=4.3×10^{22} cm^{-2} and a little cooler with <kT>$\sim$ 2.0 keV.

In Figure 11 we plot both the observed XLF and the nominal "complete" XLF of the ONC, which was parameterized by Feigelson et al. (2005) as a log-normal distribution with <log L$_x$ >$\sim$ 29.3 and $\sigma \pm 1.0$.[4] We normalized the log–normal distribution to fit the RCW 38 bins with log L$_x$ > 31.0. The RCW 38 XLF becomes incomplete around log L$_x$ $\sim$ 30.75 and is essentially cutoff near log L$_x$ $\sim$ 30.0. For the case of RCW 38 at 1.7 kpc with a mean log $N_{\rm H}$=22.4 the estimated point source sensitivity limit is log L$_x$ $\sim$ 30.1 consistent with the empirical result from Feigelson et al. (2005).

5.3. Diffuse Emission

Wolk et al. (2002) reported the detection of extensive and bright diffuse emission throughout RCW 38. In light of the estimate of over 1000 undetected cluster members, it is worthwhile to briefly revisit here whether the diffuse emission may be simply those undetected sources. We find this explanation for the diffuse emission unlikely for several reasons. First, one can attempt to count up the missing photons in Figure 11 by assigning the mean number of missing counts in the first incomplete bin to be 4 (This number is chosen, since sources as faint as 5 counts on axis are generally detected. It is clearly an over estimate since the mean value will be lower than the maximum) and then summing the counts from each bin. The result is about 1000 counts, which is significantly less than 6200 counts detected in the diffuse emission. Second, the region of emission extends about $2'$ ($\sim$ 1 pc) in the southeast–northwest direction and about $3'$ ($\sim$ 1.5 pc) in the northeast–southwest direction (see Figure 2 of Wolk et al. 2002). Ninety percent of the cluster members are within $1'$ of the cluster center and there are essentially no members outside of $2'$. Third, the spectrum of the diffuse emission outside of the cluster center is very hard with temperatures greater than 10 keV if fitted as a thermal spectrum and more accurately fit as a power-law. This is not the result of the sum of thermal spectra. It is likely that flux from unresolved point sources in the core contributes

[3]Since the mean temperature is about 2 or 3 keV and the total fit range is 0-50 keV the outlying values are vary non–symmetric. A high outlier can have a value more than 45 keV above the mean, while a low outlier is within 3 keV of the mean. Hence, we reject 5 σ outliers (high and low) before calculating the final mean.

[4]since we are using photon energies from 0.3keV to 8.0 keV we are using the formulation for total luminosity from Feigelson et al. (2005).

significantly to the emission detected there and may account for the thermal nature of the diffuse emission measured in the core. But stars cannot account for the diffuse emission more than 0.15 pc ($\sim$15″) from the cluster center.

6. Infrared Properties of X-ray Sources

Since the RCW 38 region is optically obscured there is little optical data on the X-ray sources. The region has been explored in the near-IR however. A search of the 2MASS point source catalog returns about 2500 sources in the X-ray field. About 500 of these have photometric errors of $< 5\%$ in all 3 bands. However there are only 16 such 2MASS sources in the central $2\farcm5 \times 2\farcm5$. This is because most sources are embedded in extended emission and cannot be properly measured by 2MASS with its 2″ nominal resolution. Because of this, the central region of RCW 38 was observed by Very Large Telescope (VLT) in November 1998 as part of the first light observations on VLT - UT1 (ESO Messenger 1998, 94, 7). Data in J, H and K_s bands were obtained using the ISAAC imager with exposure times of 320, 320 and 210 seconds, respectively (Figure 12). The field measures $2\farcm5 \times 2\farcm5$ and was reduced to colors and magnitudes using the standard apphot and photcal packages in IRAF[5]. There were 447 sources detected in all three filter bands. Minimum photometric errors reach 5% at J, H and K_s magnitudes of 17.6, 18 and 17.1 respectively. The errors were dominated by variability in the nebular background. The 5 σ level detections had measured magnitudes of 19.8, 19.0 and 18.0 in J, H and K_s filters respectively.

There were 36 sources detected in one or two of the VLT filters, but not all three. This usually occurred when the source was highly obscured and no H and/or J band detection was made. If there was an X-ray source coincident with one of these objects, we estimated magnitudes in the filters in which they were detected by calculating the mean conversion from instrumental magnitude to the standard scale for the 447 sources which had good IR colors and applying this linear factor to the observed instrumental magnitude. The resulting magnitude estimates have errors of about 20% since no color term could be applied. We performed astrometry on this image by matching against 10 X-ray sources spread around the field using the WCStools program imwcs (Mink 2001) which automatically finds stars in an image, matches them to stars in a reference catalog and computes the relation between sky coordinates and image coordinates. Typical offsets were $< 0\farcs3$. Direct comparison of 2MASS and VLT positions for sources near the edge of the VLT field showed similar offsets although 1″ offsets were seen in some cases. We then matched all the X-ray sources in the central region to this VLT catalog. For VLT sources, our matching procedure was to match to the nearest source, rejecting all matches with offsets $< 1''$. The median offset is $0\farcs45$. Outside the

[5]IRAF is the Image Reduction and Analysis Facility, a general purpose software system for the reduction and analysis of astronomical data. IRAF is written and supported by the IRAF programming group at the National Optical Astronomy Observatories (NOAO) in Tucson, Arizona. NOAO is operated by the Association of Universities for Research in Astronomy (AURA), Inc. under cooperative agreement with the National Science Foundation.

central pointing we matched sources against the 2MASS catalog. The maximum offset between X-ray and 2MASS IR positions allowed in matching was $1\farcs5$. This added error budget was due to the fact that 2MASS was used primarily for sources away from the *Chandra* aimpoint, hence there is larger positional uncertainty in these *Chandra* sources. 2MASS colors and magnitudes have typical errors of less than 20% at magnitudes of about 17, 16 and 15 respectively with errors of about 5% for sources which are one magnitude brighter than these limits.

Near IR matches were found for 349 of the X-ray sources listed in Table 1. Of the 360 cluster members, 294 have near–IR matches, these are listed in Table 10. Column 1 of this table is the X-ray source number. Column 2 is the 2MASS name or a VLT name (J2000) depending on which data are used. Column 3 is the offset between the X-ray and IR positions. Columns 4-9 are the J, H and K_s band observations and errors. Column 10 indicates the A_V as calculated later in this section. Column 11 indicates the type of emitting surface assumed in the calculation of A_V – this is either a cool M star photosphere (M star), a higher mass star photosphere (bright) or a star + disk combination (Bright). Column 12 contains the 2MASS flags for the 2MASS sources. For the VLT sources, the notation faint is used to indicate sources which were not detected in all three bands and hence subject to large errors due to the lack of color information. Table 11 lists the same information for 55 X-ray sources which do not appear to be cluster members. We determine extinctions to 36 of these; none have near IR-excesses which require a disk.

There are 55 matches to the 81 non-members as determined in §3. The color-color diagrams for the cluster members and non-members are shown in Figure 13. In these plots, we restrict the sources to those with errors in J and K_s of < 0.2 magnitudes and highlight sources with errors of less than 0.05 magnitudes. Most non–member sources appear to be unobscured blackbodies, although two are obscured by $A_V \sim 10$. Among the cluster members, none appear to be normal unobscured photospheres. Most of the X-ray sources which are candidate cluster members appear quite obscured. Twenty-six of the 184 (14%) IR sources with errors of $< 20\%$ lie within the classical T Tauri star (cTTs) region of the color–color diagram as described by Meyer et al. (1997). If we restrict ourselves to the 104 X-ray members with $< 5\%$ errors, 9 stars lie in the disk region. While $H-K_s$ is a not very sensitive to disk excess (Lada & Lada 2003), this is still a very small disk fraction for X-ray sources in such a young cluster.

If the IR data are of high enough quality ($err_{mag} < 0.2$) they allow a tentative extinction estimate. We simply calculate the amount of reddening required to move the object from zero reddening to the observed location. The zero reddening location is different for a star with and without a disk and varies depending on spectral type for pure photospheres. To calculate the extinction we first assume the least obscured case, that all the stars have disks and deredden the photometric colors until they intersect the cTTs locus. This is the only possible solution for stars outside the pure reddening box (Lada & Adams 1992). For stars inside the box two disk solutions exist where the extinction correction crosses the main sequence. One of these solutions roughly corresponds to the star being an M star the other with the photosphere being warmer. We measure the extinction for stars inside the box for each hypothesis (disk, M star, higher mass (HM) star).

Thus, we determine up to three possible extinctions for each star. For stars which lie either below the cTTs locus or to the left of the main–sequence, no estimate of extinction is possible. In addition there are stars outside the reddening box due to observational errors, not disks. If the dereddened star is within 2σ of the reddening box on the low mass side of the main sequence (high H−K) we calculate the M star reddening. We do not calculate the reddening of the HM star hypothesis because the angle between the ZAMS and the extinction curve is very shallow leading to large errors. If the dereddened star is outside the reddening box on the high mass side, falling near the elbow of the main sequence in the color–color diagram then no additional reddening is possible beyond the disk/M star hypothesis which yield the same result. We label these "GK stars" in the table since this is their inferred spectral type on the main sequence.

The IR-extinction of stars which are bright Xray sources can be cross-checked against the $N_{\rm H}$ column derived from spectral fits to the X-ray data. To start this process we use the relation of $N_{\rm H}$ to A_V recently derived for *Chandra* ACIS-I data by Vuong (2003) of $N_{\rm H}$= $A_V \times 1.6 \times 10^{21}{\rm cm}^{-2}$ and find which model hypothesis (disk, M star or HM star) minimizes the difference in the A_V estimates. The hypothesis which most closely matched the measured $N_{\rm H}$ absorption column was chosen as the probable source extinction in Table 10. In about half the cases the difference between the IR determined A_V and the A_V inferred from $N_{\rm H}$ was <1 magnitude. However, in about 20% of cases the difference was greater than 5 magnitudes. This large scatter led to some concern about the appropriateness of the $N_{\rm H}$ to A_V relation that was used. The mean difference between A_V calculated using the infrared extinction correction method and A_V calculated using the Vuong relation is 2.62 magnitudes, (MAD=0.35).

To assess and refine the formulation of $N_{\rm H}$ to A_V relation we fitted the extinction, as determined above, to the measured $N_{\rm H}$ values. We restricted the fit to 31 bright X-ray and IR objects with a magnitude error of less than 5% in J and an uncertainty of less than 30% in $N_{\rm H}$. Using a regression fit which rejected outliers we find a relation of $N_{\rm H} = A_V \times 1.7 \times 10^{21}$ cm^{-2}. Forcing zero extinction at zero column of $N_{\rm H}$ we get a best fit of $N_{\rm H} = A_V \times 2.0 \times 10^{21}$ cm^{-2} that is shown in Figure 14. These are intermediate to results derived using *ROSAT* data (Ryter 1996) and those of Vuong et al. (2003). Using $N_{\rm H} = A_V \times 2.0 \times 10^{21}$ cm^{-2} the mean difference between A_V calculated using the infrared extinction correction method and A_V calculated using the $N_{\rm H}$ relation drops to 0.28 magnitudes. The mean absolute deviation of this fit is 0.29, consistent with no offset.

At this point we revisited the choices we made amongst the 3extinction possibilities of each star to verify that the selection made when we assumed $N_{\rm H} = A_V \times 1.6 \times 10^{21}$ cm^{-2} was still the best fit to the updated $N_{\rm H}$ to A_V relation. We found that in all cases, the extinction as derived using the infrared method was insensitive to the choice of $N_{\rm H}$ to A_V conversion despite the fact that the conversion is used for vetting the models. This was because the differences in the possible near-IR extinction hypothesis are more significant than the difference modest 20% difference between the $N_{\rm H}$ to A_V relations.

The extinction to 160 X-ray selected cluster members was determined via infrared photometry.

Sixteen of these stars have K-band excesses indicative of disks based on their infrared colors. Most of the remainder had multiple viable extinction solutions. Using the X-ray absorption as a guide, 33 of these are most consistent with disks for a total of 49 (31%). Thirty-five appear to be obscured M stars without K-band disk signatures while 49 appear near the "elbow" of the main sequence and while no disk is in evidence there is little which can be determined about the photosphere either. The remaining 28 stars have colors too blue to be K or M stars or have optically thick disks at K_s band.

We create an intrinsic KLF by correcting the observed K_s band magnitude for extinction by $A_k = 0.109 \times A_V$ (Bessell & Brett 1988). In Figure 15, we find the KLF is peaked at $K_s = 12$. At a distance modulus of 11.15 this is an absolute K magnitude of about 0.85. Masses are estimated using the theoretical isochrones of Siess et al. (SDF; 2000) with metallicity =0.02 and no convective overshooting and a cluster age of 0.5 Myr.[6] Metallicity was varied from 0.03 to 0.01 with only a 3% effect on the K_s band magnitude at 2.7 $M_\odot$. The error induced by the age estimates, which range between 0.5 and 1.0 Myr was almost 50%. At an assumed age of 0.5 Myr a star with absolute K_s magnitude of 0.85 has a mass range of about 1.05 $M_\odot$. Completeness appears to become an issue at $K_s \approx 13$ which corresponds to 0.5 $M_\odot$. The ratio of non-X-ray stars per magnitude with corrected K magnitudes between 10 and 12 and those with corrected K magnitudes between 13 and 14 is about 1:4. The same ratio for the X-ray detected sources is about 1:2. Thus, we detect about 50% of the stars at an extinction corrected $K_s \approx 13$ (0.5 $M_\odot$). This is consistent with the prediction given in §3. We have 50 detections at 14^{th} magnitude in K_s. These sources have masses ranging from 0.25 $M_\odot$ down to the brown dwarf limit.

6.1. Other IR sources in the VLT field.

Examination of the VLT non–X–ray detected sources can be used to analyze the completeness of the X–ray data. Since the VLT image is centered near the core of a very dense cluster with a dense molecular cloud behind it we expect the stellar sources in the VLT field to be dominated by the cluster members. Using the galactic models of Wainscoat et al. (1992) we expect minimal contamination, perhaps 6 sources brighter than $K_s = 17$ in this small field of view. None of the 129 X-ray sources in the VLT field of view has been excluded as a cluster member based on its X-ray properties.

There are a total of 482 stars in the VLT field with good colors in J, H and K_S. Of these, 129 are X-ray sources. We assume the bulk of the remaining 353 are cluster members. We note that about 25% of the IR sources were detected in the X-ray observation (after a small correction

[6]All manner of evolutionary tracks are estimates and concerns about accuracy of the estimates become larger at younger ages (see Hillenbrand & White 2004 for a full discussion). Initially, the age is estimated as 0.5 Myr based on the degree of embeddedness of the sources, but we expect a range of ages as seen in the ONC. We use the Siess et al. tracks because of their large mass coverage, especially at high masses.

for VLT sources detected in less than 3 bands). This is somewhat at odds with the prediction of a 16% detection rate based on ONC data (Feigelson et al. 2005). The VLT data reach K_s of 17.1. This should be complete to 0.1 $M_\odot$ even through 30 magnitudes of visual extinction according to the SDF tracks at 0.5 Myr and 1.0 Myr. However, very low mass stars may be 0.5 magnitudes fainter than this and 20 Jupiter mass brown dwarfs similar to those detected in the ONC may be 3 magnitudes fainter than the faintest sources of stellar mass (Hillenbrand & Carpenter 2000). Thus the VLT image is somewhat incomplete. The IR color–magnitude shown in Figure 16 uses SDF isochrones set at 0.5 Myr, 1.0 Myr and the ZAMS. The dashed lines indicate 30 magnitudes of visual extinction. X-ray sources are noted with "X" and non-X-ray sources with open circles. We find about 10 of the 482 stars are too faint and unobscured to be cluster members. Thus, there is some contamination by non-cluster members in the VLT dataset. If we take the 16% detection fraction as a minimum fraction of cluster members detected in X–rays and 25% as the maximum, then the total cluster membership is between 1450 and 2400.

In Figure 16, it appears the X-ray sample is not uniform compared with the non-X-ray sample. The X-ray sample seems more sensitive to very embedded, high–mass sources and less sensitive to embedded lower mass sources. The 353 VLT sources not detected in X-rays are indicated in the color–color diagram shown in Figure 17. The minimum extinction to each star was derived using the same procedure as in the previous section. One–hundred and seventy–three stars (49%) in the non–X–ray group needed to be modeled as stars with disks. This fraction is much higher than the 14% disk fraction among the X-ray sources. Further the 49% disk fraction is a lower limit. The remainder of the stars may or may not have disks as the near-IR is only sensitive to the hot part of the inner disks. Without additional data (e.g. X-ray spectra or mid-IR photometry) it cannot be determined which of the other 51% have disks.

This indicates that the X-ray sample is biased away from stars with inner disks. There are two possible, non–exclusive, explanations for this. First, the disk itself will absorb X-rays. Second, the X-ray production mechanism for stars with disks may be different and lower in luminosity than it is for PMS stars without disks. These possibilities are discussed further by Preibisch et al. (2005). The intrinsic K_s band luminosity is *not* the primary difference between the X-ray detected and non–X-ray detected populations. Of the 152 VLT stars detected in X-rays, 8 are fainter than K= 16 and 2 are fainter than K=18. Out of the remaining 353 VLT detected sources 36 are fainter than K= 16 and 1 is fainter than K=18. The ratios are statistically indistinguishable. The KLF of the non–X–ray detected sources (bottom of Figure 15) shows a similar shape to the KLF of the X-ray detected members. Finally a two-sided KS test comparing the colors of the brightest 100 X-ray and non-X-ray detected sources found a 4% probability that they were drawn from the same population. Even when all sources were included the KS test found a 1% chance that they were drawn from the same source population. We conclude that the X-ray sample, while not complete and certainly biased against disks, is not particularly mass biased down to the sub-stellar limit. Only one X-ray source is detected significantly below the nominal brown dwarf limit, Source 281 at $0\farcs68$ from VLT085907.79-473122.2, a very likely cluster member since its extinction is about 5.25

A_V.

6.2. Possible O and B stars

Using the extinction corrected KLF we performed a survey of the cluster for O and B star candidates. On the ZAMS a star of 2.7 $M_\odot$ is a late B star. On the SDF mass tracks, at 0.5 Myr a 2.7 $M_\odot$ star has an absolute K_s band luminosity of -0.35 as calculated using the on-line SDF model isochrones as discussed in §6. We chose an age of 0.5 Myr and solar metallicity (Z=0.02). To convert the effective temperatures resulting from the models to colors, we used the conversion table from Kenyon and Hartmann (1995). Both mass and luminosity were derived from the models using the extinction corrected K_s magnitude of the X-ray selected members as estimated earlier in this section and the distance modulus of 11.15.

This use of the SDF isochrones leads the identification of 31 X-ray sources as candidate OB stars. One star (Source 390) was excluded since it had no measurable extinction and hence is probably foreground.[7] Another, Source 435, is also excluded because it is both a very faint X-ray source and somewhat softer than the rest of the group. Including Source 221/IRS 2, which has been discussed elsewhere as an ∼O5 star (Smith et al. 1999, Wolk et al. 2002) and Source 251 which is a very absorbed and luminous X-ray source, there are 29 X-ray detected candidate OB stars.

There are 2 additional stars in the VLT field, which while not detected in X–rays are still identified as O or B star candidates based on their extinction corrected luminosity. VLT085905.44-473045.2 (VLT232) is in the wings of several X-ray sources which could easily obscure X-ray emission from this source, up to about 30 counts. This would provide a perfectly reasonable log (L_x/L_{bol}) of -5.89. It is somewhat surprising that VLT085906.96-473023.2 (VLT453) is not an X-ray source if it is indeed a B star. While it is in the vicinity of Source 251, it is 3″ away and the background contamination is only about 0.5 counts. If this is a B star is would be very weak X-ray source, perhaps due to an unusually weak wind.

Figure 18 shows the location of the 31 OB star candidates. In Table 13 we list the OB stars in RCW 38. Columns 1–4 of the table list the Source ID, RA, DEC and distance from the cluster center respectively. Columns 5 and 6 list the magnitudes of visual extinction as derived from the IR (col. 5) and X–ray (col. 6) methods. The absolute K_s magnitude derived from the measured K_s magnitude, the distance modulus and the infrared extinction is given in column 7. In general, the infrared extinction is lower than the estimate derived from the $N_{\rm H}$ column. This occurs for stars fitted with the disk model since we stop the dereddening process when we reach a model consistent with a late type star with a disk. For the most part the agreement between the extinction measurements (infrared derived and X-ray derived) is very good leaving less than

[7]Source 390 had less than 30 X-ray counts, hence its identification as a cluster member was already on questionable footing.

0.3 magnitudes of variation in the derived absolute K_s magnitude. This contributes about a 25% uncertainty to the mass estimate. This is usually in the sense of a mass underestimate. The last 2 columns list the bolometric luminosity (derived from the age and absolute K_s magnitude and the relative X-ray luminosity (log (L_x/L_{bol})). The latter values are consistent with known O and B stars.

The distribution of the OB candidates mimics the roughly symmetrical and peaked distribution of the cluster as a whole. Twenty–one of the candidates are within 111″ of the cluster centroid. Four candidates lie more than 300″ from the cluster centroid. The most distant candidates tend to have extreme values of L_x/L_{bol} indicating that they may not be at the distance of RCW 38. The finding of $\sim$ 31 candidate OB stars is consistent with our estimate for the overall membership cluster as about 1.7 times that of the ONC. The ONC has about 15 O and B stars (Stelzer et al. 2005). Although 31 OB stars is a little on the high side, this number is non disallowed by the radio data (Vigil et al. in prep.) since the luminosity is dominated by IRS 2. The large number of candidates may indicate that the 4 off-axis candidates may not be cluster members. If we assume the cluster is 1 Myr instead of 0.5 Myr the cutoff for O and B stars become more than 0.5 magnitudes fainter (Abs K = 0.32) and would bring the total population of O and B stars in the cluster over 60 which we consider unlikely.

7. Specific Interesting Sources

For the analysis presented here, the primary utility of X-ray emission in young stars is as a tracer of youth and to measure the gas and dust along the line–of–sight. The former is especially useful, since other, more obvious tracers of youth, such as near-IR emission fade more quickly with age than X-ray emission. However, several of the X-ray sources, both cluster members and non-cluster members are interesting for their X-ray characteristics. In our data set we found two remarkably cool objects, and several sources with very hot plasma and others which were extremely embedded. We discuss them and the brightest 10μm source below.

7.1. Very Bright IR sources

RCW 38 was identified as a star forming region through the presence of several bright infrared sources. IRS 2 (Frogel & Persson 1974) is clearly the revealed central O star. As we discussed previously (Wolk et al. 2002), this is coincident with the brightest X-ray source in the field, Source 221. The X-ray count rate is 0.062 counts s^{-1} so the pile up fraction is very small. The X–ray spectrum was not well fitted by any single component thermal model. Our best fit was to a two–temperature Raymond-Smith plasma dominated by a cool component at 0.77 keV and a warm component at 2.5 keV. These temperatures are very consistent with those of strong wind sources in the ONC (Stelzer et al. 2005). Strong wind X-ray sources were modeled by Stelzer et al. to have a hydrodynamic

wind with many small shocks. IRS 2 has an X-ray luminosity 10% greater than that of θ^1 Orionis C. While this star was too bright to be measured in the VLT observations, good 2MASS data are available and demonstrate that IRS 2 is about 5–10 times more luminous than θ^1 Orionis C at K-band.

IRS 1, the brightest 10 μm source (Frogel & Persson 1974), appears not to be a point source at all. Rather it is a complex region to the west of IRS 2. Mid-infrared 10 and 20 μm observations by Smith et al. (1999) find that IRS 1 is a dust ridge with a number of peaks, including one at the location of IRS 1 and others noted by the letters A–D in Figure 1 of Smith et al. They propose that the region can be explained in terms of a wind-blown cavity, where the stellar wind from the hot young star IRS 2 has cleared a cavity about itself, and the ridge of emission near IRS 1 represents the material which has been swept up into the shell around IRS 2. Vigil et al. (in prep.) find that there is a peak in the cm continuum emission within this ridge. They conclude that the density enhancement could lead to future star formation.

The dust enhancements identified as regions A, B and E by Smith et al. are associated with X-ray emission – sources 187, 197 and 174 respectively. Source 187 is among the fainter sources with only 18 counts, the absolute K magnitude is very close to that expected of a 0.4–0.5 $M_\odot$ star. Source 197 on the other hand is among the brightest 5% of X-ray sources in the field. Its absolute K magnitude is consistent with that of a 2.2 $M_\odot$ star. Both sources appear to be typical thermal plasmas. Mid–infrared regions C and D are not coincident with X-ray sources.

Source 174 (08h59m03.67s, -47°30′40.″1) is the strongest X–ray source in the IRS 1 region. This source is well matched to the westernmost star in a triplet located on the NIR dust ridge that is clearly visible in the center of Figure 2. The IR counterpart to Source 174 is highly reddened with a K magnitude near 13, H-$K_s \sim 1.7$ and no J detection. The visual extinction inferred from the $N_{\rm H}$ column is about 17. From this we infer a mass of about 2.0 $M_\odot$. The best fit to the X–ray spectrum is a fairly hot 5.1 keV plasma. The high temperature may be indicative of very long (perhaps ten's of stellar radii), low density, magnetic structures in this object supporting the idea that the IRS 1 is in a region of ongoing star formation. Any soft X-ray component would be absorbed so we cannot comment on whether there is a bright soft component to the X-ray emission here.

7.2. Cool Objects

Sources 39 and 447 are both very cool and bright. Both exceed 300 counts with almost all the emission below 2.0 keV. They are the only 2 sources in the data set which are well fitted by blackbodies. Figure 19 shows the detailed blackbody fits. Both fits have null probabilities in excess of 0.95. The $N_{\rm H}$ columns fitted to the sources are 6.0 and 7.5 $\times 10^{21}$ cm^{-2} respectively, thus we conclude that they are foreground objects. The derived blackbody temperatures are 100 and 150 eV, consistent with the emission expected from the surface of a neutron star or, more likely, a white

dwarf. Neither shows evidence of variability.

Both are associated with bright 2MASS sources. Source 39 is 0.″1 offset from 2MASS085850.39-473319.5 with K= 8.9, J−H=0.44 and H−K=0.15. This is consistent with the star lying near the G, K, early M stars portion of the color–color diagram with little reddening (less than 0.03 magnitudes at V). Further this source has Tycho BT and VT magnitudes of 11.93 and 11.40 respectively and a proper motion of 47.1 ±2.5 mas/yr (Høg et al. 2000). The colors are consistent with an unabsorbed K3-4 main sequence star (Koornneef 1983) within 100 pc. The X-ray source is most likely an unseen degenerate companion.

Source 447 is 0.35″ offset from 2MASS085956.09-473304.3 which has K= 8.1, J−H=0.33 and H−K=0.18, colors that are consistent with a late K type star. However the source is also coincident with LS 1223 with V_{mag}=11.48, B−V=0.86 and U−V=-0.19, consistent with a moderately reddened ($E_{(B-V)}$ =0.4) early B star. This extinction is not consistent with the measured $N_{\rm H}$ column or the IR extinction which are A_V of 3.75 and 3.0 respectively. Further, the derived V−K_s of 3.4 is consistent with an unobscured K4-K5 star. To obtain consistent colors we need to model source 447 as a K4 star with a young white dwarf companion (which may account for the blue excess) at about 50 pc.

7.3. Very Hot objects

At the other end of the spectrum there are five bright sources which were best fitted by a single temperature plasma with a temperature exceeding 100 MK (kT > 8.6 keV) and in excess of 100 counts so we have good confidence in the fits.[8] Such stars are interesting because the underlying physics required to generate these high temperatures is probably quite different from the physics required to generate the roughly 2.5 keV characteristic plasma seen around most million year old stars. At a minimum, such temperatures probably require magnetic structures exceeding a stellar radius (Favata et al. 2005). Further, the physics required to sustain such plasmas for the entire observing window are probably not related to the loop reconnection seen in flares. We discuss the sources in order of descending temperature. Two of the five stars flared during the observation, for these stars the high temperatures are at least partially related to the flare episodes. The other three sources showed no evidence of strong flares. The spectra of all five are shown in Figure 20.

Source 56 – This source, with about 309 counts, is fitted with the hottest plasma in the field. The fit with a 14.7 keV thermal plasma with $N_{\rm H}$= 3.9 $\times 10^{22}$ cm^{-2} is very good with a reduced χ^2 of < 0.5. It is not in our VLT field and has neither 2MASS, nor MSX counterpart so it could be an AGN or other exotic object. Fits with a power-law yield a slightly poorer fit with reduced χ^2 of

[8]There are three sources fitted with two–temperature plasma in which the warmer plasma exceeds 100 MK. However, in all three of these cases the emission measure is biased towards the cool component such that there are less than 50 counts in the hot component.

0.33 but perfectly reasonable values of $N_{\rm H}$=4.05 $\pm$0.07 $\times 10^{22}$ cm^{-2} and $\Gamma = 1.83 \pm 0.21$, indicating it could be powered by synchrotron electrons. However, it is 166″ from the cluster center which puts it on the edge of the cluster core. While it is possible that this is a chance superposition of a background object, its location and count rate make a protostellar hypothesis more likely.

Source 147 – This source, with almost 200 counts is best fitted with an 11.0 keV thermal plasma with $N_{\rm H}$=1.7 $\times 10^{22}$ cm^{-2} with a reduced χ^2 of < 0.6. Fits to a power-law yield a poorer fit with reduced χ^2 of ~ 0.45 and reasonable values of $N_{\rm H}$=0.9$\times 10^{22}$ cm^{-2} and $\Gamma = 1.07$ but, the residuals are systematic indicating that the power-law model expects too much flux at the hard end. Further, since it is only 50″ from the cluster center it is within the VLT field of view. Indeed it is quiet bright in the near-IR with K=11.5 and an $A_V \sim 10$ consistent with the $N_{\rm H}$ measurement. The absolute magnitude of -0.65 at the 1.7 kpc distance of RCW 38 is consistent with a 3.5 $M_\odot$ star near the birthline (Palla & Stahler 1993). The mass of this star could be significantly higher due to the non-monotonic relation between K magnitude and mass in this regime.

Source 251 – This source, with over 280 counts, is the closest to the cluster center among this group, $< 22''$ off–axis. It is the only one of the five hottest sources coincident with the molecular ring discussed by Vigil et al. (in prep.). It lies on the inner edge of the molecular and dust rings. It is fitted with a 10.7 keV thermal plasma with a very high column, $N_{\rm H}$= 2.3 $\times 10^{23}$ cm^{-2} with a reduced χ^2 of 0.95. Fits to a power-law yield a negative slope or forcing a positive slope yields reduced χ^2 of > 9. Since the star is highly embedded it is not detected at J band. Our K_s band detection is 14.9 with H-K_s of 1.5. Based on the $N_{\rm H}$ column we estimate A_K to be about 12.5. This yields an absolute K magnitude of -8.75. This corresponds to about 25,000 $L_\odot$ which is similar to that of the Becklin–Neugebauer object (Becklin & Neugebauer 1967) and consistent with an O star of greater than 10 $M_\odot$. This star has a clear flare, about 80% of the observed flux from the star is associated with that flare.

Source 149 – This is a 300 count source 95″ off–axis. It is outside of the VLT field but coincident with the very red 2MASS085902.07-473209.4 (0.″3 offset). The observed K magnitude is 13.2 with H$-K_s < 1.2$ (the H value is an upper limit). It is well fitted to a 9.6 keV thermal plasma with a very high column, $N_{\rm H}$= 3.8 $\times 10^{22}$ cm^{-2} with a reduced χ^2 of 0.4. The equivalent A_K is about 2.1 which gives an absolute K magnitude of about 0. About 50% the flux from this star emanated during a flare. This flare would have to be extremely hot $\sim$ 150 MK to interpret this as a normal T Tauri star with a flare.

Source 108 – This source is located just southwest of Source 149, 132″ off axis. Its X-ray spectrum is very similar to nearby Sources 147 and 149, kT= 8.9, $N_{\rm H}$= 5.37 $\times 10^{22}$ cm^{-2} with a reduced χ^2 of 0.4. There is no near-IR detection at this location in the 2MASS database, nor would we expect any if the source is similar to 149 and 147 given the additional extinction present.

These stars are all interpreted as O or B stars which should, in principle, have strong, optically thick winds. However, in the sample of 8 such stars in the ONC by Stelzer et al. (2005) only 2 sources needed thermal plasma in excess of 3.33 keV to fit the data. In both cases the hot component

was a fit artifact listed as "kT> 15 keV", in one case the hot component was less than 10% of the X-ray flux, in the other case it was < 1%. We do not believe there is evidence for a strong optically thick wind giving rise to such temperatures. The rate of flaring, 2/5 in 100 ks is also inconsistent with a collisional wind model. This leads us to conclude that these are good candidates for objects undergoing extremely high rates of accretion.

We note sources 251, 147, 149 and 108 lie on a nearly straight line running from northeast to southwest. This line is parallel to the dust extension seen in the mm observation reported by Vigil et al. and the axis of the diffuse plasma emission reported by Wolk et al. (2002). Source 251 lies near the northern extent of the peak plasma emission (Figure 21). There is an additional cluster member associated with very hot plasma and over 50 counts, Source 345, which also lies close to this line. Source 345 is unusual among the hot sources because it is a fairly low extinction $N_{\rm H}$= 7.5 $\times 10^{21}\,{\rm cm}^{-2}$ and corresponds to a fairly bright (K=13.46) 2MASS source. This is the luminosity expected from a 1.5 $M_\odot$ star at about 0.5 Myr.

In addition to Source 251 there in only one bright source with a measured column with $N_{\rm H}$> $10^{23}\,{\rm cm}^{-2}$ – Source 118. This appears to be a normal PMS star with a hot component of about 3.7 keV and cool component of about 0.9 keV. The spectrum is well fitted with a two-temperature Raymond–Smith plasma with a reduced χ^2 of about 0.25. From the fit we derive a very high X-ray luminosity log $L_x = 32.9$. The source is marginally detected by the VLT in the K-band giving it a K-band magnitude of < 18.6. Three other sources with over 50 counts were found to be absorbed by columns with $N_{\rm H}$> $10^{23}\,{\rm cm}^{-2}$ – Sources 28, 78 and 322. These sources all lie along the same line as the stars with very hot plasma (Figure 21). Perhaps this is a filament of gas and dust behind the currently active region of star formation.

8. Summary

We observed the massive, embedded young cluster RCW 38 and the surrounding region using the *Chandra* X-ray Observatory and in the near-IR using the VLT. Here we summarize our results.

- We detected 460 X-ray point sources in the field. The limiting luminosity for sources in the cluster is about log $L_x \sim 30.0$. We detect over half of all stars down to 0.5 $M_\odot$. Some of the detections appear to be <0.1 $M_\odot$
- Using quartile analysis we identify 360 of the X–ray sources as cluster members. Since this approach is unusual we verify the veracity of the sources identified this way using variability as an independent tracer of stellar nature. Of the 35 stars seen to vary with 99% confidence, 34 of them are identified as cluster members by the quartile approach. This gives us great confidence in this method among the bright sources. Ten percent of the cluster members with over 30 counts are seen to flare. This gives a flare rate of one flare per 775 ks.
- We studied several thermal plasma models and conclude that the Raymond–Smith model is

most appropriate for these sources. The cluster members have a typical plasma temperature of 2.9 keV with a mean absorption of $2.8{\times}10^{22}$ cm^{-2}. By comparing the infrared observed extinction with the fitted $N_{\rm H}$ we derive a best fit of $N_{\rm H} = {\rm A}_V \times 2.0 \times 10^{21}$ cm^{-2}.

- The center of the cluster is located at 08h 59d 04.64s, -47d 30m 44.00s (J2000) and has a peak central density of $\approx$ 400 X-ray sources parsec^{-2} in the central 0.1 parsec^{-2} assuming a 1.7 kpc distance of RCW 38. The density of the number of sources per parsec^2 is $\sim exp(-5.0d)$ where d is the distance in parsecs from the cluster center. The cluster is highly centrally condensed with a half-width at half maximum density of 0.2 pc.

- Since the exposure only reached log $L_x \sim 30$ we only detected between 15 and 25% of the members based on comparison with the ONC. So the true peak density is about 1600 stars parsec^{-2} in the central 0.1 parsec. A similar extrapolation of X-ray detected members to total membership puts the total membership between 1400 and 2400.

- We find it highly unlikely that the diffuse emission reported by Wolk et al. (2002) is the result of the 1000–2000 stars not detected as individual X-rays sources. This is because the spectrum of the diffuse emission is distinctly non-stellar, the extent of the diffuse emission is greater than that of the cluster and there are more photons present in the diffuse emission than would be expected from the non-detected point sources. The point sources may be responsible for the diffuse emission in the central $0.25'$.

- The KLF of the X–ray sources appears quantitatively similar to that of the non–X–ray selected sample indicating that the X-ray sample is not particularly biased except at the lowest masses. Uncertainties in the various mass tracks make stating a value for the completeness limit, in terms of stellar mass, meaningless.

- About 150 of the X-ray cluster members are matched to near infrared sources in the 2MASS catalog or in our VLT observations of the center of the RCW 38 cluster. Less than one-third of the X-ray selected sample of cluster members with near infrared colors appears to have optically thick disks. In addition, there are 353 non-X-ray emitting infrared sources in the central $2.5' \times 2.5'$ detected by the VLT. The bulk of these (at least 90%) are cluster members. Based on the near IR colors, at least 50% of these non–X–ray detected infrared sources possess disks. This indicates a bias of the X-ray sources against having disks which are optically thick at K-band.

- We identify 31 OB star candidates in the field assuming an age of 0.5 Myr. This number is consistent with the number of OB stars expected for a cluster with about 2000 members. If we assume a cluster age of 1 Myr, we would have identified over 60 OB stars. This is inconsistent with the size of the cluster and is taken as evidence for the younger age. A continuum of stellar ages is probably present as there are still protostellar candidates in the cluster, in particular associated with the IRS 1 ridge.

This publication makes use of data products from the Two Micron All Sky Survey, which is a joint project of the University of Massachusetts and the Infrared Processing and Analysis Center, funded by the National Aeronautics and Space Administration and the National Science Foundation. This work was supported by CXC guest investigator grant GO2-3103X. We also thank the referee Leisa Townsley for many helpful comments.

REFERENCES

Becklin, E. E., Neugebauer, G. 1967, ApJ 147, 799.

Bessell M. S., Brett J. M., 1988, PASP, 100, 1134

Bourke, T. L., Wolk, S. J., Vigil, M., & Alves, J. 2004, The Dense Interstellar Medium in Galaxies, 637

Casanova S., Montmerle T., Feigelson E. D., Andre P., 1995, ApJ, 439, 752

Cash, W. 1979, ApJ, 228, 939

Churchwell E., et al., 2004, ApJS, 154, 322

Favata F., Flaccomio E., Reale F., Micela G., Sciortino S., Shang H., Stassun K. G., Feigelson E. D., 2005, ApJS, 160, 469

Favata F., Micela G., 2003, SSRv, 108, 577

Feigelson E. D., et al., 2005, ApJS, 160, 379

Feigelson E. D., Casanova S., Montmerle T., Guibert J., 1993, ApJ, 416, 623

Freeman, P.E., Doe, S. & Siemiginowska A., SPIE Proceedings vol.4477, 76

Frogel J. A., Persson S. E., 1974, ApJ, 192, 351

Güdel M., 2004, A&ARv, 12, 71

Getman K. V., Feigelson E. D., Townsley L., Bally J., Lada C. J., Reipurth B., 2002, ApJ, 575, 354

Getman K. V., et al., 2005, ApJS, 160, 319

Hillenbrand, L. A., Carpenter, J. M., 2000, ApJ 540, 236-254.

Hillenbrand L. A., White R. J., 2004, ApJ, 604, 741

Høg E., et al., 2000, A&A, 355, L27

Hong J., Schlegel E. M., Grindlay J. E., 2004, ApJ, 614, 508

Hong J., van den Berg M., Schlegel E. M., Grindlay J. E., Koenig X., Laycock S., Zhao P., 2005, ApJ, 635, 907

Kaastra, J.S. 1992, An X-Ray Spectral Code for Optically Thin Plasmas (Internal SRON-Leiden Report, updated version 2.0)

Kellogg E., Baldwin J. R., Koch D., 1975, ApJ, 199, 299

Kenyon, S., Hartmann, L., 1995 ApJS, 101, 117

Koornneef J., 1983, A&A, 128, 84

Lada C. J., Adams F. C., 1992, ApJ, 393, 278

Lada C. J., Lada E. A., 2003, ARA&A, 41, 57

Lada C. J., Shu F. A., 1990, Science, 248, 564

Liedahl, D.A., Osterheld, A.L., and Goldstein, W.H. 1995, ApJL, 438, 115

Mewe, R., Gronenschild, E.H.B.M., and van den Oord, G.H.J. 1985, A&AS, 62, 197

Mewe, R., Lemen, J.R., and van den Oord, G.H.J. 1986, A&AS, 65, 511

Meyer M. R., Calvet N., Hillenbrand L. A., 1997, AJ, 114, 288

Morrison, R., McCammon, D. 1983. ApJ 270, 119-122.

Palla F., Stahler S. W., 1993, ApJ, 418, 414

Raymond, J.C. and Smith B.W., 1977 ,ApJS 35, 419

Rho, J., Reach, W. T., Lefloch, B., & Fazio, G. 2006, ArXiv Astrophysics e-prints, arXiv:astro-ph/0601633

Rodgers A. W., Campbell C. T., Whiteoak J. B., 1960, MNRAS, 121, 103

Ryter C. E., 1996, Ap&SS, 236, 285

Sanz-Forcada, J., Brickhouse, N. S., & Dupree, A. K. 2003, ApJS, 145, 147

Scargle J. D., 1998, ApJ, 504, 405

Siess L., Dufour E., Forestini M., 2000, A&A, 358, 593

Smith C. H., et al., 1999, MNRAS, 303, 367

Stelzer B., Flaccomio E., Montmerle T., Micela G., Sciortino S., Favata F., Preibisch T., Feigelson E. D., 2005, ApJS, 160, 557

Townsley L. K., Feigelson E. D., Montmerle T., Broos P. S., Chu Y.-H., Garmire G. P., 2003, ApJ, 593, 874

Vigil, M.C., Bourke, T.L., & Wolk, S.J., in prep.

Vuong M. H., Montmerle T., Grosso N., Feigelson E. D., Verstraete L., Ozawa H., 2003, A&A, 408, 581

Wainscoat R. J., Cohen M., Volk K., Walker H. J., Schwartz D. E., 1992, ApJS, 83, 111

Whitney B. A., et al., 2004, ApJS, 154, 315

Wolk S. J., Harnden F. R., Flaccomio E., Micela G., Favata F., Shang H., Feigelson E. D., 2005, ApJS, 160, 423

Wolk S. J., et al., 2004, ApJ, 606, 466

Wolk S. J., Bourke T. L., Smith R. K., Spitzbart B., Alves J., 2002, ApJ, 580, L161

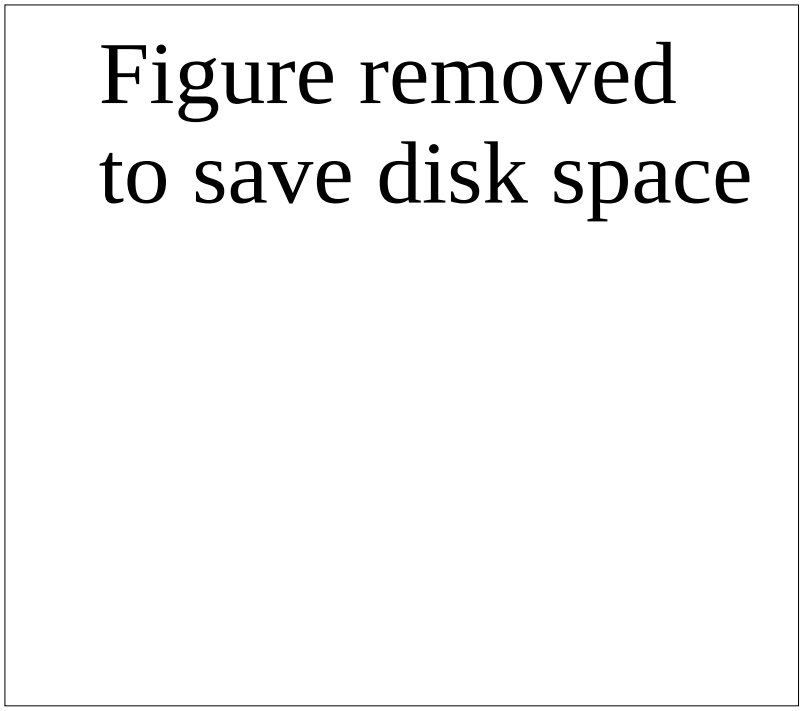

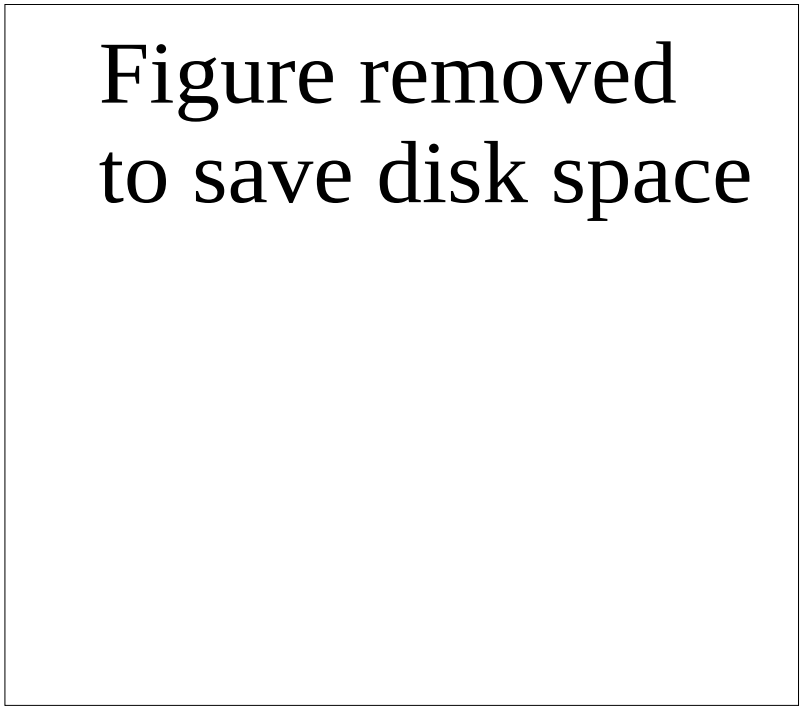

Fig. 1.— Top - The bulk of ACIS-I image of RCW 38 at low resolution. Bottom - Matching field in a 2MASS K-band image. The field of view in these figures is $16' \times 16'$. Regions of interest are identified. The small ovals near the core are the "common background regions" used for sources in the core as discussed in §2.2. At 1.7 kpc $121'' = 1$ parsec.

Fig. 2.— VLT ISAAC K_s band image of the central $2\farcm5 \times 2\farcm5$ region of RCW 38. The image uses square–root scaling. Contours of 0.5, 1 and 4 X-ray counts/pixel are overlaid.

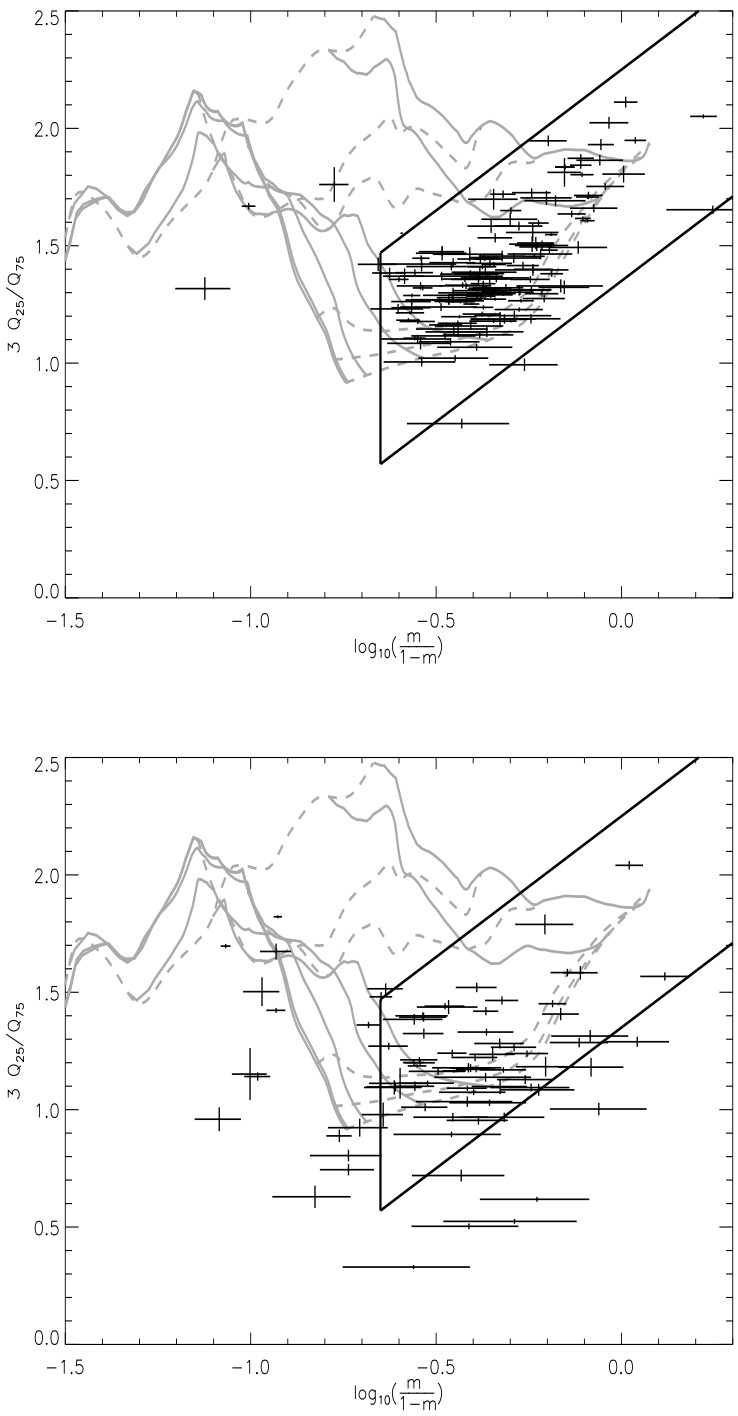

Fig. 3.— Top: Plot of the normalized quartile values for stars within 200″ of the cluster center. A grid of temperature and absorption is overlaid following Hong et al. (2004). The solid lines are lines of constant $N_{\rm H}$ 0.1, 0.5, 1.0, 5.0 and 10 $\times 10^{22}$ from bottom to top. The dashed lines are lines of constant temperature kT= 0.1, 0.5, 1.0, 5.0, 10 and 30 keV from left to right. Errors are plotted. The parallelogram outlines the region occupied by probable cluster members. The diagonal lines are offset ± three deviations from a fit to all the bright sources to the right of the vertical demarcation. See text for details. Bottom: Same as top, but for sources more than 200″ of the cluster center. For clarity, only stars with more than 30 counts are plotted.

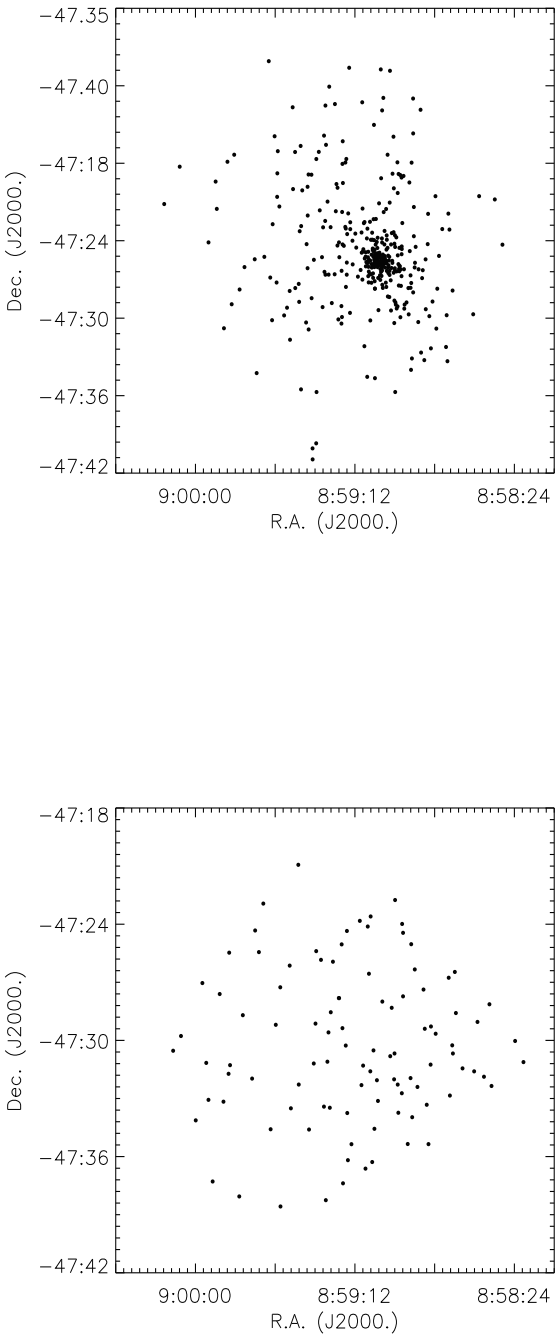

Fig. 4.— Top: Position plot of all probable X-ray cluster members as determined by quartile analysis. Bottom: Position of non–members. A density analysis shows that this distribution is uniform.

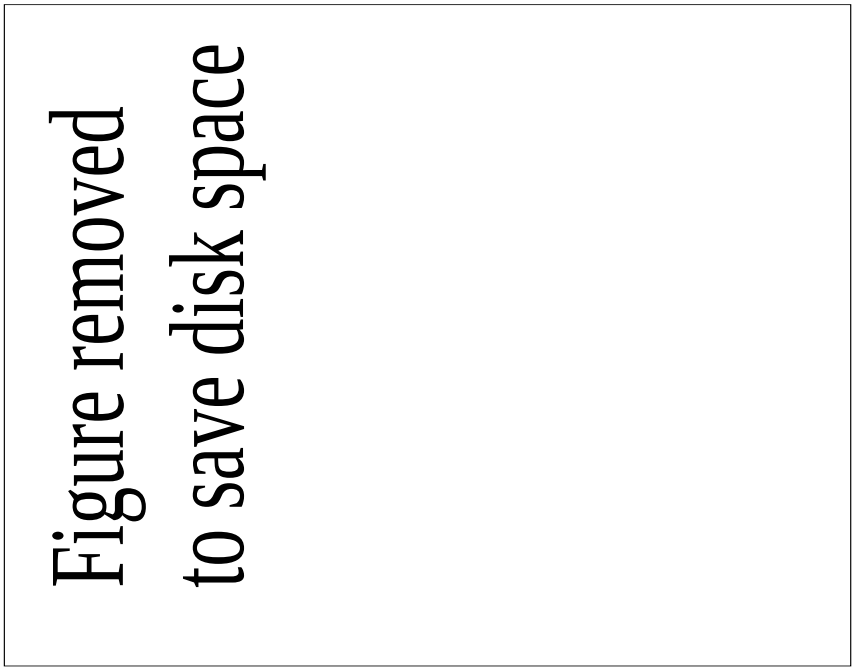

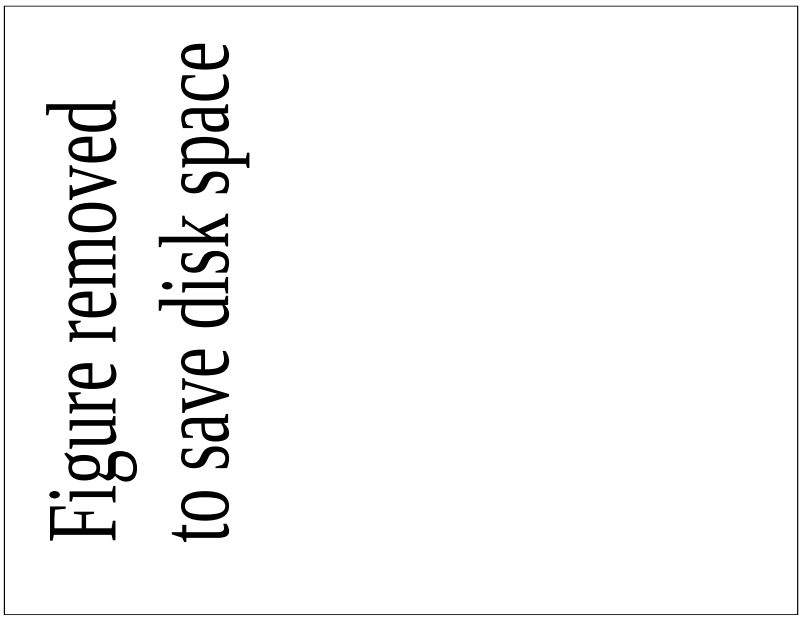

Fig. 5.— The X–ray source density profile of the RCW 38 cluster. Top: For each probable cluster member the distance from the cluster center and the number of cluster sources within 0.25 pc (15″) are plotted. The line is fitted to the data. Bottom: A similar plot for the probable non-members. The bimodal behavior is due to the results being scaled up from 15″ samples.

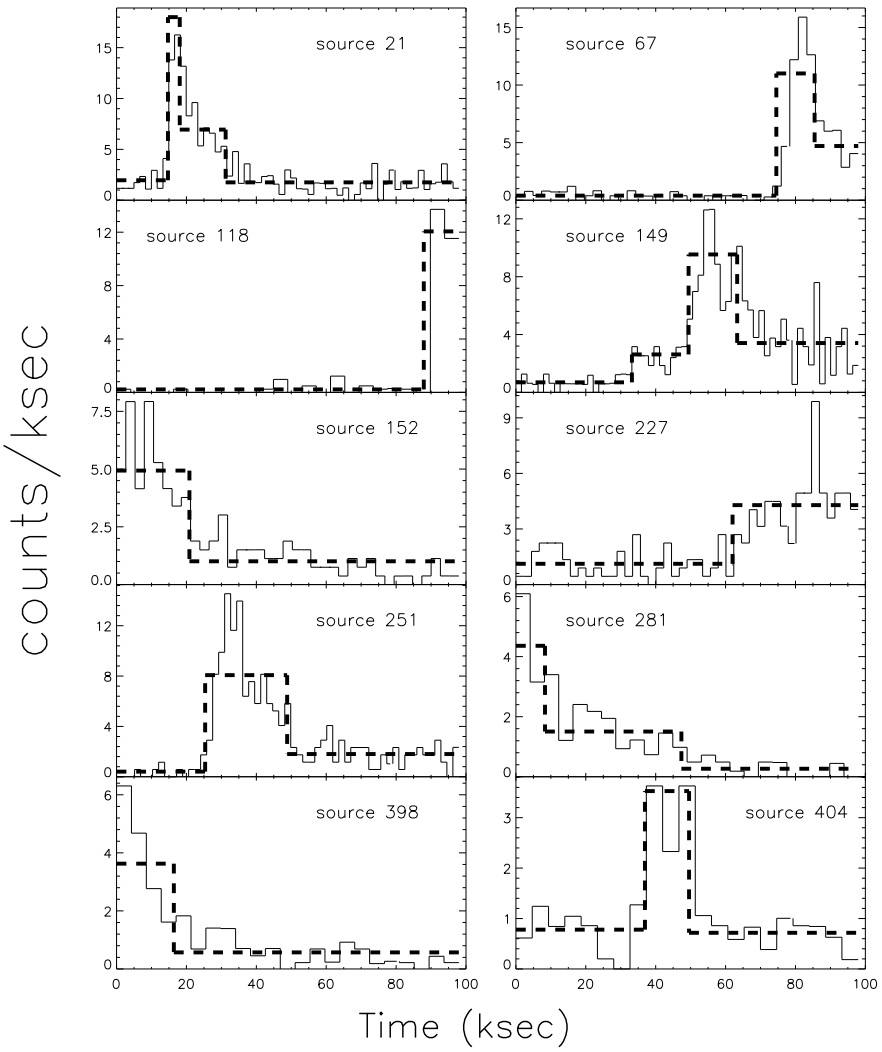

Fig. 6.— Flares on bright stars. The Figures show lightcurves of all sources with over 100 counts and flares (21, 67, 118, 149, 152, 227, 251, 281, 398 and 404). All are cluster members. Sources 149 and 251 are among the hardest X-ray sources, Source 251 is a possible embedded massive star. Source 118 is also deeply embedded (see text). Histogram bins traced with a thin solid line are to guide the eye (Bin sizes were selected to yield an average of 10 counts per bin). Blocks of constant flux (99% confidence according to Bayesian statistics) are traced in by the thick-dashed line.

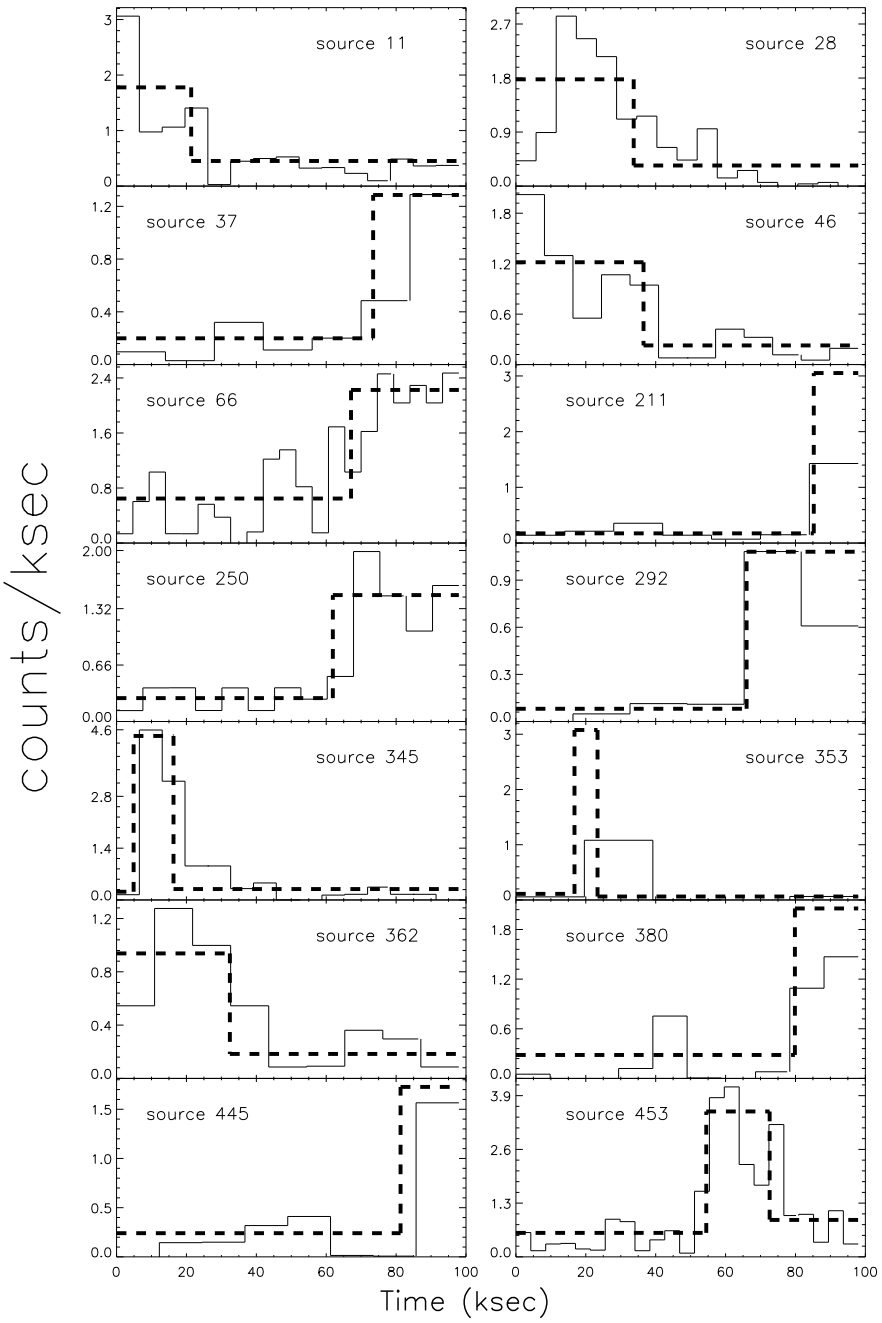

Fig. 7.— Flares on fainter sources. Lightcurves of 14 X-rays sources with flares and < 100 total counts. Sources: 11, 28, 37, 46, 66, 211, 250, 292, 345, 353, 362, 380, 445 and 453.

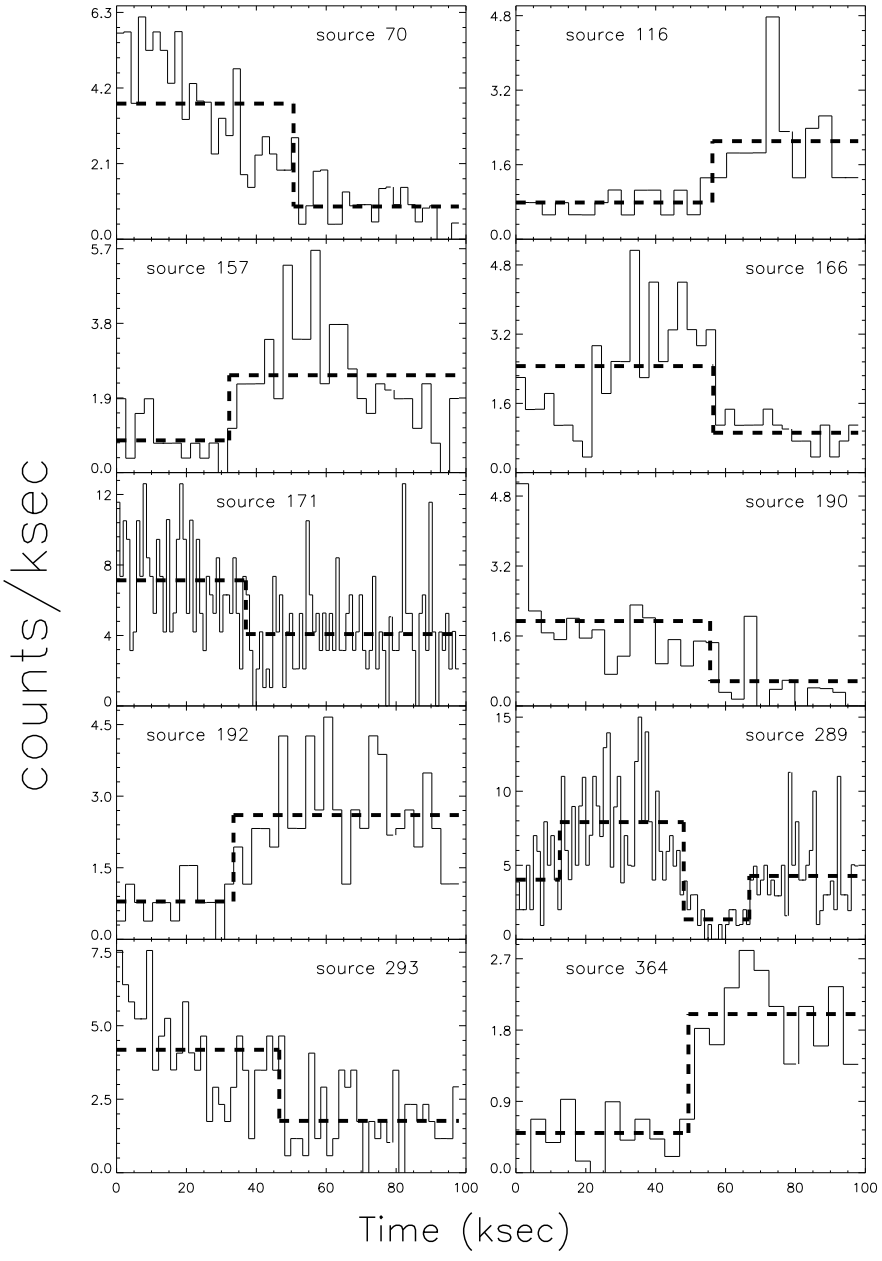

Fig. 8.— Lightcurves of the 10 X-rays sources seen to vary at 99.9% confidence and which did not flare based on the criteria given in Wolk et al. (2005). All of these sources are probable cluster members. Source 289 is the only source in the cluster to show 4 distinct flux levels at 99.9% confidence.

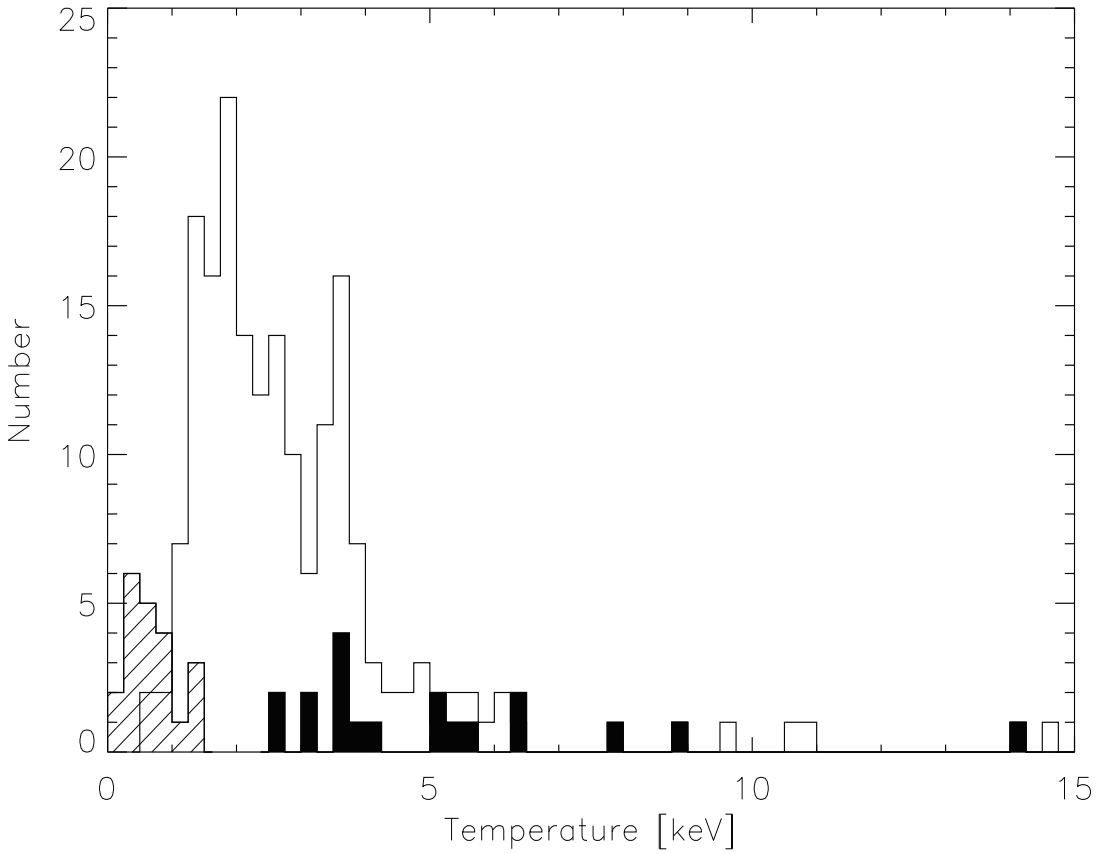

Fig. 9.— Histogram of derived plasma temperatures for each cluster member. Fits for 188 sources fitted with one temperature Raymond–Smith plasma are indicated with the unshaded histogram. The solid-filled histogram represents the high temperature component of the two–temperature fits. The line-filled histogram represents the low temperature component from these fits. The bins are 0.25 keV wide.

Fig. 10.— Top: Histogram of $N_{\rm H}$ derived through spectral fits of the 209 brightest cluster members. While the distribution is peaked at $2.8{\times}10^{22}{\rm cm}^{-2}$ at least two cluster members have an order of magnitude more absorption. Bottom: Histogram of $N_{\rm H}$ for the 157 cluster members with < 30 counts.

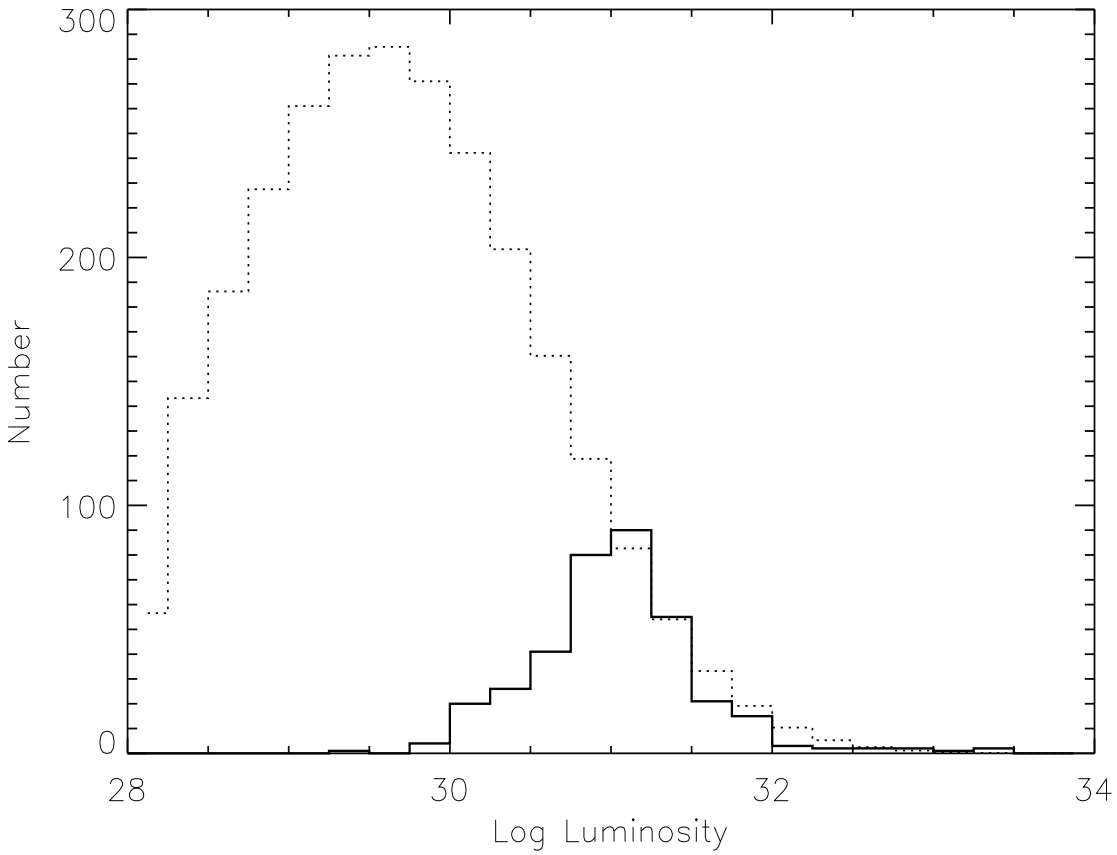

Fig. 11.— Histogram showing the X-ray luminosity distribution in RCW 38. The solid line show the distribution of 365 candidate cluster members with spectral fits. The dotted line is the expected full distribution of X-ray luminosities assuming a log-normal distribution (After Feigelson et al. 2005).

Fig. 12.— Composite J (blue), H (green) and K_s (red) band VLT near-infrared image of RCW 38. The overexposed bright star is the O5 star IRS 2, and the overexposed "X" shaped nebulosity at $\sim$ 08h59m04s –47d30m40s near the center of the image is the IRS 1 ridge (Smith et al. 1999). The grayscale version of this figure is only the K_s band image.

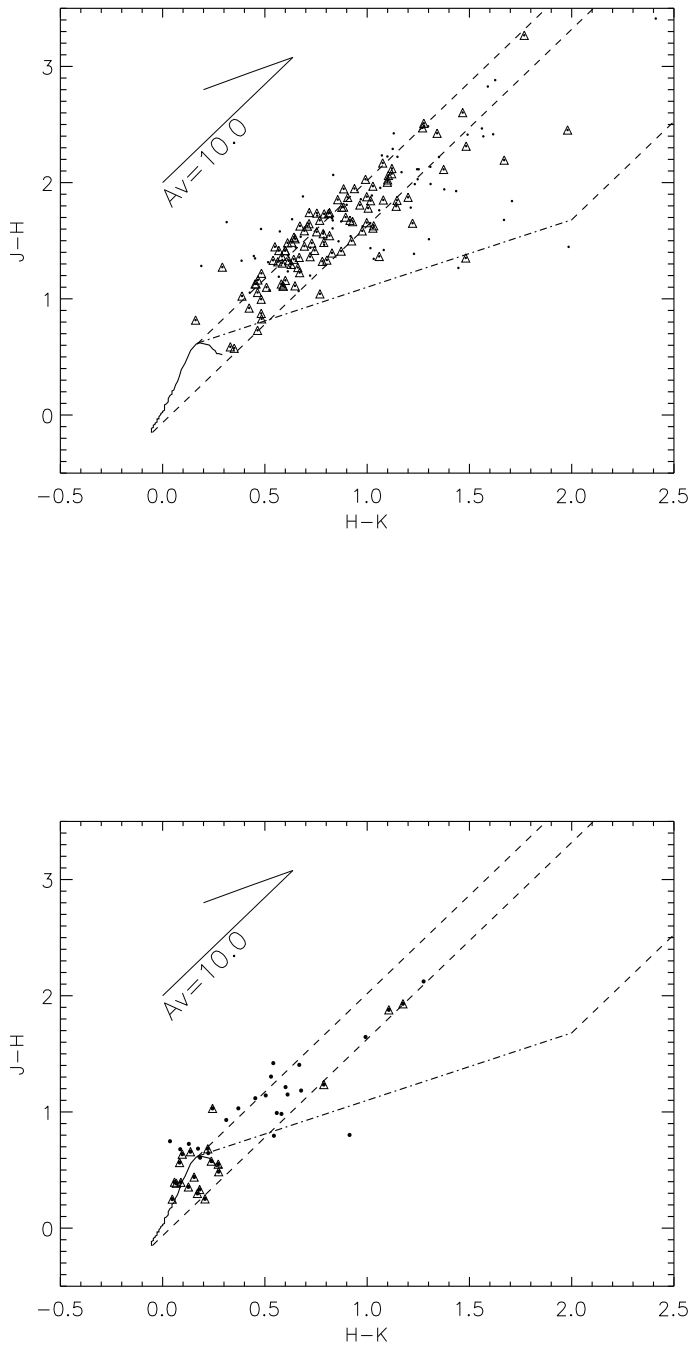

Fig. 13.— Infrared color-color diagrams (J-H vs. H-K) for counterparts to all X–ray sources in the RCW 38 *Chandra* field. The solid line indicates the main sequence, the dashed line running parallel to the reddening vector and the dot-dashed line is the cTTs locus (after Lada & Adams 1990 and Meyer et al. 1997). A reddening vector indicative of $A_V = 10$ is marked. Sources marked as points have errors < 0.2 magnitudes. Sources marked also with triangles have errors of < 0.05

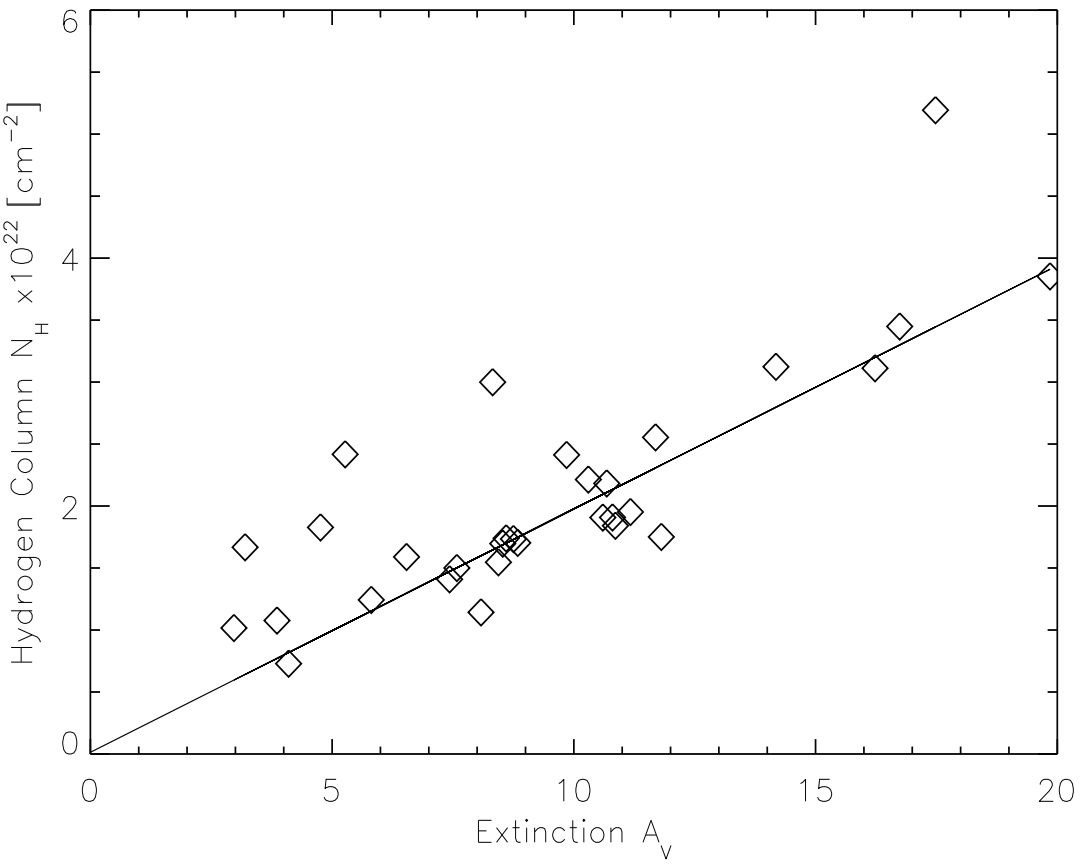

Fig. 14.— Plot of the hydrogen column as derived by X-ray spectral fits versus derived near-IR extinction. The line is the best fit line passing through the origin $N_{\rm H} = {\rm A}_V \times 2.0 \times 10^{21}$ cm^{-2}.

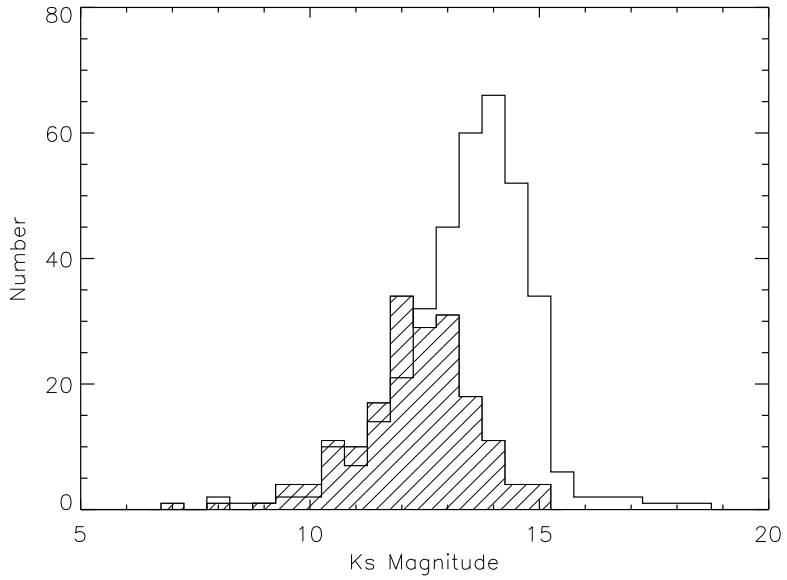

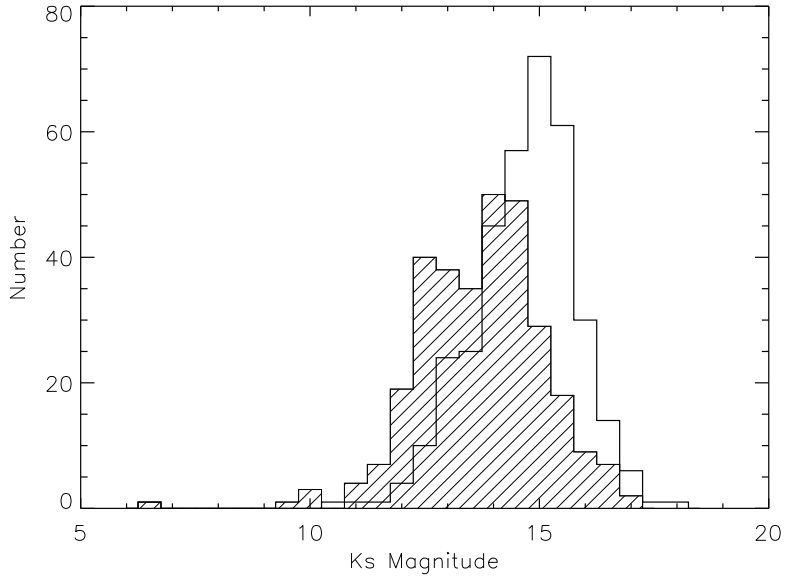

Fig. 15.— Plot of the KLF of the X-ray detected members of RCW 38. Open histogram are data

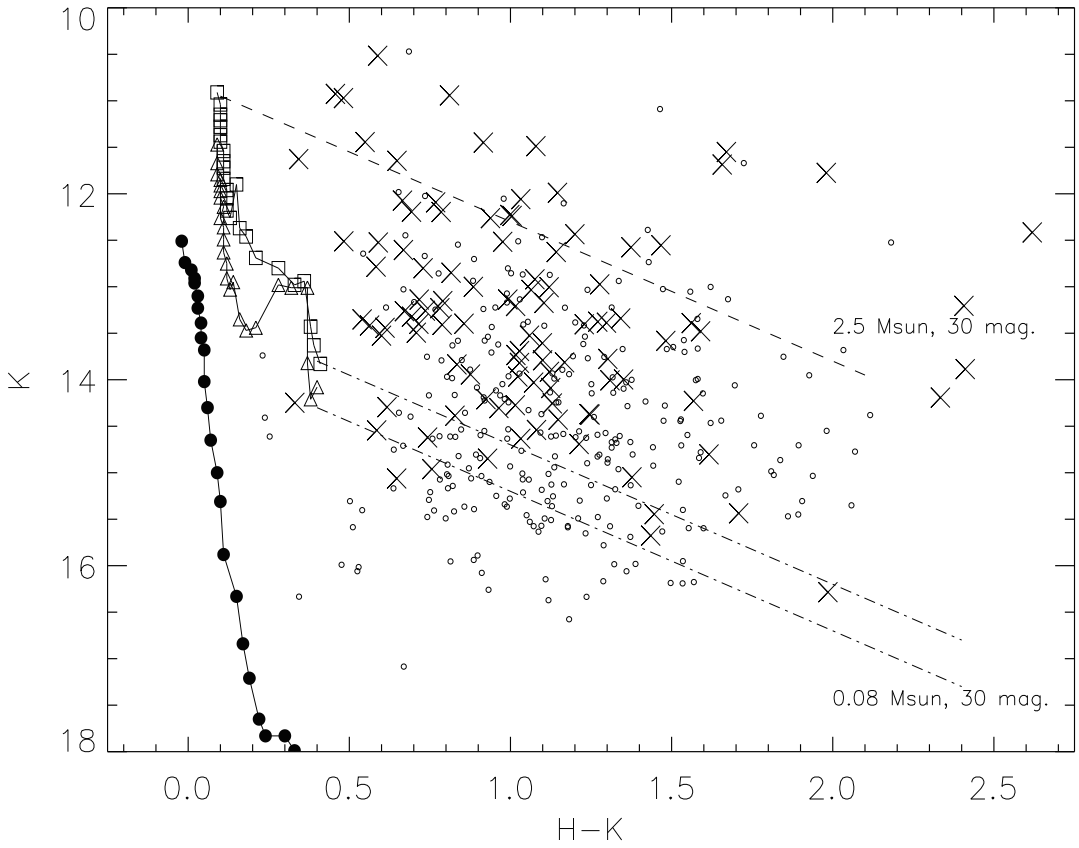

Fig. 16.— Infrared color-magnitude diagram for all sources in the VLT field. X-ray sources are indicated as "X's", non–X–ray sources are indicated with small circles. The 0.5 Myr (open squares) 1.0 Myr (open triangles) and ZAMS (filled circles) isochrones for 2.5 $M_\odot$ to 0.08 $M_\odot$ are plotted (Siess et al. 2000). Extinction of 30 visual magnitudes for a 2.5 $M_\odot$ star is indicated by the dashed lines. The dot dashed lines indicate 30 visual magnitudes for 0.08 $M_\odot$ stars at ages of 0.5 Myr (upper) and 1.0 Myr (lower).

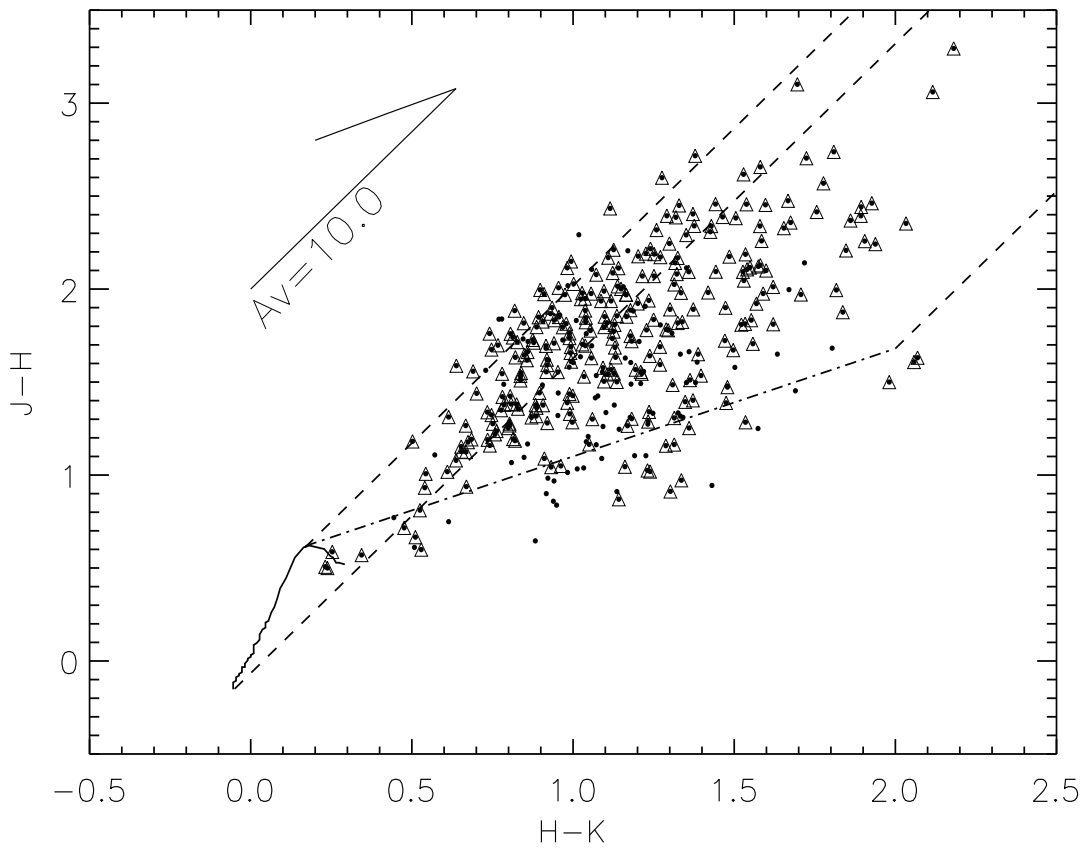

Fig. 17.— Infrared color-color diagram (J-H vs. H-K) for VLT sources without X–ray counterparts in the RCW 38 *Chandra* field. Symbols are the same as Figure 13.

Fig. 18.— Location of the OB star candidates. Left: Location of OB star candidates within $8'$ of the cluster center noted on a 2MASS K-band image. The circle indicates $200''$ from the cluster center. The box indicates the VLT field shown in the figure to the right. Right: Location of OB star candidates within $1.25'$ of the cluster center overlain on the VLT K_s band image. The numbers indicate the X-ray source number, except in the case of the two VLT only sources. To avoid clutter, only the seconds of declination are listed for the VLT sources.

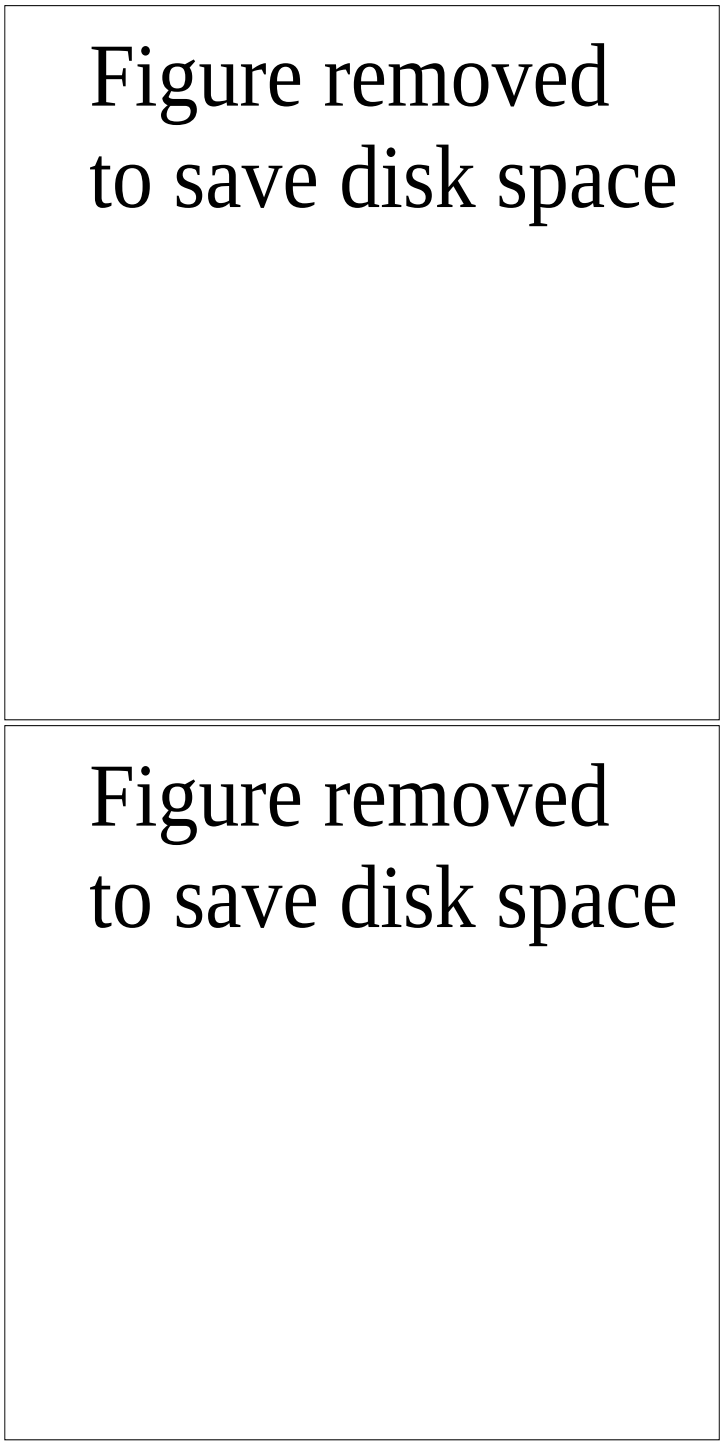

Fig. 19.— X-ray spectra of two cool white dwarf candidates. These spectra are unusual in their lack of flux above 2.5 keV. They have been fitted with blackbodies with temperatures below 150 eV (histogram), consistent with the emission expected from a degenerate star.

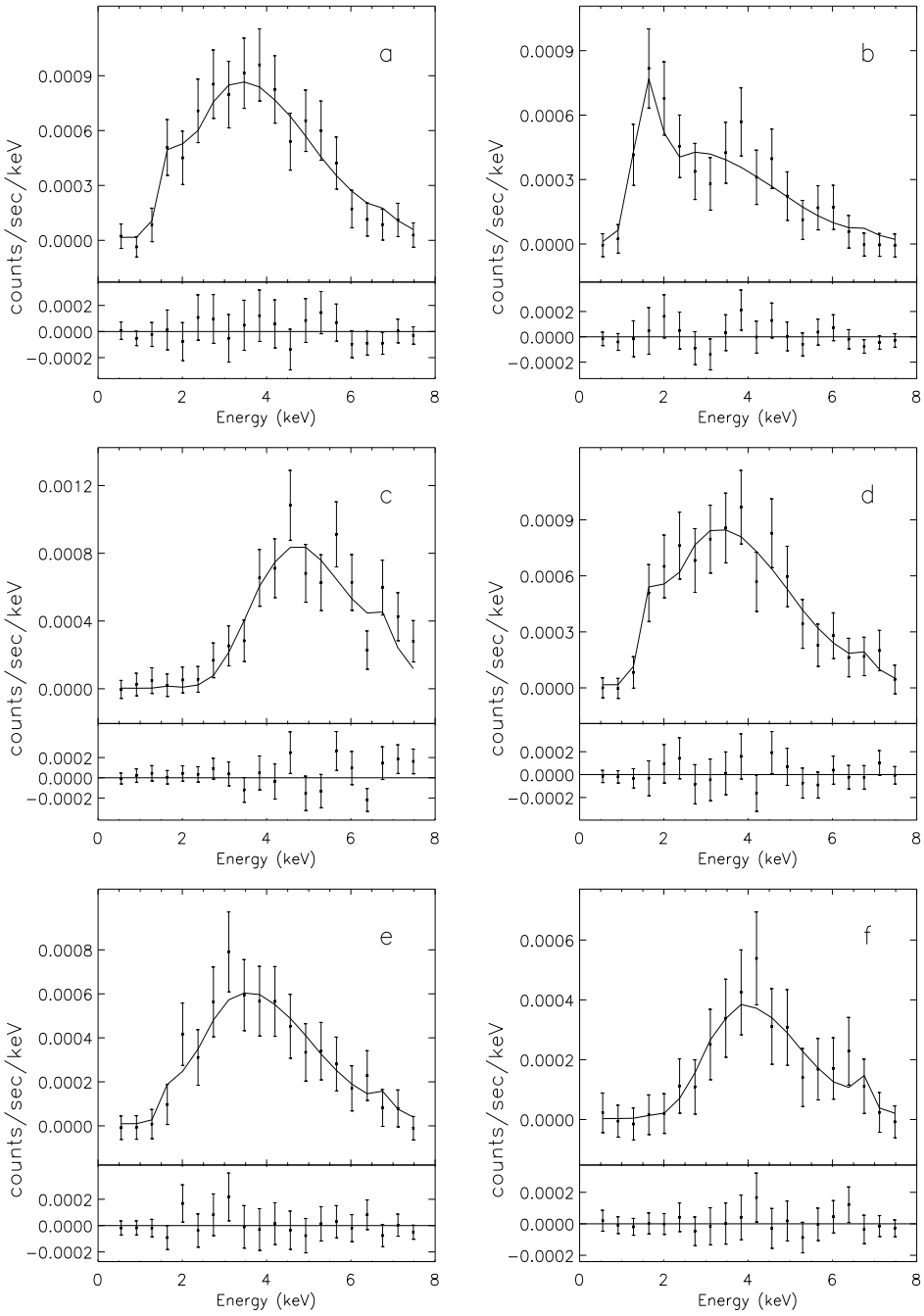

Fig. 20.— Spectra of the hottest, most embedded sources in our sample. Source 56 (a) is fitted with a 14.7 keV thermal plasma with $N_{\rm H}\sim$ 3.9 $\times 10^{22}$ cm^{-2}. Source 147 (b) is fitted with a 11.0 keV thermal plasma with $N_{\rm H}\sim$ 2.7 $\times 10^{22}$ cm^{-2}. Source 251 (c) is fitted with a 10.7 keV thermal plasma with $N_{\rm H}\sim$ 2.3 $\times 10^{23}$ cm^{-2}. Source 149 (d) is fitted with a 9.6 keV thermal plasma with $N_{\rm H}\sim$ 3.8 $\times 10^{22}$ cm^{-2}. Source 108 (e) is fitted with a 8.9 keV thermal plasma with $N_{\rm H}\sim$ 5.37 $\times 10^{22}$ cm^{-2}. Source 118 (f) is fitted with a 3.7 keV thermal plasma but a large $N_{\rm H}> 10^{23}$ cm^{-2}. All sources have a reduced $\chi^2 < 0.6$ except for 251 which has a reduced $\chi^2 \sim 0.95$. Residuals to the fits are shown beneath each fit.

Fig. 21.— Left: Location of the X-ray sources with hot (> 8keV) corona or embedded with a measured column with $N_{\rm H}> 10^{23}\,{\rm cm}^{-2}$, overlaid on a 2MASS K_s band image $8'$ on a side. Right: Close up view of the central $2.5'$. In both figures, the hot (circles) and embedded (squares) sources are co-aligned with the cold dust indicated by the mm data (contours from Vigil et al. in prep.). The thick contour is 60% of the 1.2 mm peak. Source 251 is both hot and embedded.

Table 1. X-ray sources detected in the RCW 38 Field

SRC #	CXOJ	RA (J2000.0)	DEC (J2000.0)	Off-axis angle (″)	Net counts	Baysian Blocks 95% sig.	Baysian Blocks 99% sig.
1	085821.3-473107	8:58:21.26	-47:31:07.2	604.6	54.1	1	1
2	085823.8-473001	8:58:23.77	-47:30:01.8	577.1	38.5	1	1
3	085827.6-473009	8:58:27.59	-47:30:09.2	538.3	68	1	1
4	085829.9-472824	8:58:29.89	-47:28:24.1	526.6	96.6	1	1
5	085830.9-473221	8:58:30.87	-47:32:21.2	520.6	28	1	1
6	085831.5-472808	8:58:31.51	-47:28:08.1	514.3	60.3	1	1
7	085833.1-473152	8:58:33.15	-47:31:52.6	491.8	24.1	1	1
8	085834.6-472816	8:58:34.61	-47:28:16.5	481.8	119.3	2	1
9	085835.1-472902	8:58:35.10	-47:29:02.8	467.6	15.6	1	1
10	085836.1-473135	8:58:36.11	-47:31:35.9	459.2	24.2	1	1
11	085836.4-473250	8:58:36.39	-47:32:50.9	475.5	64.6	2	2
12	085839.6-473126	8:58:39.60	-47:31:26.7	422.7	19.5	1	1
13	085841.6-472835	8:58:41.60	-47:28:35.2	408.4	36.6	1	1
14	085841.9-472627	8:58:41.92	-47:26:27.9	453.5	29.1	1	1
15	085842.5-473040	8:58:42.50	-47:30:40.5	388.0	10.9	1	1
16	085842.6-473155	8:58:42.60	-47:31:55.8	399.3	40.4	1	1
17	085842.7-473015	8:58:42.70	-47:30:15.3	385.1	19.1	1	1
18	085843.4-473250	8:58:43.41	-47:32:50.9	409.1	25.7	1	1
19	085843.5-472934	8:58:43.54	-47:29:34.1	378.7	39.2	1	1
20	085843.8-472645	8:58:43.77	-47:26:45.9	428.4	22.7	1	1
21	085843.9-472857	8:58:43.87	-47:28:57.1	381.1	311.7	4	4
22	085844.1-473440	8:58:44.15	-47:34:40.0	455.9	40.6	1	1
23	085844.4-473253	8:58:44.38	-47:32:53.1	400.9	116.7	1	1
24	085844.6-473406	8:58:44.57	-47:34:06.9	433.8	36.8	1	1
25	085845.7-472932	8:58:45.70	-47:29:32.9	357.1	53.5	2	1
26	085846.7-473035	8:58:46.69	-47:30:35.3	345.3	18.7	1	1
27	085847.2-473151	8:58:47.21	-47:31:51.5	353.1	19.5	1	1
28	085847.5-473324	8:58:47.49	-47:33:24.2	386.5	71.1	2	2
29	085847.7-472939	8:58:47.69	-47:29:39.4	336.3	14.7	1	1
30	085847.8-472816	8:58:47.75	-47:28:16.6	354.0	90.1	1	1
31	085848.6-473221	8:58:48.64	-47:32:21.4	349.0	94.6	1	1

Table 1—Continued

SRC #	CXOJ	RA (J2000.0)	DEC (J2000.0)	Off-axis angle (″)	Net counts	Baysian Blocks 95% sig.	Baysian Blocks 99% sig.
32	085849.1-472916	8:58:49.10	-47:29:16.9	325.3	32.4	1	1
33	085849.1-473410	8:58:49.12	-47:34:10.1	397.6	64.9	1	1
34	085849.2-473115	8:58:49.21	-47:31:15.0	324.9	40	1	1
35	085849.6-473255	8:58:49.59	-47:32:55.3	354.1	43	1	1
36	085849.9-473521	8:58:49.85	-47:35:21.4	438.3	16.4	1	1
37	085850.0-472857	8:58:49.97	-47:28:57.6	320.7	33.5	2	2
38	085850.1-473007	8:58:50.09	-47:30:07.9	310.3	27.4	1	1
39	085850.4-473319	8:58:50.37	-47:33:19.4	358.9	327.1	1	1
40	085850.7-473239	8:58:50.67	-47:32:39.1	337.1	53.3	1	1
41	085850.7-473043	8:58:50.72	-47:30:43.3	305.2	16.1	1	1
42	085851.0-472924	8:58:50.97	-47:29:24.0	305.4	19.9	1	1
43	085851.1-473437	8:58:51.11	-47:34:37.5	399.1	28.2	2	1
44	085851.4-472722	8:58:51.35	-47:27:22.5	343.4	17	1	1
45	085851.6-473108	8:58:51.57	-47:31:08.5	300.1	23.5	1	1
46	085851.8-473126	8:58:51.77	-47:31:26.9	302.1	58	2	2
47	085852.1-473419	8:58:52.08	-47:34:19.9	380.2	20.5	1	1
48	085852.2-472455	8:58:52.24	-47:24:55.7	429.6	25.5	1	1
49	085852.8-473106	8:58:52.83	-47:31:06.3	287.2	9.7	1	1
50	085852.9-473309	8:58:52.93	-47:33:09.0	331.3	46.5	1	1
51	085853.2-473224	8:58:53.18	-47:32:24.2	307.8	13.2	1	1
52	085853.7-473014	8:58:53.72	-47:30:14.3	273.5	16.8	1	1
53	085853.9-473051	8:58:53.92	-47:30:51.3	274.0	728.4	1	1
54	085854.0-472620	8:58:53.97	-47:26:20.2	357.9	34.9	1	1
55	085854.0-473102	8:58:54.02	-47:31:02.2	274.7	42.1	1	1
56	085854.2-472841	8:58:54.25	-47:28:41.7	283.5	328.9	1	1
57	085854.3-472949	8:58:54.26	-47:29:49.6	269.1	161.9	2	1
58	085854.5-472550	8:58:54.46	-47:25:50.7	374.2	10.9	1	1
59	085854.5-472429	8:58:54.49	-47:24:29.6	435.0	111.4	1	1
60	085854.5-473200	8:58:54.46	-47:32:00.1	286.3	13.6	1	1
61	085854.8-473358	8:58:54.75	-47:33:58.0	345.4	26.2	1	1
62	085854.8-473433	8:58:54.84	-47:34:33.6	368.9	100.7	1	1

Table 1—Continued

SRC #	CXOJ	RA (J2000.0)	DEC (J2000.0)	Off-axis angle (″)	Net counts	Baysian Blocks 95% sig.	Baysian Blocks 99% sig.
63	085854.9-472658	8:58:54.94	-47:26:58.6	326.1	20.6	1	1
64	085855.0-472502	8:58:55.05	-47:25:02.0	406.1	37.6	1	1
65	085855.0-473138	8:58:55.04	-47:31:38.2	273.3	21.7	1	1
66	085855.1-473500	8:58:55.11	-47:35:00.0	386.1	110.7	2	2
67	085855.2-473149	8:58:55.24	-47:31:49.4	275.1	212.4	4	3
68	085855.2-473120	8:58:55.25	-47:31:20.5	266.3	16	1	1
69	085855.3-473156	8:58:55.26	-47:31:56.8	277.6	201.3	1	1
70	085855.5-473024	8:58:55.49	-47:30:24.1	255.7	251.1	2	2
71	085855.6-472744	8:58:55.60	-47:27:44.7	295.0	33.1	1	1
72	085855.8-473251	8:58:55.81	-47:32:51.1	297.2	115.8	1	1
73	085855.9-473150	8:58:55.91	-47:31:50.0	268.9	32.6	1	1
74	085856.1-473521	8:58:56.10	-47:35:21.0	395.5	26.5	1	1
75	085856.5-473223	8:58:56.46	-47:32:23.4	277.7	11.9	1	1
76	085857.0-473228	8:58:57.04	-47:32:28.5	274.9	26.4	1	1
77	085857.1-473237	8:58:57.14	-47:32:37.8	278.7	21.8	1	1
78	085857.2-473106	8:58:57.22	-47:31:06.3	243.6	60.8	1	1
79	085857.4-472729	8:58:57.36	-47:27:29.5	288.1	8.6	1	1
80	085857.5-472426	8:58:57.50	-47:24:26.7	419.4	44.6	1	1
81	085857.5-472743	8:58:57.51	-47:27:43.6	279.0	18.8	1	1
82	085857.7-472918	8:58:57.73	-47:29:18.9	239.2	43.2	1	1
83	085857.8-472359	8:58:57.78	-47:23:59.2	440.9	23.4	1	1
84	085857.9-473243	8:58:57.88	-47:32:43.7	275.5	23.5	1	1
85	085857.9-473019	8:58:57.88	-47:30:19.3	231.3	29.5	1	1
86	085857.9-473031	8:58:57.94	-47:30:31.3	231.3	34.6	1	1
87	085858.0-472733	8:58:57.97	-47:27:33.2	281.0	19.6	1	1
88	085857.9-473013	8:58:57.91	-47:30:13.3	231.0	24.3	1	1
89	085858.0-473122	8:58:57.96	-47:31:22.4	240.4	23.1	1	1
90	085858.1-473144	8:58:58.13	-47:31:44.9	246.1	24.1	1	1
91	085858.2-473106	8:58:58.17	-47:31:06.5	234.3	24.2	1	1
92	085858.3-473257	8:58:58.30	-47:32:57.8	279.9	56.1	1	1
93	085858.3-472727	8:58:58.34	-47:27:27.4	281.2	54	1	1

Table 1—Continued

SRC #	CXOJ	RA (J2000.0)	DEC (J2000.0)	Off-axis angle (″)	Net counts	Baysian Blocks 95% sig.	Baysian Blocks 99% sig.
94	085858.5-473059	8:58:58.53	-47:30:59.0	229.2	174.9	1	1
96	085858.6-473016	8:58:58.62	-47:30:16.6	223.8	12.1	1	1
97	085858.6-473110	8:58:58.62	-47:31:10.9	230.9	145	3	1
98	085858.7-473105	8:58:58.73	-47:31:05.6	228.6	77	1	1
99	085858.8-473144	8:58:58.79	-47:31:44.1	239.7	20.4	1	1
100	085858.9-472725	8:58:58.86	-47:27:25.0	278.5	18.9	1	1
101	085858.9-473054	8:58:58.91	-47:30:54.4	224.5	123.1	1	1
102	085858.9-473344	8:58:58.93	-47:33:44.2	304.7	7.3	1	1
103	085859.1-473034	8:58:59.10	-47:30:34.0	219.8	39.1	1	1
104	085859.1-472809	8:58:59.12	-47:28:09.1	251.9	150.5	1	1
105	085859.1-473216	8:58:59.11	-47:32:16.9	250.9	16.8	1	1
106	085859.2-473232	8:58:59.16	-47:32:32.7	258.6	30.2	1	1
107	085859.2-472657	8:58:59.20	-47:26:57.9	293.1	58.6	1	1
108	085859.4-473237	8:58:59.43	-47:32:37.5	258.9	221.3	1	1
109	085859.5-473111	8:58:59.46	-47:31:11.3	222.8	31	1	1
110	085859.5-472952	8:58:59.53	-47:29:52.1	215.6	37.3	1	1
111	085859.7-473228	8:58:59.69	-47:32:28.6	251.9	20.9	1	1
112	085859.8-473223	8:58:59.79	-47:32:23.5	248.4	45	1	1
113	085859.9-472245	8:58:59.90	-47:22:45.1	495.9	43.5	1	1
114	085859.9-473014	8:58:59.89	-47:30:14.5	210.9	40.5	1	1
115	085859.9-473551	8:58:59.87	-47:35:51.6	398.2	39.5	1	1
116	085860.0-472947	8:58:59.95	-47:29:47.4	212.0	130.6	2	2
117	085860.0-473104	8:58:59.98	-47:31:04.1	215.9	30.2	1	1
118	085900.0-473109	8:59:00.01	-47:31:09.5	216.9	124.9	3	2
119	085900.1-473040	8:59:00.08	-47:30:40.5	210.7	15.7	1	1
120	085900.1-473007	8:59:00.10	-47:30:07.0	208.9	62.6	1	1
121	085900.1-473219	8:59:00.12	-47:32:19.2	243.3	28.6	1	1
122	085900.1-473311	8:59:00.15	-47:33:11.3	273.5	41.8	1	1
123	085900.2-473200	8:59:00.20	-47:32:00.6	233.5	15.9	1	1
124	085900.3-472758	8:59:00.28	-47:27:58.2	247.5	12.3	1	1
125	085900.3-473114	8:59:00.33	-47:31:14.3	215.1	144.8	1	1

Table 1—Continued

SRC #	CXOJ	RA (J2000.0)	DEC (J2000.0)	Off-axis angle (″)	Net counts	Baysian Blocks 95% sig.	Baysian Blocks 99% sig.
126	085900.3-472940	8:59:00.35	-47:29:40.3	209.0	59.5	1	1
127	085900.4-472558	8:59:00.39	-47:25:58.3	328.2	108.1	1	1
128	085900.7-472724	8:59:00.68	-47:27:24.3	264.5	16.3	1	1
129	085900.7-473051	8:59:00.71	-47:30:51.4	206.0	200.2	1	1
130	085900.8-473046	8:59:00.76	-47:30:46.8	204.7	285	2	1
131	085900.9-472942	8:59:00.90	-47:29:42.3	203.2	28.4	1	1
132	085900.9-472819	8:59:00.92	-47:28:19.0	231.1	36.6	1	1
133	085901.0-473103	8:59:01.00	-47:31:03.4	205.7	104.4	2	1
134	085901.1-473008	8:59:01.12	-47:30:08.7	198.5	22.2	1	1
135	085901.1-473242	8:59:01.13	-47:32:42.2	247.6	19	1	1
136	085901.2-473132	8:59:01.22	-47:31:32.0	212.3	23	1	1
137	085901.4-473049	8:59:01.37	-47:30:49.0	199.0	23.3	1	1
138	085901.4-472325	8:59:01.45	-47:23:25.2	453.0	69	1	1
139	085901.5-472831	8:59:01.53	-47:28:31.4	219.7	15.9	1	1
140	085901.6-473110	8:59:01.56	-47:31:10.2	201.9	236.7	1	1
141	085901.6-473119	8:59:01.57	-47:31:19.5	204.7	127.3	1	1
142	085901.6-473210	8:59:01.64	-47:32:10.9	225.8	20.7	1	1
143	085901.6-473037	8:59:01.64	-47:30:37.5	194.6	117.1	1	1
144	085901.8-473046	8:59:01.75	-47:30:46.0	194.7	90	1	1
145	085901.9-473057	8:59:01.88	-47:30:57.0	195.6	170.2	1	1
146	085902.0-473034	8:59:01.99	-47:30:34.8	190.7	42.2	1	1
147	085901.9-473115	8:59:01.95	-47:31:15.0	199.6	199.3	1	1
148	085902.0-473102	8:59:01.99	-47:31:02.5	195.8	205.6	1	1
149	085902.1-473209	8:59:02.09	-47:32:09.6	221.2	321.3	4	4
150	085902.2-472640	8:59:02.16	-47:26:40.2	284.6	24.4	1	1
151	085902.2-473016	8:59:02.17	-47:30:16.6	187.8	1147.4	1	1
152	085902.4-472957	8:59:02.39	-47:29:57.7	186.3	191.2	3	2
153	085902.4-473110	8:59:02.42	-47:31:10.1	193.6	30.6	1	1
154	085902.4-472947	8:59:02.43	-47:29:47.7	187.0	37	1	1
155	085902.5-473052	8:59:02.46	-47:30:52.8	188.9	119.3	2	1
156	085902.5-473020	8:59:02.51	-47:30:20.6	184.5	28.7	1	1

Table 1—Continued

SRC #	CXOJ	RA (J2000.0)	DEC (J2000.0)	Off-axis angle (″)	Net counts	Baysian Blocks 95% sig.	Baysian Blocks 99% sig.
157	085902.5-473147	8:59:02.54	-47:31:47.5	206.4	189.8	3	2
158	085902.6-473046	8:59:02.56	-47:30:46.5	186.7	95.4	1	1
159	085902.6-472846	8:59:02.60	-47:28:46.3	203.3	44.9	1	1
160	085902.7-473137	8:59:02.70	-47:31:37.5	200.7	93	1	1
161	085902.9-473102	8:59:02.91	-47:31:02.2	186.6	24.5	1	1
162	085903.0-473040	8:59:02.96	-47:30:40.0	181.6	50.9	1	1
163	085903.0-473035	8:59:03.03	-47:30:35.6	180.4	59	1	1
164	085903.0-473044	8:59:02.98	-47:30:44.4	182.2	89.8	1	1
165	085903.0-473051	8:59:03.03	-47:30:51.8	183.0	48.5	1	1
166	085903.1-472937	8:59:03.08	-47:29:37.3	182.4	184	3	2
167	085903.1-473008	8:59:03.12	-47:30:08.7	178.3	17.4	1	1
168	085903.3-472853	8:59:03.34	-47:28:53.4	193.5	33.3	1	1
169	085903.4-473045	8:59:03.37	-47:30:45.6	178.5	166.3	1	1
170	085903.4-472428	8:59:03.44	-47:24:28.1	387.5	46.9	1	1
171	085903.5-473058	8:59:03.53	-47:30:58.3	179.6	535.1	2	2
172	085903.6-473032	8:59:03.58	-47:30:32.2	174.5	109.1	1	1
173	085903.6-473149	8:59:03.60	-47:31:49.7	198.0	59.7	1	1
174	085903.7-473040	8:59:03.67	-47:30:40.1	174.6	538.3	2	1
175	085903.7-472759	8:59:03.74	-47:27:59.8	218.0	35.4	1	1
176	085903.8-473142	8:59:03.76	-47:31:42.5	193.1	31.7	1	1
177	085903.8-472457	8:59:03.81	-47:24:57.3	360.0	70.5	1	1
178	085903.8-473004	8:59:03.82	-47:30:04.2	171.3	27.9	1	1
179	085903.8-473048	8:59:03.82	-47:30:48.3	174.5	112.2	1	1
180	085903.8-473100	8:59:03.83	-47:31:00.8	177.3	22.6	1	1
181	085903.8-473109	8:59:03.83	-47:31:09.4	179.7	84	1	1
182	085903.9-472954	8:59:03.88	-47:29:54.8	171.6	20.6	1	1
183	085903.9-473104	8:59:03.91	-47:31:04.8	177.6	77.8	1	1
184	085904.0-473121	8:59:03.98	-47:31:21.8	182.6	39.2	1	1
185	085904.0-473055	8:59:04.03	-47:30:55.8	174.1	52.2	1	1
186	085904.0-473052	8:59:04.04	-47:30:52.9	173.3	19.6	1	1
187	085904.0-473034	8:59:04.05	-47:30:34.6	170.0	19.6	1	1

Table 1—Continued

SRC #	CXOJ	RA (J2000.0)	DEC (J2000.0)	Off-axis angle (″)	Net counts	Baysian Blocks 95% sig.	Baysian Blocks 99% sig.
188	085904.1-472734	8:59:04.11	-47:27:34.9	231.5	20.8	1	1
189	085904.2-473112	8:59:04.15	-47:31:12.7	177.7	40.3	1	1
190	085904.2-472322	8:59:04.21	-47:23:22.0	444.6	121.4	2	2
191	085904.3-473046	8:59:04.31	-47:30:46.4	169.3	25.8	1	1
192	085904.3-473105	8:59:04.34	-47:31:05.7	173.7	194.5	2	2
193	085904.3-473131	8:59:04.35	-47:31:31.0	182.8	17.3	1	1
194	085904.5-473056	8:59:04.45	-47:30:56.2	170.1	237.3	1	1
195	085904.5-473120	8:59:04.46	-47:31:20.4	177.5	13.2	1	1
196	085904.5-473038	8:59:04.46	-47:30:38.4	166.4	24.1	1	1
197	085904.6-473050	8:59:04.60	-47:30:50.8	167.3	318.6	1	1
198	085904.6-473027	8:59:04.61	-47:30:27.8	163.7	69.9	1	1
199	085904.7-472833	8:59:04.73	-47:28:33.1	190.7	9.7	1	1
200	085904.7-473036	8:59:04.72	-47:30:36.8	163.6	102.4	1	1
201	085904.8-473031	8:59:04.83	-47:30:31.4	161.8	39.4	1	1
202	085904.9-473054	8:59:04.86	-47:30:54.8	165.7	74.9	1	1
203	085904.9-473241	8:59:04.91	-47:32:41.3	217.5	37	1	1
204	085905.0-473126	8:59:05.01	-47:31:26.5	174.8	28.9	1	1
205	085905.0-473058	8:59:05.03	-47:30:58.1	164.9	162.2	1	1
206	085905.1-473307	8:59:05.06	-47:33:07.6	235.1	16.9	1	1
207	085905.1-473047	8:59:05.08	-47:30:47.3	161.8	183.2	1	1
208	085905.1-473053	8:59:05.09	-47:30:53.3	163.0	22.9	1	1
209	085905.2-473101	8:59:05.16	-47:31:01.3	164.5	81	1	1
210	085905.2-472953	8:59:05.16	-47:29:53.2	158.9	41.8	2	1
211	085905.2-473029	8:59:05.21	-47:30:29.3	157.8	42.4	2	2
212	085905.2-473016	8:59:05.24	-47:30:16.9	156.8	51.3	1	1
213	085905.3-473032	8:59:05.28	-47:30:32.8	157.4	82	1	1
214	085905.3-473042	8:59:05.30	-47:30:42.5	158.7	306.8	1	1
215	085905.4-473059	8:59:05.42	-47:30:59.0	161.3	35.5	1	1
216	085905.4-473203	8:59:05.37	-47:32:03.4	190.0	13	1	1
217	085905.4-473002	8:59:05.41	-47:30:02.9	155.4	83.8	1	1
218	085905.4-473048	8:59:05.43	-47:30:48.2	158.5	154.9	1	1

Table 1—Continued

SRC #	CXOJ	RA (J2000.0)	DEC (J2000.0)	Off-axis angle (″)	Net counts	Baysian Blocks 95% sig.	Baysian Blocks 99% sig.
219	085905.4-473030	8:59:05.44	-47:30:30.1	155.5	223.6	1	1
220	085905.5-473035	8:59:05.55	-47:30:35.8	155.1	1023	2	1
221	085905.7-473040	8:59:05.66	-47:30:40.9	154.8	6495.3	4	3
222	085905.7-472909	8:59:05.68	-47:29:09.5	165.3	12.5	1	1
223	085905.7-473046	8:59:05.70	-47:30:46.6	155.5	356	1	1
224	085905.8-473050	8:59:05.76	-47:30:50.4	155.8	36.6	1	1
225	085905.8-473009	8:59:05.77	-47:30:09.0	151.5	421	1	1
226	085905.8-473030	8:59:05.85	-47:30:30.4	151.4	282.3	1	1
227	085905.9-473036	8:59:05.87	-47:30:36.6	152.0	230.5	2	2
229	085905.9-473042	8:59:05.94	-47:30:42.7	152.3	163	1	1
230	085906.0-473054	8:59:05.97	-47:30:54.9	154.8	53.4	1	1
231	085906.0-473151	8:59:05.98	-47:31:51.3	178.1	28.8	1	1
232	085906.0-473151	8:59:05.98	-47:31:51.5	178.2	28.6	1	1
233	085906.0-473519	8:59:05.97	-47:35:19.4	340.0	145.4	1	1
234	085906.0-473134	8:59:06.05	-47:31:34.1	168.8	18.6	1	1
235	085906.1-473021	8:59:06.07	-47:30:21.0	148.4	28.4	1	1
236	085906.1-473101	8:59:06.12	-47:31:01.2	155.2	59.7	1	1
237	085906.1-473433	8:59:06.13	-47:34:33.9	299.0	13.6	1	1
238	085906.2-473035	8:59:06.16	-47:30:35.3	149.0	357.1	2	1
239	085906.2-473044	8:59:06.20	-47:30:44.4	150.0	52.5	1	1
240	085906.2-473051	8:59:06.21	-47:30:51.3	151.6	47.2	1	1
241	085906.2-472958	8:59:06.24	-47:29:58.7	147.4	35.7	1	1
242	085906.3-472530	8:59:06.27	-47:25:30.8	318.6	30.9	1	1
243	085906.3-473025	8:59:06.30	-47:30:25.9	146.5	209.5	1	1
244	085906.4-472910	8:59:06.38	-47:29:10.0	158.6	61.8	1	1
245	085906.4-473031	8:59:06.41	-47:30:31.0	145.9	33.6	1	1
246	085906.4-473037	8:59:06.44	-47:30:37.4	146.4	137.3	1	1
247	085906.5-473126	8:59:06.52	-47:31:26.3	160.9	29.2	1	1
248	085906.5-473115	8:59:06.55	-47:31:15.9	156.2	30.3	1	1
249	085906.6-473100	8:59:06.61	-47:31:00.1	150.1	82.8	2	1
250	085906.6-473018	8:59:06.64	-47:30:18.2	142.6	66.1	2	2

Table 1—Continued

SRC #	CXOJ	RA (J2000.0)	DEC (J2000.0)	Off-axis angle (″)	Net counts	Baysian Blocks 95% sig.	Baysian Blocks 99% sig.
251	085906.6-473021	8:59:06.64	-47:30:21.9	142.7	289.1	4	3
252	085906.7-472957	8:59:06.74	-47:29:57.7	142.4	44.1	1	1
253	085906.8-472941	8:59:06.82	-47:29:41.4	144.4	84.2	1	1
254	085906.8-473616	8:59:06.79	-47:36:16.8	389.3	11.2	1	1
255	085906.9-473102	8:59:06.92	-47:31:02.3	147.8	214.7	1	1
256	085907.0-473032	8:59:06.99	-47:30:32.5	140.2	14.8	1	1
257	085907.0-473137	8:59:07.02	-47:31:37.6	162.0	11.4	1	1
258	085907.0-473054	8:59:07.04	-47:30:54.3	144.3	20	1	1
259	085907.2-472957	8:59:07.19	-47:29:57.8	137.9	47.3	1	1
260	085907.3-472336	8:59:07.26	-47:23:36.1	420.5	39.3	1	1
261	085907.1-473118	8:59:07.11	-47:31:18.3	152.0	103.7	1	1
262	085907.4-473135	8:59:07.36	-47:31:35.9	158.1	25.1	1	1
263	085907.4-473305	8:59:07.37	-47:33:05.2	218.2	271.9	1	1
264	085907.4-473046	8:59:07.39	-47:30:46.2	138.7	40	1	1
265	085907.5-472916	8:59:07.46	-47:29:16.0	146.1	43.8	1	1
266	085907.5-473117	8:59:07.55	-47:31:17.3	147.6	32.5	1	1
267	085907.7-473044	8:59:07.74	-47:30:44.7	134.9	22.2	1	1
268	085907.8-472633	8:59:07.78	-47:26:33.5	256.4	12.2	1	1
269	085907.8-473111	8:59:07.82	-47:31:11.8	142.8	22.1	1	1
270	085907.9-473136	8:59:07.86	-47:31:36.9	154.3	10.5	1	1
271	085907.9-473100	8:59:07.92	-47:31:00.6	137.7	133.2	1	1
272	085908.0-473025	8:59:07.98	-47:30:25.7	129.5	78.2	1	1
273	085908.0-473122	8:59:07.99	-47:31:22.4	145.9	20	1	1
274	085908.1-473038	8:59:08.06	-47:30:38.6	130.5	75	1	1
275	085908.0-473050	8:59:08.01	-47:30:50.3	133.7	20.2	1	1
276	085908.1-473047	8:59:08.09	-47:30:47.4	132.1	87.6	1	1
277	085908.1-472407	8:59:08.13	-47:24:07.2	388.2	41.9	1	1
278	085908.2-472932	8:59:08.24	-47:29:32.0	133.1	7	1	1
279	085908.2-473051	8:59:08.24	-47:30:51.9	131.9	17.7	1	1
280	085908.3-473516	8:59:08.30	-47:35:16.3	327.5	30.2	1	1
281	085908.4-472954	8:59:08.40	-47:29:54.7	126.2	123.4	3	3

Table 1—Continued

SRC #	CXOJ	RA (J2000.0)	DEC (J2000.0)	Off-axis angle (″)	Net counts	Baysian Blocks 95% sig.	Baysian Blocks 99% sig.
282	085908.6-473049	8:59:08.57	-47:30:49.6	128.1	81.3	1	1
283	085908.7-473059	8:59:08.72	-47:30:59.6	129.8	19.2	1	1
284	085908.8-473026	8:59:08.76	-47:30:26.8	121.8	86.7	3	1
285	085908.8-473037	8:59:08.78	-47:30:37.0	123.0	300.3	1	1
286	085908.8-473637	8:59:08.81	-47:36:37.3	401.8	41.5	1	1
287	085909.1-473041	8:59:09.05	-47:30:41.3	121.2	41.4	1	1
288	085909.1-472916	8:59:09.10	-47:29:16.7	130.7	27	1	1
289	085909.2-473405	8:59:09.15	-47:34:05.1	259.2	517.4	4	4
290	085909.3-472919	8:59:09.31	-47:29:19.1	127.8	26.8	1	1
291	085909.5-473019	8:59:09.46	-47:30:19.9	114.1	19.4	1	1
292	085909.5-473118	8:59:09.53	-47:31:18.1	130.1	28.4	2	2
293	085909.6-473025	8:59:09.63	-47:30:25.4	112.8	302	2	2
294	085909.7-472845	8:59:09.70	-47:28:45.3	142.4	17.7	1	1
295	085909.7-473130	8:59:09.74	-47:31:30.3	134.8	14.3	1	1
296	085909.8-472438	8:59:09.80	-47:24:38.4	353.3	28.7	1	1
297	085910.0-473027	8:59:09.96	-47:30:27.7	109.8	33.1	2	1
298	085910.0-472940	8:59:10.00	-47:29:40.9	113.4	21.7	1	1
299	085910.3-473108	8:59:10.28	-47:31:08.0	118.7	17.8	1	1
300	085910.5-472349	8:59:10.52	-47:23:49.6	397.9	27.9	1	1
301	085911.1-473123	8:59:11.10	-47:31:23.5	119.7	8.5	1	1
302	085911.6-473016	8:59:11.60	-47:30:16.0	92.3	22.3	1	1
303	085911.9-472943	8:59:11.88	-47:29:43.5	94.5	19.6	1	1
304	085912.7-473055	8:59:12.67	-47:30:55.0	91.2	10.1	1	1
305	085912.7-472960	8:59:12.74	-47:29:60.0	81.9	29.9	1	1
306	085913.0-473521	8:59:13.04	-47:35:21.5	317.3	10.7	1	1
307	085913.4-472933	8:59:13.40	-47:29:33.1	84.5	28.1	1	1
308	085913.4-472917	8:59:13.40	-47:29:17.2	93.2	7.2	1	1
309	085913.5-473247	8:59:13.48	-47:32:47.6	170.3	16	1	1
310	085913.7-472318	8:59:13.73	-47:23:18.1	421.7	26.6	1	1
311	085914.0-472856	8:59:14.01	-47:28:56.6	102.8	11.9	1	1
312	085914.1-473611	8:59:14.11	-47:36:11.1	363.4	11.7	1	1

Table 1—Continued

SRC #	CXOJ	RA (J2000.0)	DEC (J2000.0)	Off-axis angle (″)	Net counts	Baysian Blocks 95% sig.	Baysian Blocks 99% sig.
313	085914.3-473345	8:59:14.30	-47:33:45.0	220.9	16.1	1	1
314	085914.3-472944	8:59:14.33	-47:29:44.6	70.9	15.4	1	1
315	085914.4-472421	8:59:14.41	-47:24:21.0	358.6	23.3	2	1
316	085914.4-473050	8:59:14.44	-47:30:50.8	73.4	34.5	1	1
317	085914.5-473118	8:59:14.46	-47:31:18.9	90.7	32.8	1	1
318	085914.6-472650	8:59:14.59	-47:26:50.1	213.0	28.3	1	1
319	085914.7-473147	8:59:14.71	-47:31:47.4	111.5	22.9	1	1
320	085914.8-472931	8:59:14.75	-47:29:31.6	73.6	70.3	1	1
321	085914.8-473016	8:59:14.76	-47:30:16.0	60.3	9.8	1	1
322	085914.9-472658	8:59:14.87	-47:26:58.3	204.3	56.6	1	1
323	085914.9-472927	8:59:14.90	-47:29:27.9	74.6	31.3	1	1
324	085915.3-473011	8:59:15.32	-47:30:11.8	54.5	8.4	1	1
325	085915.6-473722	8:59:15.58	-47:37:22.8	432.0	30.5	1	1
326	085915.6-472745	8:59:15.61	-47:27:45.9	156.7	28.5	1	1
327	085915.7-472608	8:59:15.67	-47:26:08.9	250.2	14.6	1	1
328	085915.7-473008	8:59:15.72	-47:30:08.7	50.8	10.6	1	1
329	085915.8-472922	8:59:15.75	-47:29:22.1	72.1	11	1	1
330	085915.8-472701	8:59:15.76	-47:27:01.5	198.8	36.8	1	1
331	085915.8-472853	8:59:15.85	-47:28:53.2	94.5	35.3	1	1
332	085915.9-473257	8:59:15.90	-47:32:57.3	170.6	31.1	1	1
333	085916.0-472502	8:59:15.99	-47:25:02.5	315.0	28.3	1	1
334	085916.0-473109	8:59:16.01	-47:31:09.9	73.5	20.7	1	1
335	085916.1-473312	8:59:16.05	-47:33:12.5	184.8	14.6	1	1
336	085916.1-473231	8:59:16.06	-47:32:31.9	145.9	6.1	1	1
337	085916.7-473038	8:59:16.69	-47:30:38.3	47.5	21.3	1	1
338	085916.8-472749	8:59:16.75	-47:27:49.0	150.3	21.6	1	1
339	085916.8-473003	8:59:16.80	-47:30:03.9	40.8	49.6	2	1
340	085916.9-472748	8:59:16.85	-47:27:48.9	150.2	15.8	1	1
341	085917.0-473302	8:59:16.99	-47:33:02.9	173.1	24.9	1	1
342	085917.2-472756	8:59:17.23	-47:27:56.9	141.4	15.7	1	1
343	085917.3-473011	8:59:17.26	-47:30:11.2	35.0	47.6	1	1

Table 1—Continued

SRC #	CXOJ	RA (J2000.0)	DEC (J2000.0)	Off-axis angle (″)	Net counts	Baysian Blocks 95% sig.	Baysian Blocks 99% sig.
344	085917.6-472748	8:59:17.55	-47:27:48.3	149.0	14.6	1	1
345	085917.8-472851	8:59:17.75	-47:28:51.5	87.6	79.3	3	2
346	085918.0-472442	8:59:18.02	-47:24:42.4	332.5	25.9	1	1
347	085918.1-473118	8:59:18.10	-47:31:18.0	69.3	11.4	1	1
348	085918.6-472556	8:59:18.62	-47:25:56.2	258.5	26.6	1	1
349	085919.0-473224	8:59:18.96	-47:32:24.9	132.2	40.5	1	1
350	085919.3-472832	8:59:19.27	-47:28:32.8	102.1	7.5	1	1
351	085919.3-472928	8:59:19.31	-47:29:28.6	47.4	21.3	2	1
352	085919.6-473328	8:59:19.55	-47:33:28.7	195.1	11.9	1	1
353	085919.7-472402	8:59:19.73	-47:24:02.1	371.9	24.4	2	2
354	085919.9-473118	8:59:19.91	-47:31:18.8	65.4	10.8	1	1
355	085920.0-472935	8:59:19.96	-47:29:35.2	39.4	14.7	1	1
356	085920.2-472829	8:59:20.24	-47:28:29.1	104.8	89.4	1	1
357	085920.3-473106	8:59:20.28	-47:31:06.0	52.3	7.5	1	1
358	085920.7-472617	8:59:20.70	-47:26:17.2	236.7	73.7	1	1
359	085920.8-473815	8:59:20.76	-47:38:15.0	481.2	22.6	1	1
360	085920.9-473118	8:59:20.88	-47:31:18.9	65.1	6.6	1	1
361	085920.9-472445	8:59:20.88	-47:24:45.9	327.9	67.8	1	1
362	085920.9-472914	8:59:20.95	-47:29:14.0	59.9	48.9	2	2
363	085921.2-473112	8:59:21.16	-47:31:12.4	58.7	7.5	1	1
364	085921.3-472555	8:59:21.29	-47:25:55.8	258.1	126.2	2	2
365	085921.3-473325	8:59:21.32	-47:33:25.2	191.4	21.6	1	1
366	085921.6-472928	8:59:21.58	-47:29:28.9	45.8	344	1	1
367	085921.7-473234	8:59:21.73	-47:32:34.2	140.8	19.7	1	1
368	085921.9-473038	8:59:21.91	-47:30:38.3	27.3	35.7	1	1
369	085922.2-472550	8:59:22.22	-47:25:50.4	263.9	22.7	1	1
370	085922.6-472849	8:59:22.58	-47:28:49.5	86.5	7.2	1	1
371	085922.9-472633	8:59:22.87	-47:26:33.6	221.4	40.6	2	1
372	085923.6-473551	8:59:23.55	-47:35:51.6	339.0	62.7	1	1
373	085923.6-472650	8:59:23.62	-47:26:50.2	205.8	20.5	1	1
374	085923.7-473750	8:59:23.66	-47:37:50.8	457.9	64.5	1	1

Table 1—Continued

SRC #	CXOJ	RA (J2000.0)	DEC (J2000.0)	Off-axis angle (″)	Net counts	Baysian Blocks 95% sig.	Baysian Blocks 99% sig.
375	085923.7-472523	8:59:23.66	-47:25:23.4	292.0	18.9	1	1
376	085923.9-472908	8:59:23.87	-47:29:08.0	73.3	9.6	1	1
377	085924.4-473044	8:59:24.36	-47:30:44.4	48.0	19.3	1	1
378	085924.4-473111	8:59:24.38	-47:31:11.6	68.7	15	1	1
379	085924.7-473828	8:59:24.73	-47:38:28.1	495.9	113.6	1	1
380	085924.8-473802	8:59:24.75	-47:38:02.5	470.5	35.9	2	2
381	085925.0-473213	8:59:25.04	-47:32:13.5	127.5	10.8	1	1
382	085925.1-472726	8:59:25.08	-47:27:26.6	173.1	11.3	1	1
383	085925.8-473436	8:59:25.82	-47:34:36.1	267.3	28.3	1	1
384	085925.9-473326	8:59:25.94	-47:33:26.2	199.5	12.8	1	1
385	085926.0-472726	8:59:25.97	-47:27:26.2	176.0	12.5	1	1
386	085926.2-472901	8:59:26.21	-47:29:01.5	91.4	9.1	1	1
387	085926.2-473103	8:59:26.25	-47:31:03.9	75.3	6.7	1	1
388	085926.2-472754	8:59:26.25	-47:27:54.7	150.1	25.2	1	1
389	085926.5-473007	8:59:26.54	-47:30:07.9	59.5	32.4	1	1
390	085926.7-473310	8:59:26.70	-47:33:10.0	186.3	9.5	1	1
391	085927.9-472803	8:59:27.86	-47:28:03.0	149.6	17.3	1	1
392	085928.2-472926	8:59:28.18	-47:29:26.0	89.6	49.4	1	1
393	085928.2-473545	8:59:28.22	-47:35:45.4	340.2	8.5	1	1
394	085928.3-472619	8:59:28.34	-47:26:19.8	246.5	118	1	1
395	085928.6-472937	8:59:28.63	-47:29:37.9	88.0	13.5	1	1
396	085928.8-473222	8:59:28.79	-47:32:22.1	152.1	72.9	1	1
397	085928.9-473216	8:59:28.91	-47:32:16.8	148.4	12.5	1	1
398	085928.9-473140	8:59:28.92	-47:31:40.4	120.0	119.5	3	2
399	085929.1-472056	8:59:29.05	-47:20:56.0	564.2	111.3	1	1
400	085930.0-473150	8:59:29.96	-47:31:50.0	134.3	55.8	1	1
401	085930.0-472633	8:59:30.01	-47:26:33.9	239.4	26.8	1	1
402	085930.6-472800	8:59:30.62	-47:28:00.0	167.4	13.2	1	1
403	085930.7-472450	8:59:30.74	-47:24:50.0	339.5	22.6	1	1
404	085931.3-473330	8:59:31.27	-47:33:30.4	223.8	107.2	3	3
405	085931.5-473350	8:59:31.53	-47:33:50.1	242.4	18.4	1	1

Table 1—Continued

SRC #	CXOJ	RA (J2000.0)	DEC (J2000.0)	Off-axis angle (″)	Net counts	Baysian Blocks 95% sig.	Baysian Blocks 99% sig.
406	085931.6-473156	8:59:31.64	-47:31:56.7	151.2	30	1	1
407	085931.6-472608	8:59:31.64	-47:26:08.3	269.4	5.8	1	1
408	085932.4-473235	8:59:32.44	-47:32:35.7	185.0	18.1	1	1
409	085933.3-473253	8:59:33.31	-47:32:53.6	204.5	37.9	1	1
410	085934.4-473834	8:59:34.40	-47:38:34.5	519.5	17.8	1	1
411	085934.5-472715	8:59:34.47	-47:27:15.5	226.5	25.5	1	1
412	085934.7-472840	8:59:34.74	-47:28:40.5	170.2	17.6	1	1
413	085935.2-472632	8:59:35.22	-47:26:32.0	266.3	58.8	1	1
414	085935.4-472723	8:59:35.36	-47:27:23.4	226.1	101.7	1	1
415	085935.4-472818	8:59:35.41	-47:28:18.1	188.7	69.5	1	1
416	085935.6-473137	8:59:35.58	-47:31:37.1	172.2	17.8	1	1
417	085935.8-472911	8:59:35.82	-47:29:11.7	165.4	8.9	1	1
418	085936.2-472557	8:59:36.17	-47:25:57.3	300.7	19	1	1
419	085936.8-472921	8:59:36.76	-47:29:21.6	170.9	10.9	1	1
420	085936.9-473304	8:59:36.93	-47:33:04.7	237.1	68.5	1	1
421	085937.4-473435	8:59:37.37	-47:34:35.3	311.2	16.6	1	1
422	085937.5-473125	8:59:37.48	-47:31:25.6	184.5	12.7	1	1
423	085937.9-472302	8:59:37.93	-47:23:02.8	465.1	39.1	1	1
424	085939.3-473037	8:59:39.27	-47:30:37.5	189.6	22.3	1	1
425	085939.6-472256	8:59:39.58	-47:22:56.1	477.8	11.1	1	1
426	085940.9-472526	8:59:40.90	-47:25:26.5	352.9	25.5	1	1
427	085941.6-473507	8:59:41.58	-47:35:07.6	361.8	173.8	2	1
428	085942.0-472419	8:59:42.03	-47:24:19.5	415.2	15.3	1	1
429	085942.2-473043	8:59:42.16	-47:30:43.1	219.4	21.8	1	1
430	085943.0-473158	8:59:42.95	-47:31:58.3	248.4	38.4	1	1
431	085945.2-473101	8:59:45.24	-47:31:01.3	253.1	15.5	1	1
432	085945.7-472841	8:59:45.74	-47:28:41.9	269.9	21.4	1	1
433	085946.7-473153	8:59:46.71	-47:31:53.4	281.7	70.4	2	1
434	085946.8-473803	8:59:46.81	-47:38:03.4	538.8	38.5	1	1
435	085948.3-472640	8:59:48.34	-47:26:40.2	352.4	30.4	1	1
436	085949.1-473227	8:59:49.09	-47:32:27.6	317.1	11.6	1	1

Table 1—Continued

SRC #	CXOJ	RA (J2000.0)	DEC (J2000.0)	Off-axis angle (″)	Net counts	Baysian Blocks 95% sig.	Baysian Blocks 99% sig.
437	085949.6-473116	8:59:49.59	-47:31:16.7	299.3	12.5	1	1
438	085949.8-472528	8:59:49.84	-47:25:28.2	411.0	16	1	1
439	085950.0-473143	8:59:50.04	-47:31:43.5	310.4	9.9	1	1
440	085950.4-472656	8:59:50.37	-47:26:56.6	359.7	69	1	1
441	085951.4-473323	8:59:51.42	-47:33:23.4	364.3	19	1	1
442	085951.6-473309	8:59:51.56	-47:33:09.9	358.7	19.3	1	1
443	085952.7-472736	8:59:52.70	-47:27:36.3	360.6	12.5	1	1
444	085953.6-472846	8:59:53.58	-47:28:46.0	344.6	94.2	1	1
445	085953.9-472742	8:59:53.93	-47:27:42.6	369.2	31.3	2	2
446	085954.8-473717	8:59:54.82	-47:37:17.1	546.3	108	1	1
447	085956.1-473304	8:59:56.09	-47:33:04.2	396.8	441.4	1	1
448	085956.1-473003	8:59:56.07	-47:30:03.9	358.5	19.2	1	1
449	085956.8-473109	8:59:56.76	-47:31:09.7	369.5	16.7	1	1
450	085957.9-472702	8:59:57.92	-47:27:02.3	423.1	192.7	1	1
451	085959.9-473407	8:59:59.92	-47:34:07.7	460.9	48.6	1	1
452	090004.4-472946	9:00:04.36	-47:29:46.4	443.2	68.1	1	1
453	090004.7-472708	9:00:04.74	-47:27:08.0	483.6	115.5	3	3
454	090006.7-473032	9:00:06.72	-47:30:32.1	466.6	24.8	1	1
455	090009.4-472834	9:00:09.41	-47:28:34.8	503.5	63.1	1	1
456	085904.8-473028	8:59:04.81	-47:30:28.5	161.8	49.2	1	1
457	085904.5-473035	8:59:04.50	-47:30:35.1	165.6	41.1	1	1
458	085907.2-473114	8:59:07.24	-47:31:14.2	149.2	47.5	1	1
459	085906.3-473107	8:59:06.27	-47:31:07.3	155.7	14.4	1	1
460	085906.2-473112	8:59:06.22	-47:31:12.7	158.1	11.4	1	1
461	085900.9-473044	8:59:00.87	-47:30:44.4	203.3	28	1	1
462	085903.0-473042	8:59:03.02	-47:30:42.3	181.4	47.2	1	1

Table 2. Quartile Values of Probable Cluster Members

SRC#	Q25	$Q25_{err}$	M	M_{err}	Q75	$Q75_{err}$	log(m/(1-m))	3*Q25/Q75
4	0.15	0.01	0.23	0.02	0.33	0.04	-0.53	1.32
8	0.18	0.01	0.29	0.03	0.45	0.03	-0.39	1.17
11	0.27	0.05	0.41	0.03	0.57	0.05	-0.16	1.41
16	0.19	0.02	0.31	0.03	0.47	0.09	-0.35	1.24
19	0.17	0.01	0.26	0.06	0.57	0.06	-0.46	0.90
21	0.16	0.01	0.22	0.01	0.39	0.02	-0.55	1.19
22	0.31	0.03	0.45	0.06	0.71	0.13	-0.08	1.31
23	0.14	0.01	0.22	0.01	0.34	0.03	-0.56	1.20
24	0.19	0.03	0.28	0.06	0.56	0.09	-0.42	1.03
25	0.19	0.03	0.32	0.04	0.53	0.14	-0.33	1.10
26	0.21	0.05	0.32	0.05	0.56	0.18	-0.33	1.12
27	0.22	0.03	0.32	0.04	0.45	0.16	-0.34	1.48
28	0.42	0.04	0.57	0.04	0.80	0.05	0.12	1.57
30	0.15	0.01	0.23	0.03	0.41	0.03	-0.52	1.11
31	0.22	0.01	0.31	0.03	0.47	0.04	-0.36	1.43
33	0.17	0.01	0.26	0.04	0.51	0.09	-0.46	0.97
35	0.19	0.01	0.31	0.05	0.56	0.06	-0.36	1.03
37	0.20	0.02	0.28	0.04	0.41	0.08	-0.41	1.46
38	0.25	0.03	0.32	0.07	0.55	0.08	-0.33	1.36
40	0.14	0.01	0.22	0.03	0.40	0.09	-0.54	1.08
41	0.29	0.10	0.43	0.05	0.51	0.13	-0.12	1.71
43	0.21	0.02	0.38	0.07	0.54	0.15	-0.22	1.19
45	0.22	0.04	0.40	0.06	0.52	0.07	-0.18	1.28
46	0.35	0.03	0.47	0.02	0.54	0.05	-0.06	1.93
47	0.32	0.04	0.48	0.05	0.70	0.18	-0.03	1.38
48	0.15	0.02	0.19	0.05	0.45	0.12	-0.63	0.99
49	0.36	0.05	0.49	0.09	0.79	0.21	-0.02	1.35
50	0.22	0.03	0.31	0.03	0.42	0.06	-0.35	1.58
52	0.31	0.08	0.40	0.05	0.57	0.14	-0.18	1.65
53	0.18	0.00	0.28	0.01	0.43	0.01	-0.41	1.25
55	0.28	0.03	0.39	0.04	0.49	0.07	-0.20	1.70
56	0.32	0.01	0.45	0.01	0.59	0.02	-0.09	1.61
57	0.15	0.01	0.21	0.02	0.37	0.02	-0.57	1.21

Table 2—Continued

SRC#	Q25	$Q25_{err}$	M	M_{err}	Q75	$Q75_{err}$	log(m/(1-m))	3*Q25/Q75
58	0.12	0.03	0.21	0.05	0.39	0.17	-0.58	0.93
59	0.15	0.01	0.19	0.02	0.34	0.03	-0.63	1.27
60	0.27	0.06	0.37	0.06	0.56	0.16	-0.23	1.43
62	0.19	0.01	0.25	0.02	0.39	0.03	-0.48	1.44
63	0.15	0.03	0.22	0.04	0.36	0.28	-0.54	1.29
65	0.29	0.05	0.43	0.06	0.67	0.09	-0.12	1.30
66	0.17	0.01	0.22	0.02	0.42	0.03	-0.55	1.21
67	0.16	0.01	0.25	0.02	0.42	0.03	-0.47	1.16
68	0.18	0.03	0.29	0.05	0.36	0.40	-0.38	1.54
70	0.25	0.02	0.39	0.01	0.51	0.02	-0.20	1.48
71	0.23	0.08	0.38	0.04	0.58	0.07	-0.21	1.18
72	0.20	0.01	0.30	0.02	0.42	0.03	-0.37	1.45
73	0.23	0.06	0.36	0.04	0.45	0.05	-0.26	1.53
75	0.24	0.06	0.37	0.07	0.48	0.07	-0.23	1.53
76	0.17	0.02	0.23	0.02	0.32	0.05	-0.52	1.57
77	0.27	0.03	0.36	0.05	0.54	0.10	-0.26	1.52
78	0.42	0.03	0.51	0.02	0.59	0.05	0.01	2.11
79	0.20	0.04	0.30	0.09	0.56	0.45	-0.37	1.08
82	0.19	0.02	0.33	0.05	0.47	0.05	-0.32	1.19
85	0.20	0.04	0.32	0.04	0.49	0.09	-0.33	1.19
86	0.15	0.01	0.20	0.03	0.36	0.05	-0.60	1.23
87	0.17	0.02	0.23	0.05	0.37	0.08	-0.54	1.37
88	0.18	0.02	0.26	0.04	0.36	0.10	-0.45	1.53
89	0.28	0.05	0.42	0.06	0.56	0.06	-0.14	1.51
90	0.31	0.06	0.40	0.04	0.53	0.13	-0.18	1.77
91	0.39	0.08	0.54	0.10	0.76	0.12	0.08	1.52
92	0.19	0.02	0.26	0.03	0.41	0.04	-0.45	1.43
93	0.13	0.01	0.20	0.03	0.36	0.06	-0.61	1.10
94	0.33	0.01	0.41	0.02	0.55	0.02	-0.15	1.84
96	0.23	0.07	0.33	0.07	0.55	0.21	-0.32	1.26
97	0.18	0.01	0.31	0.03	0.45	0.02	-0.35	1.18
98	0.30	0.02	0.36	0.03	0.52	0.04	-0.24	1.73
99	0.23	0.07	0.44	0.05	0.53	0.20	-0.10	1.31

Table 2—Continued

SRC#	Q25	$Q25_{err}$	M	M_{err}	Q75	$Q75_{err}$	log(m/(1-m))	3*Q25/Q75
100	0.16	0.02	0.22	0.08	0.44	0.20	-0.54	1.06
101	0.24	0.02	0.32	0.02	0.42	0.02	-0.32	1.72
103	0.36	0.05	0.50	0.03	0.61	0.09	0.01	1.81
104	0.15	0.01	0.21	0.01	0.38	0.02	-0.58	1.18
106	0.35	0.05	0.49	0.03	0.64	0.12	-0.02	1.63
107	0.18	0.01	0.23	0.03	0.38	0.03	-0.54	1.40
108	0.34	0.01	0.45	0.02	0.60	0.02	-0.09	1.71
109	0.32	0.03	0.41	0.03	0.52	0.17	-0.15	1.81
110	0.20	0.02	0.34	0.05	0.50	0.07	-0.29	1.20
111	0.37	0.05	0.51	0.06	0.67	0.26	0.02	1.64
112	0.26	0.03	0.37	0.03	0.52	0.10	-0.24	1.51
114	0.18	0.02	0.29	0.05	0.41	0.06	-0.39	1.30
115	0.19	0.02	0.26	0.04	0.40	0.07	-0.47	1.44
116	0.19	0.01	0.30	0.02	0.42	0.02	-0.36	1.37
117	0.41	0.05	0.49	0.03	0.58	0.04	-0.01	2.15
118	0.42	0.02	0.52	0.02	0.65	0.04	0.04	1.95
120	0.15	0.01	0.21	0.02	0.37	0.05	-0.57	1.24
121	0.32	0.04	0.41	0.05	0.60	0.10	-0.15	1.58
122	0.15	0.01	0.22	0.04	0.40	0.06	-0.55	1.10
124	0.19	0.04	0.28	0.08	0.46	0.18	-0.41	1.25
125	0.35	0.02	0.44	0.02	0.57	0.03	-0.11	1.84
126	0.16	0.02	0.25	0.04	0.39	0.03	-0.49	1.24
127	0.21	0.02	0.32	0.02	0.43	0.04	-0.32	1.47
128	0.13	0.03	0.22	0.07	0.47	0.32	-0.55	0.86
129	0.21	0.01	0.31	0.02	0.44	0.02	-0.34	1.42
130	0.15	0.00	0.21	0.01	0.35	0.02	-0.57	1.29
131	0.24	0.05	0.43	0.06	0.56	0.09	-0.13	1.28
133	0.18	0.01	0.24	0.04	0.41	0.03	-0.49	1.27
134	0.33	0.04	0.40	0.03	0.46	0.07	-0.18	2.19
135	0.32	0.06	0.39	0.05	0.52	0.10	-0.20	1.82
136	0.24	0.04	0.33	0.05	0.53	0.09	-0.31	1.33
138	0.19	0.01	0.28	0.03	0.48	0.06	-0.41	1.18
139	0.12	0.02	0.19	0.05	0.31	0.27	-0.64	1.16

Table 2—Continued

SRC#	Q25	$Q25_{err}$	M	M_{err}	Q75	$Q75_{err}$	log(m/(1-m))	3*Q25/Q75
140	0.20	0.01	0.30	0.01	0.42	0.02	-0.37	1.44
141	0.20	0.01	0.30	0.02	0.42	0.02	-0.38	1.41
142	0.18	0.02	0.22	0.04	0.38	0.10	-0.56	1.39
143	0.16	0.01	0.22	0.02	0.41	0.03	-0.55	1.18
144	0.17	0.01	0.25	0.04	0.45	0.05	-0.48	1.12
145	0.18	0.01	0.30	0.02	0.41	0.03	-0.37	1.34
146	0.15	0.02	0.22	0.04	0.44	0.07	-0.54	1.01
147	0.21	0.01	0.35	0.03	0.50	0.02	-0.28	1.23
148	0.18	0.01	0.27	0.02	0.45	0.02	-0.44	1.20
149	0.31	0.02	0.44	0.01	0.57	0.01	-0.10	1.62
150	0.23	0.04	0.35	0.05	0.53	0.09	-0.26	1.31
151	0.19	0.00	0.29	0.01	0.43	0.01	-0.39	1.30
152	0.20	0.01	0.29	0.01	0.46	0.03	-0.39	1.28
153	0.24	0.06	0.31	0.03	0.42	0.05	-0.35	1.70
154	0.19	0.02	0.30	0.04	0.41	0.09	-0.37	1.39
155	0.22	0.02	0.36	0.03	0.49	0.03	-0.24	1.31
156	0.18	0.03	0.28	0.04	0.49	0.09	-0.42	1.08
157	0.25	0.02	0.39	0.02	0.53	0.03	-0.19	1.38
158	0.20	0.01	0.30	0.02	0.45	0.03	-0.36	1.32
159	0.17	0.02	0.25	0.05	0.38	0.04	-0.49	1.37
160	0.22	0.03	0.38	0.03	0.53	0.03	-0.21	1.28
161	0.17	0.03	0.25	0.06	0.43	0.07	-0.49	1.18
162	0.19	0.01	0.30	0.04	0.43	0.04	-0.38	1.29
163	0.19	0.01	0.29	0.05	0.51	0.06	-0.38	1.12
164	0.19	0.01	0.30	0.02	0.45	0.03	-0.38	1.29
165	0.29	0.04	0.43	0.05	0.59	0.07	-0.12	1.49
166	0.22	0.02	0.35	0.02	0.50	0.02	-0.27	1.30
167	0.17	0.03	0.22	0.05	0.39	0.09	-0.56	1.28
168	0.23	0.04	0.41	0.06	0.53	0.06	-0.16	1.33
169	0.18	0.01	0.26	0.02	0.42	0.03	-0.46	1.28
170	0.18	0.01	0.28	0.04	0.45	0.07	-0.41	1.18
171	0.19	0.01	0.30	0.01	0.44	0.01	-0.36	1.32
172	0.19	0.01	0.28	0.02	0.41	0.03	-0.41	1.38

Table 2—Continued

SRC#	Q25	$Q25_{err}$	M	M_{err}	Q75	$Q75_{err}$	log(m/(1-m))	3*Q25/Q75
173	0.33	0.03	0.39	0.03	0.51	0.03	-0.20	1.95
174	0.28	0.01	0.39	0.01	0.54	0.02	-0.19	1.55
176	0.27	0.03	0.40	0.05	0.48	0.04	-0.18	1.69
177	0.21	0.02	0.34	0.03	0.51	0.05	-0.29	1.27
178	0.19	0.03	0.29	0.03	0.38	0.11	-0.39	1.48
179	0.15	0.01	0.22	0.02	0.33	0.03	-0.56	1.39
180	0.18	0.02	0.28	0.08	0.51	0.16	-0.42	1.03
181	0.19	0.02	0.33	0.02	0.44	0.03	-0.31	1.32
182	0.17	0.03	0.21	0.06	0.49	0.11	-0.58	1.03
183	0.17	0.01	0.22	0.03	0.39	0.04	-0.54	1.33
184	0.22	0.02	0.34	0.04	0.45	0.05	-0.29	1.45
185	0.18	0.01	0.27	0.04	0.49	0.09	-0.44	1.13
186	0.21	0.06	0.31	0.10	0.49	0.09	-0.34	1.24
187	0.15	0.03	0.26	0.07	0.45	0.07	-0.46	1.00
188	0.20	0.03	0.30	0.08	0.54	0.13	-0.36	1.14
189	0.20	0.04	0.31	0.02	0.43	0.05	-0.36	1.36
190	0.22	0.02	0.36	0.03	0.53	0.03	-0.26	1.24
191	0.20	0.03	0.28	0.05	0.48	0.13	-0.41	1.23
192	0.20	0.01	0.35	0.02	0.47	0.02	-0.27	1.27
193	0.29	0.06	0.38	0.03	0.41	0.14	-0.22	2.08
194	0.21	0.01	0.33	0.02	0.48	0.03	-0.32	1.30
195	0.27	0.04	0.33	0.07	0.52	0.08	-0.30	1.55
196	0.17	0.02	0.28	0.04	0.43	0.05	-0.41	1.16
197	0.20	0.01	0.32	0.02	0.45	0.01	-0.33	1.32
198	0.18	0.01	0.30	0.03	0.46	0.02	-0.38	1.21
199	0.21	0.04	0.30	0.05	0.38	0.10	-0.38	1.70
200	0.18	0.01	0.27	0.02	0.40	0.03	-0.43	1.33
201	0.18	0.02	0.26	0.04	0.43	0.06	-0.47	1.27
202	0.20	0.01	0.28	0.04	0.43	0.04	-0.41	1.38
203	0.23	0.03	0.38	0.05	0.47	0.04	-0.22	1.47
204	0.24	0.03	0.36	0.04	0.47	0.14	-0.26	1.49
205	0.26	0.02	0.34	0.02	0.46	0.03	-0.30	1.65
207	0.18	0.01	0.26	0.02	0.42	0.04	-0.47	1.26

Table 2—Continued

SRC#	Q25	$Q25_{err}$	M	M_{err}	Q75	$Q75_{err}$	log(m/(1-m))	3*Q25/Q75
208	0.19	0.01	0.23	0.05	0.34	0.05	-0.53	1.65
209	0.19	0.02	0.30	0.02	0.42	0.04	-0.37	1.31
210	0.23	0.03	0.35	0.05	0.52	0.05	-0.28	1.31
211	0.17	0.03	0.26	0.04	0.44	0.06	-0.45	1.15
212	0.16	0.02	0.26	0.04	0.48	0.04	-0.45	1.02
213	0.18	0.02	0.28	0.03	0.41	0.02	-0.42	1.33
214	0.15	0.01	0.22	0.01	0.40	0.03	-0.56	1.11
215	0.27	0.05	0.37	0.04	0.53	0.07	-0.24	1.56
217	0.23	0.02	0.31	0.02	0.44	0.04	-0.34	1.53
218	0.17	0.01	0.28	0.02	0.40	0.03	-0.42	1.27
219	0.17	0.01	0.22	0.01	0.35	0.03	-0.54	1.45
220	0.18	0.00	0.27	0.01	0.42	0.01	-0.43	1.29
221	0.15	0.00	0.20	0.00	0.30	0.00	-0.59	1.55
222	0.32	0.06	0.45	0.08	0.64	0.10	-0.09	1.53
223	0.17	0.01	0.27	0.02	0.41	0.02	-0.44	1.26
224	0.16	0.02	0.21	0.02	0.34	0.07	-0.59	1.37
225	0.20	0.01	0.31	0.02	0.47	0.02	-0.34	1.27
226	0.19	0.01	0.27	0.02	0.42	0.03	-0.42	1.36
227	0.23	0.02	0.38	0.02	0.54	0.02	-0.22	1.30
229	0.15	0.01	0.20	0.01	0.33	0.02	-0.60	1.36
230	0.19	0.02	0.30	0.04	0.44	0.05	-0.37	1.31
231	0.35	0.06	0.44	0.04	0.57	0.06	-0.10	1.87
232	0.39	0.06	0.45	0.04	0.58	0.06	-0.08	2.01
233	0.26	0.02	0.40	0.02	0.54	0.04	-0.19	1.45
234	0.40	0.05	0.47	0.03	0.56	0.15	-0.05	2.13
235	0.17	0.02	0.27	0.05	0.39	0.07	-0.44	1.31
236	0.33	0.03	0.46	0.04	0.59	0.03	-0.08	1.66
238	0.20	0.01	0.31	0.02	0.45	0.02	-0.34	1.31
239	0.16	0.01	0.25	0.03	0.32	0.03	-0.48	1.48
240	0.23	0.03	0.32	0.03	0.48	0.06	-0.32	1.46
241	0.20	0.02	0.26	0.05	0.42	0.03	-0.46	1.41
242	0.28	0.04	0.39	0.05	0.58	0.08	-0.20	1.44
243	0.19	0.01	0.30	0.01	0.46	0.02	-0.37	1.24

Table 2—Continued

SRC#	Q25	$Q25_{err}$	M	M_{err}	Q75	$Q75_{err}$	log(m/(1-m))	3*Q25/Q75
244	0.20	0.03	0.31	0.03	0.46	0.04	-0.35	1.30
246	0.18	0.01	0.27	0.02	0.45	0.04	-0.44	1.17
247	0.38	0.02	0.46	0.02	0.53	0.03	-0.07	2.14
248	0.34	0.03	0.47	0.06	0.62	0.06	-0.05	1.63
249	0.34	0.02	0.45	0.02	0.59	0.04	-0.09	1.71
250	0.26	0.03	0.37	0.03	0.51	0.07	-0.23	1.51
251	0.52	0.01	0.62	0.02	0.75	0.03	0.22	2.05
252	0.29	0.04	0.37	0.05	0.62	0.06	-0.24	1.40
253	0.34	0.03	0.44	0.02	0.55	0.03	-0.11	1.87
255	0.34	0.01	0.44	0.02	0.57	0.02	-0.11	1.80
256	0.19	0.02	0.25	0.07	0.41	0.08	-0.48	1.38
257	0.31	0.08	0.38	0.11	0.69	0.16	-0.21	1.34
258	0.22	0.02	0.28	0.06	0.50	0.09	-0.40	1.33
259	0.40	0.02	0.48	0.03	0.59	0.07	-0.03	2.02
261	0.32	0.02	0.42	0.02	0.59	0.04	-0.13	1.64
263	0.16	0.00	0.23	0.01	0.36	0.03	-0.54	1.32
264	0.19	0.04	0.29	0.03	0.40	0.04	-0.38	1.38
265	0.22	0.05	0.41	0.04	0.50	0.03	-0.15	1.32
266	0.19	0.01	0.22	0.04	0.40	0.09	-0.54	1.42
267	0.24	0.05	0.38	0.05	0.47	0.10	-0.22	1.53
269	0.38	0.05	0.49	0.04	0.58	0.07	-0.01	1.97
270	0.39	0.06	0.53	0.13	0.78	0.13	0.06	1.49
271	0.23	0.02	0.36	0.03	0.50	0.04	-0.25	1.36
272	0.25	0.02	0.37	0.03	0.54	0.04	-0.24	1.40
273	0.36	0.04	0.51	0.06	0.65	0.11	0.02	1.68
274	0.24	0.02	0.35	0.03	0.46	0.04	-0.28	1.58
275	0.23	0.09	0.39	0.05	0.47	0.12	-0.20	1.49
276	0.22	0.02	0.35	0.02	0.46	0.02	-0.27	1.42
278	0.39	0.04	0.49	0.07	0.61	0.23	-0.01	1.92
279	0.23	0.05	0.38	0.07	0.49	0.17	-0.22	1.39
280	0.18	0.02	0.30	0.06	0.45	0.08	-0.36	1.17
281	0.16	0.01	0.21	0.02	0.38	0.03	-0.57	1.26
282	0.21	0.02	0.29	0.03	0.43	0.03	-0.38	1.44

Table 2—Continued

SRC#	Q25	$Q25_{err}$	M	M_{err}	Q75	$Q75_{err}$	log(m/(1-m))	3*Q25/Q75
283	0.17	0.01	0.20	0.06	0.44	0.12	-0.60	1.14
284	0.36	0.02	0.48	0.03	0.61	0.03	-0.04	1.75
285	0.24	0.01	0.37	0.02	0.49	0.02	-0.24	1.46
287	0.20	0.02	0.32	0.05	0.44	0.05	-0.34	1.36
288	0.15	0.02	0.21	0.04	0.36	0.07	-0.58	1.23
289	0.16	0.00	0.26	0.01	0.42	0.02	-0.45	1.17
290	0.22	0.03	0.28	0.04	0.47	0.10	-0.41	1.40
291	0.29	0.04	0.39	0.07	0.60	0.10	-0.20	1.44
292	0.45	0.04	0.64	0.07	0.82	0.04	0.25	1.65
293	0.27	0.02	0.37	0.02	0.50	0.02	-0.22	1.60
294	0.24	0.05	0.37	0.05	0.48	0.13	-0.24	1.50
295	0.19	0.04	0.23	0.07	0.39	0.20	-0.52	1.43
296	0.22	0.02	0.32	0.05	0.63	0.18	-0.34	1.07
297	0.38	0.03	0.47	0.04	0.62	0.05	-0.06	1.86
298	0.15	0.02	0.27	0.05	0.35	0.06	-0.43	1.27
299	0.60	0.10	0.64	0.04	0.77	0.06	0.24	2.33
301	0.39	0.06	0.56	0.11	0.73	0.26	0.11	1.61
302	0.47	0.03	0.56	0.04	0.68	0.07	0.11	2.09
303	0.37	0.03	0.47	0.06	0.65	0.09	-0.06	1.72
304	0.41	0.05	0.46	0.14	0.80	0.10	-0.07	1.52
305	0.34	0.03	0.42	0.04	0.58	0.06	-0.15	1.74
307	0.31	0.05	0.43	0.03	0.47	0.07	-0.13	1.98
308	0.30	0.08	0.50	0.11	0.61	0.23	0.00	1.46
309	0.18	0.03	0.22	0.04	0.33	0.12	-0.56	1.66
310	0.33	0.09	0.48	0.05	0.67	0.10	-0.04	1.46
311	0.44	0.09	0.56	0.07	0.69	0.12	0.10	1.93
313	0.32	0.08	0.52	0.07	0.69	0.09	0.04	1.36
314	0.39	0.06	0.46	0.07	0.68	0.11	-0.07	1.72
316	0.25	0.03	0.33	0.04	0.46	0.05	-0.30	1.61
317	0.21	0.02	0.29	0.04	0.47	0.08	-0.39	1.36
318	0.31	0.06	0.42	0.06	0.61	0.09	-0.15	1.55
319	0.34	0.05	0.41	0.03	0.53	0.15	-0.15	1.92
320	0.18	0.01	0.26	0.04	0.49	0.07	-0.46	1.09

Table 2—Continued

SRC#	Q25	$Q25_{err}$	M	M_{err}	Q75	$Q75_{err}$	log(m/(1-m))	3*Q25/Q75
322	0.41	0.03	0.51	0.02	0.61	0.03	0.02	2.04
323	0.18	0.01	0.23	0.03	0.33	0.06	-0.54	1.62
324	0.32	0.08	0.43	0.13	0.60	0.34	-0.13	1.58
326	0.15	0.03	0.20	0.02	0.29	0.10	-0.61	1.61
327	0.15	0.03	0.24	0.05	0.33	0.26	-0.49	1.38
328	0.41	0.08	0.55	0.08	0.68	0.08	0.09	1.80
330	0.28	0.04	0.38	0.04	0.48	0.09	-0.21	1.79
331	0.19	0.02	0.25	0.03	0.39	0.08	-0.48	1.47
332	0.20	0.02	0.28	0.03	0.43	0.06	-0.41	1.36
334	0.31	0.07	0.39	0.03	0.49	0.13	-0.20	1.89
335	0.22	0.06	0.33	0.05	0.40	0.33	-0.30	1.61
336	0.57	0.02	0.63	0.05	0.68	0.05	0.23	2.52
337	0.35	0.03	0.43	0.06	0.57	0.13	-0.12	1.85
339	0.21	0.03	0.36	0.04	0.54	0.04	-0.24	1.19
341	0.36	0.05	0.48	0.06	0.59	0.09	-0.03	1.81
342	0.18	0.02	0.23	0.06	0.39	0.09	-0.52	1.37
343	0.30	0.02	0.38	0.04	0.60	0.07	-0.21	1.50
344	0.18	0.02	0.22	0.07	0.51	0.26	-0.55	1.04
345	0.17	0.02	0.29	0.05	0.47	0.03	-0.39	1.07
346	0.45	0.06	0.58	0.04	0.66	0.04	0.13	2.06
347	0.47	0.14	0.55	0.08	0.76	0.15	0.09	1.84
349	0.17	0.02	0.30	0.05	0.45	0.08	-0.36	1.13
351	0.22	0.04	0.37	0.06	0.46	0.05	-0.24	1.45
353	0.32	0.04	0.40	0.05	0.61	0.10	-0.18	1.57
354	0.15	0.03	0.21	0.11	0.49	0.20	-0.57	0.93
356	0.25	0.02	0.37	0.03	0.49	0.04	-0.23	1.50
358	0.14	0.01	0.19	0.02	0.27	0.04	-0.64	1.52
360	0.22	0.03	0.24	0.13	0.45	0.24	-0.50	1.47
361	0.30	0.02	0.42	0.03	0.57	0.04	-0.15	1.58
362	0.14	0.01	0.19	0.02	0.31	0.04	-0.63	1.38
363	0.17	0.09	0.35	0.11	0.40	0.48	-0.26	1.31
364	0.16	0.01	0.26	0.02	0.39	0.04	-0.46	1.24
366	0.20	0.01	0.30	0.02	0.44	0.01	-0.37	1.32

Table 2—Continued

SRC#	Q25	$Q25_{err}$	M	M_{err}	Q75	$Q75_{err}$	log(m/(1-m))	3*Q25/Q75
367	0.27	0.05	0.38	0.04	0.46	0.07	-0.21	1.80
368	0.18	0.02	0.26	0.03	0.43	0.09	-0.45	1.29
370	0.25	0.05	0.34	0.12	0.57	0.14	-0.28	1.34
371	0.16	0.01	0.30	0.06	0.43	0.06	-0.37	1.14
372	0.21	0.02	0.32	0.03	0.48	0.05	-0.33	1.28
373	0.13	0.02	0.21	0.06	0.34	0.05	-0.59	1.12
374	0.20	0.02	0.36	0.04	0.53	0.06	-0.26	1.13
377	0.32	0.03	0.44	0.05	0.52	0.07	-0.11	1.82
379	0.17	0.01	0.28	0.03	0.47	0.04	-0.42	1.09
380	0.14	0.01	0.19	0.02	0.43	0.22	-0.64	0.98
381	0.20	0.03	0.23	0.06	0.41	0.08	-0.51	1.45
382	0.21	0.05	0.40	0.11	0.48	0.31	-0.18	1.31
384	0.42	0.09	0.59	0.08	0.69	0.09	0.16	1.82
385	0.23	0.08	0.32	0.07	0.52	0.21	-0.33	1.35
386	0.27	0.06	0.42	0.10	0.59	0.12	-0.15	1.35
387	0.18	0.06	0.24	0.15	0.52	0.15	-0.51	1.03
388	0.16	0.02	0.21	0.03	0.32	0.08	-0.58	1.50
389	0.15	0.01	0.20	0.03	0.29	0.06	-0.61	1.54
390	0.15	0.02	0.20	0.08	0.39	0.21	-0.60	1.14
391	0.15	0.03	0.27	0.06	0.39	0.14	-0.43	1.12
392	0.15	0.02	0.22	0.03	0.33	0.04	-0.56	1.39
393	0.19	0.03	0.24	0.07	0.42	0.15	-0.49	1.39
394	0.20	0.02	0.30	0.04	0.44	0.04	-0.36	1.33
395	0.14	0.02	0.19	0.07	0.35	0.28	-0.63	1.25
396	0.19	0.01	0.29	0.04	0.52	0.05	-0.40	1.07
398	0.19	0.01	0.30	0.02	0.41	0.04	-0.37	1.42
400	0.21	0.02	0.29	0.03	0.41	0.04	-0.39	1.52
401	0.14	0.01	0.20	0.06	0.41	0.07	-0.59	1.02
402	0.19	0.03	0.22	0.12	0.63	0.23	-0.56	0.88
403	0.20	0.06	0.35	0.04	0.47	0.19	-0.27	1.27
405	0.17	0.03	0.27	0.04	0.37	0.22	-0.43	1.34
406	0.32	0.03	0.41	0.04	0.54	0.05	-0.16	1.78
408	0.11	0.02	0.20	0.06	0.41	0.40	-0.60	0.81

Table 2—Continued

SRC#	Q25	$Q25_{err}$	M	M_{err}	Q75	$Q75_{err}$	log(m/(1-m))	3*Q25/Q75
409	0.13	0.02	0.20	0.03	0.37	0.09	-0.61	1.10
412	0.29	0.04	0.38	0.09	0.57	0.06	-0.22	1.55
413	0.31	0.03	0.44	0.03	0.59	0.10	-0.11	1.58
414	0.13	0.01	0.18	0.01	0.27	0.04	-0.65	1.48
415	0.17	0.01	0.23	0.03	0.36	0.05	-0.53	1.39
416	0.16	0.02	0.21	0.05	0.42	0.16	-0.57	1.11
418	0.16	0.03	0.27	0.08	0.50	0.28	-0.44	0.94
419	0.21	0.05	0.27	0.06	0.39	0.31	-0.44	1.60
420	0.19	0.02	0.29	0.03	0.47	0.04	-0.40	1.22
422	0.18	0.05	0.23	0.05	0.30	0.08	-0.52	1.81
424	0.32	0.05	0.39	0.05	0.58	0.08	-0.19	1.65
427	0.15	0.01	0.22	0.02	0.38	0.02	-0.54	1.20
429	0.47	0.07	0.61	0.06	0.81	0.12	0.19	1.73
431	0.36	0.07	0.41	0.08	0.66	0.18	-0.16	1.61
433	0.14	0.01	0.24	0.03	0.37	0.04	-0.50	1.16
435	0.15	0.02	0.20	0.03	0.28	0.11	-0.62	1.55
436	0.23	0.06	0.34	0.06	0.58	0.35	-0.30	1.16
440	0.14	0.02	0.22	0.02	0.37	0.05	-0.56	1.10
441	0.17	0.03	0.25	0.06	0.42	0.33	-0.47	1.21
444	0.19	0.01	0.32	0.03	0.48	0.03	-0.32	1.17
445	0.15	0.01	0.20	0.03	0.39	0.23	-0.60	1.11
448	0.20	0.04	0.32	0.09	0.56	0.09	-0.33	1.06
453	0.14	0.01	0.23	0.03	0.41	0.06	-0.53	1.01
455	0.26	0.03	0.44	0.04	0.62	0.07	-0.11	1.29

Table 3. Quartile Values of Probable Non-Members

SRC#	Q25	$Q25_{err}$	M	M_{err}	Q75	$Q75_{err}$	log(m/(1-m))	3*Q25/Q75
1	0.11	0.01	0.16	0.02	0.44	0.14	-0.74	0.74
2	0.20	0.02	0.37	0.08	0.95	0.13	-0.23	0.62
3	0.19	0.01	0.29	0.04	0.60	0.11	-0.39	0.95
5	0.19	0.03	0.41	0.09	0.68	0.19	-0.15	0.85
6	0.11	0.01	0.16	0.03	0.35	0.14	-0.71	0.92
7	0.31	0.06	0.68	0.08	1.16	0.13	0.32	0.80
9	0.20	0.03	0.34	0.14	1.10	0.21	-0.28	0.53
10	0.20	0.03	0.37	0.05	0.71	0.28	-0.24	0.84
12	0.27	0.04	0.41	0.08	0.94	0.23	-0.16	0.85
13	0.14	0.02	0.27	0.06	0.60	0.20	-0.43	0.72
14	0.31	0.05	0.45	0.05	0.78	0.23	-0.08	1.18
15	0.09	0.02	0.13	0.10	0.60	0.40	-0.82	0.44
17	0.09	0.01	0.11	0.03	0.25	0.34	-0.91	1.08
18	0.17	0.03	0.39	0.08	0.67	0.21	-0.20	0.77
20	0.31	0.06	0.47	0.08	0.93	0.16	-0.06	0.99
29	0.14	0.03	0.29	0.10	0.61	0.20	-0.38	0.67
32	0.13	0.02	0.27	0.06	0.53	0.14	-0.43	0.74
34	0.05	0.01	0.07	0.01	0.12	0.04	-1.12	1.32
36	0.24	0.04	0.40	0.07	0.65	0.26	-0.17	1.12
39	0.06	0.00	0.08	0.00	0.11	0.01	-1.07	1.70
42	0.09	0.01	0.13	0.02	0.19	0.23	-0.84	1.38
44	0.19	0.06	0.43	0.10	0.86	0.20	-0.12	0.65
51	0.19	0.04	0.30	0.13	0.66	0.14	-0.36	0.87
54	0.07	0.01	0.10	0.01	0.14	0.06	-0.97	1.50
61	0.28	0.05	0.47	0.07	0.83	0.15	-0.06	1.00
64	0.07	0.01	0.13	0.03	0.35	0.27	-0.83	0.63
69	0.07	0.00	0.09	0.00	0.13	0.01	-1.01	1.67
74	0.19	0.03	0.34	0.08	0.59	0.13	-0.28	0.97
80	0.11	0.01	0.16	0.03	0.42	0.12	-0.74	0.81
81	0.29	0.07	0.44	0.08	0.73	0.13	-0.11	1.19
83	0.14	0.02	0.20	0.08	0.72	0.17	-0.60	0.59
84	0.22	0.05	0.39	0.06	0.59	0.08	-0.20	1.10
102	0.16	0.04	0.23	0.20	1.05	0.49	-0.54	0.46

Table 3—Continued

SRC#	Q25	$Q25_{err}$	M	M_{err}	Q75	$Q75_{err}$	log(m/(1-m))	3*Q25/Q75
105	0.17	0.07	0.41	0.10	0.61	0.15	-0.15	0.86
113	0.14	0.02	0.28	0.07	0.84	0.19	-0.41	0.50
119	0.30	0.06	0.45	0.09	0.77	0.22	-0.10	1.18
123	0.23	0.06	0.42	0.08	0.83	0.18	-0.15	0.83
132	0.18	0.04	0.35	0.05	0.55	0.09	-0.26	0.99
137	0.09	0.02	0.20	0.08	0.43	0.10	-0.60	0.65
175	0.11	0.01	0.14	0.01	0.19	0.08	-0.77	1.76
206	0.06	0.01	0.10	0.05	0.31	0.20	-0.96	0.61
216	0.21	0.08	0.42	0.12	0.76	0.18	-0.15	0.84
237	0.32	0.13	0.55	0.08	0.69	0.15	0.09	1.41
245	0.14	0.01	0.18	0.02	0.29	0.05	-0.66	1.42
254	0.14	0.04	0.36	0.16	0.96	0.27	-0.24	0.43
260	0.19	0.03	0.33	0.06	0.58	0.09	-0.32	0.97
262	0.16	0.04	0.32	0.06	0.56	0.12	-0.33	0.83
268	0.30	0.05	0.40	0.16	0.95	0.24	-0.18	0.96
277	0.08	0.01	0.11	0.01	0.15	0.02	-0.93	1.67
286	0.06	0.00	0.08	0.01	0.19	0.10	-1.09	0.96
300	0.12	0.01	0.17	0.03	0.44	0.14	-0.69	0.80
306	0.26	0.12	0.49	0.10	0.59	0.29	-0.01	1.29
312	0.25	0.07	0.49	0.13	0.71	0.15	-0.01	1.04
315	0.14	0.02	0.21	0.06	0.66	0.25	-0.58	0.63
321	0.34	0.13	0.59	0.11	0.70	0.25	0.16	1.48
325	0.24	0.07	0.48	0.06	0.67	0.08	-0.03	1.07
329	0.11	0.03	0.17	0.03	0.21	0.11	-0.70	1.63
333	0.26	0.04	0.49	0.07	0.68	0.12	-0.03	1.12
338	0.26	0.07	0.50	0.12	0.75	0.06	0.00	1.04
340	0.35	0.08	0.64	0.13	0.76	0.06	0.25	1.36
348	0.06	0.01	0.10	0.01	0.15	0.03	-0.94	1.11
350	0.23	0.12	0.42	0.17	0.63	0.21	-0.14	1.08
352	0.20	0.08	0.41	0.11	0.64	0.22	-0.17	0.94
355	0.08	0.01	0.09	0.01	0.10	0.02	-0.98	2.40
357	0.24	0.09	0.47	0.22	0.77	0.32	-0.06	0.93
359	0.22	0.07	0.39	0.07	0.65	0.11	-0.20	1.03

Table 3—Continued

SRC#	Q25	$Q25_{err}$	M	M_{err}	Q75	$Q75_{err}$	log(m/(1-m))	3*Q25/Q75
365	0.28	0.07	0.49	0.07	0.65	0.14	-0.02	1.27
369	0.15	0.01	0.18	0.02	0.29	0.13	-0.66	1.52
375	0.12	0.02	0.17	0.05	0.36	0.18	-0.68	0.96
376	0.17	0.07	0.37	0.12	0.51	0.08	-0.24	1.01
378	0.19	0.06	0.40	0.10	0.50	0.10	-0.18	1.12
383	0.09	0.01	0.11	0.04	0.35	0.16	-0.91	0.78
397	0.07	0.02	0.08	0.06	0.15	0.40	-1.07	1.29
399	0.13	0.01	0.17	0.01	0.28	0.02	-0.68	1.36
404	0.06	0.00	0.10	0.01	0.17	0.02	-0.98	1.14
407	0.06	0.02	0.07	0.02	0.10	0.01	-1.14	1.77
410	0.12	0.04	0.31	0.16	1.17	0.21	-0.34	0.30
411	0.13	0.02	0.17	0.02	0.28	0.19	-0.68	1.37
417	0.26	0.04	0.37	0.21	1.00	0.34	-0.23	0.77
421	0.20	0.04	0.32	0.09	0.65	0.28	-0.34	0.91
423	0.25	0.03	0.36	0.06	0.67	0.07	-0.24	1.09
425	0.26	0.06	0.42	0.10	0.79	0.17	-0.15	0.99
426	0.10	0.02	0.16	0.02	0.23	0.24	-0.73	1.32
428	0.18	0.03	0.35	0.12	0.78	0.24	-0.27	0.68
430	0.21	0.04	0.37	0.05	0.58	0.07	-0.22	1.09
432	0.08	0.01	0.12	0.02	0.17	0.13	-0.88	1.49
434	0.16	0.02	0.34	0.09	0.91	0.11	-0.29	0.52
437	0.14	0.04	0.36	0.10	0.50	0.14	-0.25	0.84
438	0.13	0.02	0.22	0.09	0.92	0.40	-0.54	0.41
439	0.29	0.08	0.50	0.09	0.65	0.10	-0.01	1.35
442	0.11	0.02	0.15	0.04	0.39	0.29	-0.74	0.86
443	0.12	0.02	0.22	0.22	1.16	0.27	-0.55	0.31
446	0.10	0.01	0.15	0.01	0.33	0.10	-0.76	0.89
447	0.08	0.00	0.11	0.00	0.14	0.00	-0.93	1.82
449	0.20	0.08	0.42	0.11	0.79	0.27	-0.14	0.76
450	0.08	0.00	0.11	0.01	0.16	0.01	-0.93	1.42
451	0.35	0.04	0.52	0.05	0.82	0.10	0.04	1.29
452	0.06	0.01	0.09	0.01	0.15	0.15	-1.00	1.15
454	0.13	0.02	0.22	0.07	1.18	0.28	-0.56	0.33

Table 4. Summary Model Fit Data

Model	RS	2temp RS	APEC	MeKaL	TB	BB	Power Law
mean	0.41	0.44	0.41	0.45	0.44	1.44	1.23
MAD	0.017	0.019	0.016	0.020	0.019	0.090	0.069
Num. Rej.	14	9	19	32	16	16	11

Table 5. Sources with Two–Temperature Spectra

SRC#	χ^2 per d.o.f.	$N_{\rm H}$ 10^{22} cm^{-2}	$N_{{\rm H}err}$	kT_1 keV	$kT_{1\ err}$	kT_2 keV	$kT_{2\ err}$	Unabs. Flux log ergs $cm^{-2}s^{-1}$	EMR[a] kT_1/kT_2	L_x log $ergss^{-1}$
8	0.28	2.30	0.26	1.37	0.50	6.47	–	-13.23	2.79	31.31
23	0.47	1.24	0.12	0.60	0.34	3.04	1.45	-13.31	1.61	31.23
39	0.10	0.67	0.02	0.08	0.00	0.35	0.06	-11.31	32.41	b
97	0.29	1.78	0.21	0.49	–	4.02	–	-13.29	0.12	31.25
104	0.39	2.88	0.14	0.31	0.08	5.67	3.85	-11.82	54.04	32.72
118	0.24	21.36	1.70	0.90	0.18	3.67	3.11	-11.64	12.65	32.90
129	0.42	3.50	0.24	1.44	0.20	>15	–	-12.80	8.70	31.74
133	0.12	1.25	0.19	0.47	–	3.74	0.00	-13.54	0.07	31.00
157	0.19	3.60	0.28	0.18	0.02	5.48	–	-11.32	50.33	33.22
169	0.53	4.08	0.19	0.38	0.09	6.25	–	-11.68	49.03	32.86
172	0.22	3.06	0.26	0.72	0.22	3.98	2.58	-12.76	5.43	31.78
179	0.25	1.76	0.17	1.14	0.26	7.78	–	-13.31	4.30	31.23
192	0.52	3.73	0.21	0.36	0.03	5.01	3.74	-11.93	14.75	32.61
207	0.31	2.79	0.16	0.65	0.18	8.78	0.00	-12.47	8.69	32.07
219	0.54	2.54	0.11	0.56	0.09	3.19	–	-12.27	6.76	32.26
221	0.77	2.29	0.02	0.77	0.02	2.52	0.20	-11.11	7.13	33.43
225	0.38	2.33	0.12	0.47	0.32	3.58	0.56	-12.62	0.49	31.92
226	0.37	2.73	0.18	0.90	0.32	2.67	0.61	-12.79	1.01	31.75
227	0.80	2.40	0.26	0.14	0.02	>15	3.67	-11.24	68.77	33.29
285	0.36	4.26	0.23	1.41	–	14.22	–	-12.55	4.18	31.99
364	0.23	1.78	0.18	0.83	0.57	3.60	–	-13.24	0.94	31.30
394	0.33	2.27	0.26	0.72	0.59	5.04	0.00	-13.14	1.21	31.39
404	0.21	0.00	0.02	0.08	–	1.05	0.10	-14.16	0.31	b
450	0.23	0.47	0.03	0.32	0.08	1.14	0.15	-13.30	2.56	b

Table 6. Cluster Members Fit with 1 Temperature Spectra

SRC#	χ^2 per d.o.f.	$N_{\rm H}$ 10^{22} cm^{-2}	$N_{{\rm H}err}$	kT keV	kT$_{err}$	Unabs. Flux log ergs cm^{-2}s^{-1}	L$_x$ log ergss^{-1}
3	0.23	3.19	1.06	1.04	0.46	-13.08	31.45
4	0.36	1.22	–	1.72	–	-13.42	31.11
11	0.41	3.54	0.63	3.72	–	-13.43	31.11
14	0.17	4.80	1.79	3.51	1.16	-13.60	30.94
16	0.19	2.22	1.37	2.08	1.59	-13.69	30.85
19	1.01	2.48	1.14	0.73	0.40	-13.28	31.26
21	0.48	0.90	0.16	3.87	1.09	-13.17	31.36
22	0.32	4.46	1.04	3.67	–	-13.54	30.99
24	0.14	1.71	0.73	2.83	1.55	-13.91	30.63
25	0.23	2.20	–	2.06	–	-13.67	30.87
28	0.38	14.04	5.99	6.14	4.52	-13.08	31.46
30	0.24	0.95	0.28	3.01	0.06	-13.69	30.85
31	0.26	3.64	0.69	1.54	0.27	-13.10	31.44
33	0.19	1.31	0.42	2.56	0.94	-13.76	30.78
35	0.67	2.97	–	1.41	–	-13.50	31.04
37	0.14	2.28	0.79	1.97	0.72	-13.75	30.78
40	0.30	1.28	0.44	1.48	0.40	-13.84	30.70
46	0.20	9.17	2.96	2.15	0.54	-13.03	31.51
50	0.32	4.77	1.40	1.17	0.28	-13.09	31.45
53	0.48	1.77	0.18	3.31	0.61	-12.60	31.94
55	0.32	5.66	0.33	1.62	–	-13.25	31.29
56	0.46	3.89	0.42	14.73	0.00	-12.77	31.76
57	0.40	0.91	0.19	3.29	0.90	-13.45	31.09
59	0.29	0.96	0.28	1.98	0.75	-13.57	30.97
62	0.15	2.68	0.66	1.58	0.50	-13.23	31.31
66	0.49	2.10	0.51	1.32	0.35	-13.27	31.27
67	0.51	0.96	–	5.42	–	-13.35	31.19
70	0.34	3.37	0.41	3.82	0.82	-12.88	31.66
71	0.76	6.15	–	6.42	–	-13.72	30.82
72	0.28	3.21	–	1.52	–	-13.03	31.50
78	0.25	10.92	3.94	2.39	0.84	-12.96	31.57
82	0.28	2.10	0.26	2.92	–	-13.75	30.79

Table 6—Continued

SRC#	χ^2 per d.o.f.	$N_{\rm H}$ 10^{22} cm^{-2}	$N_{{\rm H}err}$	kT keV	kT$_{err}$	Unabs. Flux log ergs cm^{-2}s^{-1}	L$_x$ log ergss^{-1}
85	0.21	3.06	2.10	1.86	1.59	-13.68	30.86
86	0.10	0.91	0.02	2.55	–	-14.10	30.44
92	0.19	2.25	1.04	1.58	0.78	-13.57	30.97
93	0.22	0.90	–	1.43	–	-13.94	30.60
94	0.40	6.96	–	2.31	–	-12.66	31.88
98	0.52	6.77	0.74	1.68	–	-12.96	31.57
101	0.20	4.79	0.46	1.39	–	-12.76	31.78
103	0.53	7.54	4.50	4.29	2.58	-13.51	31.03
107	0.28	2.43	–	1.44	–	-12.97	31.57
108	0.43	5.37	0.68	8.91	0.08	-12.86	31.67
109	0.45	6.22	2.47	1.56	0.95	-13.31	31.22
110	0.35	3.20	0.96	1.99	0.75	-13.64	30.89
112	0.42	5.37	2.25	1.38	0.87	-13.20	31.34
114	0.33	1.36	0.53	3.26	0.13	-13.90	30.64
115	0.11	2.79	–	1.27	–	-13.47	31.07
116	0.29	2.99	0.60	1.84	0.46	-13.09	31.45
120	0.13	1.38	–	2.20	–	-13.74	30.80
122	0.33	0.43	0.35	5.62	0.11	-14.21	30.33
125	0.42	6.23	2.80	3.40	2.77	-12.91	31.63
126	0.16	1.04	0.41	3.52	1.51	-13.85	30.69
127	0.17	3.40	–	1.78	–	-13.06	31.48
130	0.68	1.18	0.29	2.27	0.63	-13.11	31.43
132	0.40	0.90	–	>15	–	-14.05	30.49
138	0.35	2.21	0.64	1.89	0.81	-13.47	31.07
140	0.43	2.98	1.00	1.83	0.67	-12.84	31.70
141	0.44	2.90	–	1.69	–	-13.11	31.43
143	0.23	1.32	–	2.65	–	-13.50	31.04
144	0.15	1.30	0.13	3.64	–	-13.61	30.93
145	0.90	1.24	0.32	6.00	0.05	-13.40	31.13
146	0.11	0.43	–	>15	–	-14.11	30.42
147	0.60	1.65	0.24	10.95	0.04	-13.22	31.31
148	0.57	1.92	0.27	2.71	0.61	-13.12	31.42

Table 6—Continued

SRC#	χ^2 per d.o.f.	$N_{\rm H}$ 10^{22} cm^{-2}	$N_{{\rm H}err}$	kT keV	kT$_{err}$	Unabs. Flux log ergs cm^{-2}s^{-1}	L$_x$ log ergss^{-1}
149	0.39	3.84	0.40	9.57	0.02	-12.79	31.75
151	0.65	1.99	0.19	2.91	0.42	-12.36	32.18
152	0.51	2.80	0.32	1.98	0.29	-12.97	31.57
153	0.73	5.96	1.01	1.32	–	-13.30	31.24
154	0.47	2.97	–	1.34	–	-13.55	30.99
155	0.26	2.47	–	3.52	–	-13.31	31.23
158	0.18	2.90	0.65	1.89	0.63	-13.25	31.29
159	0.32	1.38	0.61	3.26	2.02	-13.85	30.69
160	0.28	2.74	0.38	4.69	–	-13.41	31.13
162	0.08	2.81	1.31	1.82	1.20	-13.59	30.95
163	0.19	1.89	1.15	2.68	2.67	-13.74	30.80
164	0.46	1.95	0.39	3.81	1.50	-13.20	31.34
165	0.16	2.79	–	14.22	–	-13.71	30.82
166	0.26	2.54	0.37	4.33	0.71	-13.11	31.43
168	0.23	2.57	1.12	5.67	0.23	-13.84	30.70
170	0.22	1.34	–	2.84	–	-13.79	30.75
171	0.53	1.86	0.18	3.59	0.50	-12.73	31.81
173	0.49	8.28	–	1.83	–	-13.04	31.50
174	0.73	3.37	0.26	5.13	0.69	-12.58	31.96
176	0.32	6.58	0.86	1.63	–	-13.28	31.25
177	0.21	3.46	1.06	1.86	0.72	-13.33	31.21
181	0.27	2.79	0.70	2.56	1.12	-13.38	31.16
183	0.37	1.95	0.43	1.49	0.39	-13.48	31.05
184	0.11	3.43	–	2.07	–	-13.58	30.96
185	0.47	1.81	–	2.67	–	-13.74	30.79
189	0.10	4.73	2.83	1.30	1.01	-13.21	31.33
190	0.45	3.85	0.42	2.58	–	-13.13	31.40
194	0.36	2.30	–	3.63	–	-13.00	31.53
197	0.47	2.07	–	3.60	–	-12.91	31.63
198	0.32	1.89	0.92	3.15	3.34	-13.34	31.19
200	0.24	1.83	0.43	2.36	0.76	-13.28	31.26
201	0.21	1.71	0.69	2.02	0.94	-13.90	30.64

Table 6—Continued

SRC#	χ^2 per d.o.f.	$N_{\rm H}$ 10^{22} cm^{-2}	$N_{{\rm H}err}$	kT keV	kT$_{err}$	Unabs. Flux log ergs cm^{-2}s^{-1}	L$_x$ log ergss^{-1}
202	0.33	2.17	0.61	2.56	0.74	-13.57	30.97
203	0.29	3.18	1.34	2.33	0.85	-13.64	30.90
205	0.38	4.39	–	1.83	–	-12.81	31.73
209	0.45	1.68	–	3.50	–	-13.61	30.92
210	0.26	2.81	0.21	2.94	–	-13.69	30.85
211	0.10	1.57	0.76	3.37	1.69	-13.96	30.58
212	0.75	1.09	0.46	3.66	1.69	-13.91	30.62
213	0.18	1.90	0.05	2.81	–	-13.60	30.93
214	0.37	0.86	0.11	4.38	0.76	-13.17	31.37
215	0.11	5.63	2.15	2.02	0.80	-13.43	31.11
217	0.18	3.53	0.72	1.69	0.29	-13.19	31.35
218	0.49	1.72	0.32	2.64	0.59	-13.29	31.25
220	0.72	1.89	–	2.83	–	-12.38	32.15
223	0.62	1.87	0.33	2.64	0.69	-12.87	31.67
224	0.16	2.11	0.71	1.06	0.38	-13.57	30.97
229	0.41	1.72	0.26	1.56	0.28	-13.19	31.35
230	0.16	1.82	0.82	3.01	1.65	-13.72	30.81
233	0.59	3.51	1.00	3.94	3.15	-13.14	31.39
236	0.12	4.75	1.66	4.91	2.64	-13.41	31.12
238	0.41	1.99	0.29	3.92	1.22	-12.89	31.65
239	0.33	3.21	1.14	0.97	0.35	-13.14	31.40
240	0.26	3.44	2.60	1.98	1.97	-13.44	31.09
241	0.26	2.41	1.33	1.66	1.20	-13.72	30.82
243	0.36	2.21	0.98	2.91	2.10	-13.02	31.51
244	0.24	2.83	1.08	3.00	1.95	-13.56	30.98
246	0.15	1.59	0.36	3.64	1.38	-13.35	31.18
249	0.24	5.72	–	3.57	–	-13.20	31.34
250	0.25	4.33	1.18	2.14	0.51	-13.32	31.22
251	0.95	23.04	–	10.69	–	-12.26	32.28
252	0.33	3.55	0.76	3.62	–	-13.64	30.90
253	0.33	5.22	1.81	4.75	2.42	-13.25	31.28
255	0.73	6.05	1.41	3.36	1.64	-12.77	31.77

Table 6—Continued

SRC#	χ^2 per d.o.f.	$N_{\rm H}$ 10^{22} cm^{-2}	$N_{{\rm H}err}$	kT keV	kT$_{err}$	Unabs. Flux log ergs cm^{-2}s^{-1}	L$_x$ log ergss^{-1}
259	0.57	9.61	2.64	2.50	0.95	-13.18	31.36
260	0.29	0.91	–	>15	–	-13.94	30.60
261	0.15	5.99	0.38	2.85	–	-13.01	31.53
263	0.28	1.50	0.25	2.05	0.43	-13.06	31.48
264	0.53	4.66	2.27	1.42	0.57	-13.35	31.19
265	0.50	2.88	1.19	3.87	1.94	-13.69	30.84
266	0.21	3.15	0.96	1.08	0.62	-13.44	31.10
271	0.28	3.07	0.56	3.13	1.18	-13.19	31.34
272	0.35	3.81	0.77	2.65	0.64	-13.32	31.22
274	0.13	4.20	–	1.78	–	-13.18	31.36
276	0.15	3.77	0.82	1.92	0.53	-13.16	31.37
281	0.31	1.64	0.59	1.83	0.77	-13.38	31.15
282	0.36	3.90	1.11	1.49	0.49	-13.14	31.40
284	0.13	6.08	1.10	5.79	–	-13.21	31.32
287	0.27	2.59	0.84	2.38	0.93	-13.69	30.85
289	0.37	1.16	0.16	4.95	1.64	-12.89	31.64
292	0.39	14.58	–	>15	–	-13.56	30.98
293	0.35	3.93	0.58	2.64	0.70	-12.70	31.84
297	0.12	8.83	3.90	3.28	1.23	-13.40	31.13
316	0.28	4.18	–	1.80	–	-13.54	31.00
317	0.40	3.79	1.37	1.48	0.76	-13.54	31.00
320	0.31	2.34	0.58	1.69	0.49	-13.52	31.02
322	0.18	11.90	–	3.51	–	-13.09	31.45
330	0.39	5.88	–	1.31	–	-13.19	31.35
331	0.34	2.95	1.04	1.09	0.52	-13.53	31.01
339	0.25	3.07	0.93	3.83	1.90	-13.63	30.91
343	0.38	5.29	–	1.99	–	-13.35	31.18
345	0.46	0.75	–	>15	–	-13.85	30.69
349	0.10	2.01	0.70	3.38	0.17	-13.84	30.70
356	0.20	4.14	0.78	2.12	0.42	-13.19	31.35
358	0.15	1.14	–	1.24	–	-13.68	30.85
361	0.20	4.78	0.94	3.41	–	-13.31	31.23

Table 6—Continued

SRC#	χ^2 per d.o.f.	$N_{\rm H}$ 10^{22} cm^{-2}	$N_{{\rm H}err}$	kT keV	kT$_{err}$	Unabs. Flux log ergs cm^{-2}s^{-1}	L$_x$ log ergss^{-1}
362	0.10	0.94	0.46	2.21	1.35	-13.98	30.56
366	0.52	2.58	–	2.43	–	-12.81	31.73
368	0.21	2.60	0.92	1.02	0.31	-13.31	31.23
371	0.25	1.47	0.56	3.26	0.13	-13.94	30.60
372	0.23	2.85	0.92	2.26	0.78	-13.47	31.07
374	0.34	2.33	0.69	3.14	1.06	-13.58	30.96
379	0.26	1.33	0.37	4.04	1.39	-13.51	31.02
380	0.19	1.81	1.07	0.62	0.66	-13.21	31.33
392	0.16	1.30	0.75	1.88	1.10	-13.51	31.03
396	0.33	2.02	0.19	3.55	–	-13.66	30.88
398	0.38	2.62	0.88	1.96	1.09	-13.25	31.28
400	0.14	3.99	1.24	1.25	0.48	-13.18	31.36
409	0.14	1.22	0.62	1.63	0.84	-14.01	30.53
413	0.48	5.94	3.03	2.32	1.17	-13.33	31.20
414	0.21	1.09	–	1.44	–	-13.56	30.98
415	0.16	1.98	0.51	1.69	0.42	-13.38	31.15
420	0.19	2.04	0.19	2.79	–	-13.60	30.94
423	0.57	3.29	–	2.07	–	-13.60	30.93
427	0.47	1.07	0.33	2.43	1.12	-13.42	31.12
430	0.16	1.70	–	>15	–	-13.96	30.58
433	0.33	0.73	–	4.03	–	-13.90	30.64
440	0.27	0.33	–	5.39	–	-14.02	30.52
444	0.23	1.92	0.47	4.17	1.43	-13.47	31.06
445	0.05	2.13	–	0.78	–	-13.40	31.13
451	0.19	7.26	–	4.73	–	-13.39	31.15
453	0.59	0.81	–	2.21	–	-13.70	30.84
455	0.60	4.93	1.89	2.47	1.30	-13.27	31.27

Table 7. Faint Cluster Members Fit with 1 Temperature Spectra

SRC#	χ^2 per d.o.f.	$N_{\rm H}$ 10^{22} cm^{-2}	$N_{\rm H}{}_{err}$	kT keV	kT$_{err}$	Unabs. Flux log ergs cm^{-2}s^{-1}	L$_x$ log ergss^{-1}
26	0.26	3.39	0.94	2.06	0.63	-13.84	30.00
27	0.26	8.80	1.12	0.46	0.05	-11.64	29.88
38	0.27	1.39	0.57	>15	–	-13.98	30.39
41	0.22	16.87	3.19	0.87	0.12	-12.22	29.98
43	0.31	2.03	0.55	3.01	1.05	-13.85	30.20
45	0.24	2.12	0.73	4.70	1.99	-13.96	30.21
47	0.27	7.15	1.74	2.09	0.49	-13.41	30.21
48	0.30	0.85	0.29	1.88	0.59	-14.07	29.98
49	0.24	7.94	2.55	1.98	0.60	-13.67	29.91
52	0.21	7.23	2.62	2.92	0.94	-13.67	30.15
58	0.32	1.88	0.44	0.71	0.17	-13.62	29.48
60	0.23	2.72	0.88	2.50	0.94	-14.02	29.93
63	0.26	1.69	0.48	1.39	0.40	-13.93	29.86
65	0.24	2.96	1.02	7.82	–	-13.92	30.28
68	0.17	3.86	0.62	0.60	0.09	-12.80	29.74
75	0.22	9.52	2.18	0.96	0.17	-12.89	29.82
76	0.20	2.13	0.45	1.44	0.33	-13.73	30.00
77	0.23	6.39	1.21	1.20	0.21	-13.15	30.07
79	0.23	2.44	0.80	1.44	0.51	-14.07	29.63
85	0.55	2.44	0.59	2.22	0.59	-13.77	30.16
87	0.25	1.31	0.39	1.68	0.52	-14.07	29.86
88	0.53	2.22	0.52	1.68	0.42	-13.82	30.01
89	0.54	4.94	1.30	2.76	0.82	-13.69	30.18
90	0.21	3.48	0.85	2.32	0.59	-13.71	30.15
91	0.55	3.34	1.27	>15	–	-13.88	30.43
96	0.52	1.91	0.84	4.72	2.75	-14.32	29.88
99	0.21	3.85	1.18	2.93	0.94	-13.85	30.11
100	0.24	1.31	0.40	1.83	0.58	-14.09	29.88
106	0.24	4.93	1.52	> 15	–	-13.67	30.54
109	0.56	12.72	1.63	0.71	0.07	-11.83	30.15
111	0.21	8.35	2.06	1.82	0.36	-13.34	30.15
117	0.55	21.67	3.22	1.19	0.12	-12.27	30.36

Table 7—Continued

SRC#	χ^2 per d.o.f.	$N_{\rm H}$ 10^{22} cm^{-2}	$N_{{\rm H}err}$	kT keV	kT$_{err}$	Unabs. Flux log ergs cm^{-2}s^{-1}	L$_x$ log ergss^{-1}
121	0.22	6.09	1.37	2.32	0.52	-13.45	30.29
123	0.29	4.13	1.38	3.72	1.48	-13.92	30.11
124	0.15	1.83	0.70	2.93	1.32	-14.23	29.83
128	0.18	0.77	0.32	1.75	0.70	-14.28	29.76
131	0.55	2.33	0.85	14.10	–	-13.90	30.39
134	0.53	11.31	1.75	0.81	0.08	-12.23	30.10
135	0.20	3.85	1.12	2.77	0.96	-13.85	30.07
136	0.54	3.38	0.81	1.83	0.42	-13.68	30.08
139	0.19	1.35	0.28	0.75	0.17	-13.77	29.59
142	0.18	2.91	0.52	0.90	0.15	-13.36	29.85
150	0.20	5.14	0.93	1.26	0.22	-13.24	30.10
153	0.56	1.22	0.42	5.41	2.57	-14.03	30.23
156	0.55	1.18	0.38	3.71	1.47	-14.06	30.14
161	0.54	1.05	0.37	3.71	1.49	-14.15	30.06
167	0.51	1.35	0.42	1.83	0.61	-14.17	29.80
178	0.54	3.15	0.55	1.19	0.21	-13.47	30.01
180	0.52	2.34	0.47	1.25	0.25	-13.69	29.93
182	0.53	0.99	0.45	4.15	2.00	-14.25	29.98
186	0.53	1.27	0.60	>15	–	-14.14	30.19
187	0.53	1.16	0.39	2.17	0.80	-14.20	29.85
188	0.12	2.15	0.69	4.49	1.96	-13.48	30.68
191	0.54	1.47	0.41	2.32	0.72	-14.02	30.02
193	0.52	5.39	1.14	1.24	0.25	-13.40	29.93
195	0.51	5.15	1.16	1.21	0.26	-13.50	29.82
196	0.52	2.94	0.72	1.83	0.44	-13.75	29.97
199	0.15	7.27	1.53	0.70	0.12	-12.71	29.64
204	0.55	4.52	0.86	1.42	0.25	-13.41	30.10
208	0.51	4.33	0.67	0.68	0.09	-12.74	29.83
222	0.15	6.59	2.24	2.82	1.01	-13.83	30.00
231	0.56	6.17	2.08	9.55	5.08	-13.67	30.49
232	0.17	6.06	1.98	9.55	4.99	-13.66	30.49
234	0.52	11.86	2.46	1.36	0.20	-13.00	30.11

Table 7—Continued

SRC#	χ^2 per d.o.f.	$N_{\rm H}$ 10^{22} cm^{-2}	$N_{{\rm H}err}$	kT keV	kT$_{err}$	Unabs. Flux log ergs cm^{-2}s^{-1}	L$_x$ log ergss^{-1}
235	0.54	1.18	0.37	2.87	1.06	-14.07	30.07
242	0.25	2.31	0.75	>15	–	-13.81	30.51
247	0.54	17.13	2.67	1.11	0.12	-12.36	30.28
248	0.56	4.66	1.34	>15	–	-13.70	30.52
256	0.51	3.04	0.81	1.65	0.46	-13.88	29.85
257	0.51	2.49	1.08	6.18	–	-14.26	29.94
258	0.53	2.59	0.74	2.68	0.93	-13.96	30.03
267	0.53	2.75	0.72	2.32	0.67	-13.88	30.04
269	0.54	8.15	2.46	4.70	1.58	-13.62	30.36
270	0.51	5.41	2.55	>15	–	-14.12	30.14
273	0.53	10.22	2.62	2.60	0.68	-13.46	30.22
275	0.52	2.54	0.77	2.32	0.73	-13.96	29.88
278	13	22.10	5.07	0.94	0.16	-12.43	29.75
279	0.51	3.23	0.90	1.88	0.52	-13.85	29.85
280	0.23	1.41	0.40	3.15	1.04	-13.94	30.19
283	0.52	1.64	0.50	2.24	0.76	-14.11	29.89
288	0.14	1.07	0.34	2.48	0.87	-14.10	30.00
290	0.16	2.97	0.64	1.62	0.35	-13.66	30.06
291	0.53	5.55	1.45	2.48	0.68	-13.68	30.12
292	0.15	22.11	4.95	4.44	1.16	-13.13	30.61
294	0.16	3.93	0.98	1.83	0.45	-13.75	29.98
295	0.13	1.95	0.65	1.99	0.75	-14.20	29.73
296	0.26	3.00	0.64	1.52	0.36	-13.60	30.09
298	0.18	1.86	0.45	1.48	0.34	-13.89	29.90
299	0.16	18.77	6.07	>15	–	-13.53	30.56
301	0.13	9.30	3.99	8.95	–	-14.01	30.07
302	0.13	32.96	5.13	1.35	0.15	-12.26	30.34
303	0.15	3.89	1.40	>15	–	-13.93	30.31
304	0.12	11.69	4.67	7.66	–	-13.89	30.13
305	0.18	8.70	1.62	1.69	0.25	-13.14	30.29
307	0.12	4.57	1.10	2.89	0.75	-13.64	30.27
308	0.14	8.14	2.57	1.29	0.35	-13.57	29.63

Table 7—Continued

SRC#	χ^2 per d.o.f.	$N_{\rm H}$ 10^{22} cm^{-2}	$N_{{\rm H}err}$	kT keV	kT$_{err}$	Unabs. Flux log ergs cm^{-2}s^{-1}	L$_x$ log ergss^{-1}
309	0.13	2.04	0.51	1.17	0.32	-13.63	29.98
310	0.31	11.10	3.14	3.59	1.07	-13.35	30.46
311	0.10	30.18	6.91	1.44	0.24	-12.03	30.71
314	0.14	8.12	2.62	3.71	1.28	-13.74	30.15
318	0.44	3.09	1.04	>15	–	-13.83	30.49
319	0.14	4.35	1.21	2.93	0.85	-13.76	30.17
323	0.19	2.94	0.48	1.12	0.19	-13.40	30.04
324	0.10	4.27	1.67	2.93	1.22	-14.17	29.76
326	0.20	0.75	0.27	2.58	1.02	-14.18	29.98
327	0.12	1.47	0.44	1.29	0.37	-14.13	29.63
328	0.10	13.33	4.54	3.16	1.05	-13.67	30.04
332	0.19	3.34	0.57	1.25	0.23	-13.40	30.10
334	0.15	2.35	0.86	12.09	8.31	-14.04	30.23
335	0.15	1.74	0.56	1.83	0.57	-14.18	29.74
336	0.09	62.65	14.24	1.44	0.28	-12.32	30.00
337	0.13	9.83	1.98	1.44	0.23	-13.12	30.12
341	0.15	8.00	2.16	3.71	1.08	-13.56	30.34
342	0.19	2.09	0.61	1.83	0.55	-14.07	29.80
344	0.19	1.87	0.50	1.27	0.35	-14.03	29.66
346	0.20	23.27	4.52	2.31	0.41	-12.81	30.56
347	0.11	22.02	6.14	2.08	0.49	-13.15	30.13
351	0.09	2.92	0.79	2.60	0.80	-13.65	30.30
353	0.23	3.37	1.12	8.52	–	-13.73	30.45
354	0.10	1.04	0.54	3.57	2.03	-13.99	30.20
360	0.08	2.80	1.11	1.73	0.76	-14.15	29.62
363	0.09	4.38	1.31	1.14	0.31	-13.57	29.73
367	0.12	4.62	1.18	2.32	0.61	-13.73	30.08
370	0.05	2.78	1.50	13.92	–	-14.42	29.84
373	0.13	0.58	0.27	2.90	1.21	-14.34	29.89
377	0.12	7.74	1.91	1.83	0.35	-13.42	30.10
381	0.08	3.55	0.85	0.99	0.23	-13.65	29.59
382	0.15	3.28	0.99	1.83	0.55	-14.00	29.77

Table 7—Continued

SRC#	χ^2 per d.o.f.	$N_{\rm H}$ 10^{22} cm^{-2}	$N_{{\rm H}err}$	kT keV	kT$_{err}$	Unabs. Flux log ergs cm^{-2}s^{-1}	L$_x$ log ergss^{-1}
384	0.14	12.62	5.13	16.21	–	-13.79	30.31
385	0.14	2.04	0.83	4.13	2.06	-14.27	29.88
386	0.12	5.92	2.29	3.29	1.43	-14.05	29.85
387	0.08	1.05	0.74	>15	–	-14.69	29.65
388	0.13	2.02	0.44	1.34	0.32	-13.75	29.96
390	0.13	1.96	0.58	1.07	0.34	-14.10	29.44
391	0.13	0.98	0.37	2.01	0.83	-14.32	29.74
393	0.21	3.83	0.90	0.75	0.19	-13.34	29.50
395	0.08	1.10	0.44	1.83	0.71	-14.05	29.95
401	0.17	0.73	0.28	3.29	1.31	-14.18	30.05
402	0.12	2.99	0.70	0.97	0.25	-13.69	29.58
403	0.25	2.29	0.63	2.32	0.70	-13.92	30.05
405	0.12	1.25	0.43	1.83	0.58	-14.21	29.76
406	0.16	8.30	1.57	1.57	0.22	-13.12	30.27
408	0.12	0.36	0.22	2.32	0.89	-14.50	29.73
412	0.13	4.37	1.27	3.00	0.97	-13.78	30.16
416	0.11	1.55	0.47	1.70	0.56	-14.00	29.91
418	0.15	0.84	0.35	2.84	1.25	-14.28	29.89
419	0.12	3.03	0.79	0.90	0.22	-13.67	29.52
422	0.14	3.86	0.97	1.04	0.24	-13.59	29.66
424	0.19	4.85	1.34	2.93	0.84	-13.70	30.22
429	0.17	11.76	3.95	7.54	3.26	-13.55	30.47
431	0.17	5.80	2.43	3.72	1.43	-13.86	30.10
435	0.27	1.18	0.29	1.44	0.34	-13.92	29.98
436	0.21	5.30	1.21	0.90	0.18	-13.18	29.74
441	0.27	1.70	0.46	1.36	0.36	-13.92	29.81
445	0.32	1.94	0.31	0.78	0.14	-13.29	29.90
448	0.23	1.26	0.60	>15	–	-14.15	30.21
459	0.51	5.66	1.48	1.71	0.40	-13.68	29.92
460	0.50	5.94	1.45	1.22	0.27	-13.52	29.76
461	0.53	0.88	0.30	2.74	0.98	-14.14	30.03

Table 8. X-ray Spectral fits to Bright Non-member X-ray Sources.

SRC#	χ^2 per d.o.f.	$N_{\rm H}$ 10^{22} cm^{-2}	$N_{{\rm H}err}$	kT keV	kT$_{err}$	Unabs. Flux log ergs cm^{-2}s^{-1}
1	0.54	1.24	0.42	0.34	0.08	-13.00
2	0.14	2.43	–	1.82	–	-13.70
6	0.20	1.00	0.39	0.72	0.29	-13.57
13	0.34	0.46	0.34	4.60	0.15	-14.22
32	0.62	0.26	0.37	4.28	0.13	-14.41
34	0.12	0.00	0.17	0.30	–	-14.46
54	0.06	0.01	–	1.04	–	-14.32
61	0.21	4.82	0.66	3.31	–	-13.72
64	0.18	0.53	0.48	0.76	0.44	-14.19
69	0.53	0.60	0.15	0.37	0.07	-13.11
80	0.35	0.51	–	0.82	–	-14.17
113	0.50	0.56	0.43	2.46	1.17	-14.09
175	0.16	0.64	0.37	0.90	0.27	-14.10
214	0.37	0.86	0.11	4.38	0.76	-13.17
245	0.09	1.02	–	1.76	–	-14.01
277	0.16	0.16	–	0.91	–	-14.50
286	0.30	0.40	–	0.60	–	-14.21
399	0.34	1.25	–	1.14	–	-13.39
434	0.08	0.75	0.03	1.89	–	-14.22
446	0.37	0.49	0.25	1.00	0.19	-13.63
447	0.40	1.18	0.12	0.29	0.04	-11.95
452	0.24	0.75	0.21	0.14	0.03	-12.30
454	0.22	1.84	0.62	0.64	0.27	-13.37

Table 9. X-ray Spectral fits to Faint Non-member Sources.

SRC#	χ^2 per d.o.f.	$N_{\rm H}$ 10^{22} cm^{-2}	$N_{{\rm H}err}$	kT keV	kT$_{err}$	Unabs. Flux log ergs cm^{-2}s^{-1}
5	0.37	0.27	–	>15	–	-14.15
7	0.40	3.26	1.27	>15	–	-13.82
9	0.33	6.69	0.85	0.39	0.03	-11.72
10	0.35	3.32	0.64	1.27	0.27	-13.44
12	0.33	2.97	0.97	2.80	1.06	-13.85
14	0.35	3.64	1.12	3.71	1.28	-13.67
15	0.25	0.63	0.15	0.34	0.06	-13.87
17	0.25	1.28	0.14	0.17	0.02	-12.02
18	0.35	0.79	0.34	5.47	2.95	-14.13
20	0.38	2.43	1.02	>15	–	-13.90
29	0.22	0.56	0.34	4.95	–	-14.46
36	0.31	4.95	1.34	1.58	0.42	-13.56
42	0.21	0.80	0.15	0.49	0.09	-13.81
44	0.27	0.68	0.44	>15	–	-14.29
51	0.26	1.18	0.60	9.55	–	-14.33
61	0.28	2.47	0.91	>15	–	-13.90
74	0.28	1.55	0.48	3.05	1.21	-13.98
81	0.25	4.31	1.54	8.19	–	-13.90
83	0.23	1.24	0.23	0.64	0.14	-13.58
84	0.25	2.40	0.76	4.30	1.84	-13.94
102	0.14	1.34	0.48	1.14	0.33	-14.35
105	0.20	1.44	0.83	>15	–	-14.20
119	0.52	5.68	1.61	1.95	0.53	-13.71
137	0.54	0.01	–	>15	–	-14.40
206	0.17	0.46	0.12	0.25	0.03	-13.83
216	0.52	2.97	0.88	1.37	0.44	-14.00
237	0.16	7.56	3.41	>15	–	-13.95
254	0.23	1.88	0.40	0.44	0.10	-13.40
262	0.55	1.02	0.42	12.09	8.19	-14.14
268	0.16	8.97	1.78	0.72	0.12	-12.46
300	0.28	0.01	–	4.51	–	-14.39
306	0.20	7.55	2.65	2.32	0.78	-13.82

Table 9—Continued

SRC#	χ^2 per d.o.f.	$N_{\rm H}$ 10^{22} cm^{-2}	$N_{{\rm H}err}$	kT keV	kT$_{err}$	Unabs. Flux log ergs cm^{-2}s^{-1}
312	0.23	2.58	1.35	>15	12.78	-14.24
313	0.14	3.74	1.54	>15	–	-13.99
315	0.23	1.49	0.24	0.54	0.10	-13.42
321	0.10	3.07	1.62	>15	–	-14.29
325	0.33	2.42	0.81	>15	–	-13.76
329	0.08	0.92	0.32	1.01	0.39	-14.17
333	0.22	3.85	1.21	>15	–	-13.71
338	0.20	2.46	0.96	>15	–	-14.01
340	0.19	4.91	2.03	>15	–	-13.98
348	0.19	0.65	0.11	0.28	0.04	-13.43
350	0.11	1.46	1.00	>15	–	-14.61
352	0.13	0.81	0.55	>15	–	-14.46
355	0.06	0.83	0.16	0.35	0.06	-13.45
357	0.09	2.22	1.35	>15	–	-14.09
359	0.42	3.93	1.28	4.35	1.90	-13.74
365	0.15	2.86	1.11	>15	–	-13.96
369	0.20	1.34	0.31	1.14	0.21	-13.93
375	0.18	0.43	0.23	1.88	0.72	-14.47
376	0.10	1.33	0.75	>15	–	-14.48
378	0.11	2.32	0.81	3.51	1.47	-14.14
383	0.16	0.01	–	2.14	1.09	-14.55
397	0.13	0.01	–	0.32	0.07	-14.83
407	0.12	0.01	–	0.44	0.14	-15.08
410	0.39	0.01	–	0.77	0.37	-14.77
411	0.28	0.31	0.19	2.76	1.38	-14.40
417	0.11	10.20	1.73	0.45	0.07	-11.81
421	0.19	0.93	0.44	4.70	2.53	-14.29
425	0.47	6.16	2.49	2.42	0.96	-13.81
426	0.22	0.82	0.21	0.87	0.17	-14.01
428	0.23	0.92	0.41	2.58	1.22	-14.33
432	0.14	1.20	0.14	0.20	0.02	-12.53
437	0.18	0.14	–	>15	–	-14.57

Table 9—Continued

SRC#	χ^2 per d.o.f.	$N_{\rm H}$ 10^{22} cm^{-2}	$N_{{\rm H}err}$	kT keV	kT$_{err}$	Unabs. Flux log ergs cm^{-2}s^{-1}
438	0.19	0.32	0.22	1.83	0.71	-14.43
439	0.17	5.10	2.22	15.32	–	-14.05
442	0.30	0.95	0.19	0.69	0.16	-13.88
443	0.30	0.28	0.22	1.14	0.29	-14.67
449	0.24	1.57	0.79	19.40	>15	-14.19
454	0.35	1.31	0.21	0.70	0.13	-13.51

Table 10. IR Photometry of X-ray Sources (members)

SRC#	IR ID	offset	J	Jerr	H	Herr	K	Kerr	A_V	Model	flags
4	2MASS085829.85-472823.0	1.11	14.058	0.028	12.895	0.026	12.429	0.019	5.16	GK STAR	AAA
8	2MASS085834.64-472816.4	0.30	14.968	0.032	13.312	0.02	12.314	0.019	10.32	M STAR	AAA
14	2MASS085842.04-472628.3	1.29	15.459	0.047	14.406	0.054	13.98	0.06	4.4	Bright	AAA
16	2MASS085842.58-473156.7	0.91	14.599	0.033	13.602	0.046	13.12	0.036	2.74	Bright	AAA
19	2MASS085843.51-472934.3	0.40	16.556	0.161	14.881	0.062	14.049	0.068	11.14	Bright	CAA
21	2MASS085843.88-472856.9	0.22	12.572	0.023	11.529	0.027	10.76	0.023	5.35	M STAR	AAA
22	2MASS085844.19-473441.4	1.44	17.086	—	15.336	0.113	13.536	0.067	—	—	UBA
23	2MASS085844.40-473253.3	0.26	14.64	0.042	13.299	0.03	12.658	0.035	6.22	Disk	AAA
24	2MASS085844.53-473406.5	0.57	16.619	0.165	14.394	0.048	13.295	0.042	14.77	GK STAR	CAA
26	2MASS085846.69-473035.7	0.43	16.357	—	15.065	0.085	13.843	0.063	—	—	UAA
27	2MASS085847.18-473151.3	0.38	18.017	—	15.759	0.149	14.791	0.126	—	—	UBB
28	2MASS085847.53-473322.9	1.38	16.381	—	15.673	0.133	14.687	0.122	—	—	UBB
30	2MASS085847.70-472817.4	0.97	13.966	—	15.087	0.09	14.443	0.113	—	—	UAB
31	2MASS085848.63-473221.4	0.05	16.987	0.23	14.336	0.047	13.106	0.044	—	—	DAA
33	2MASS085849.15-473409.1	1.02	15.509	0.093	13.652	0.062	12.683	0.054	10.72	Disk	AAA
35	2MASS085849.59-473255.4	0.06	15.873	—	15.077	0.086	14.326	0.092	—	—	UAA
36	2MASS085849.83-473520.6	0.79	17.246	—	15.83	0.144	14.501	0.096	—	—	UBA
37	2MASS085849.96-472857.5	0.15	16.972	0.217	15.446	0.1	14.975	0.148	—	—	DAB
38	2MASS085850.11-473008.3	0.49	17.893	—	15.271	—	14.729	0.141	—	—	UUB
40	2MASS085850.66-473239.6	0.53	15.354	0.056	14.039	0.041	13.523	0.044	6.86	GK STAR	AAA
43	2MASS085851.15-473437.3	0.35	14.631	—	14.548	0.06	13.897	0.069	—	—	UAA
50	2MASS085852.94-473309.1	0.16	15.91	0.095	14.101	0.048	13.201	0.057	10.61	—	AAA
53	2MASS085853.91-473051.4	0.11	12.48	0.018	10.949	0.023	10.307	0.021	8.84	GK STAR	AAA
55	2MASS085854.03-473102.2	0.17	17.188	—	15.608	0.137	13.535	0.051	—	—	UBA
57	2MASS085854.25-472949.8	0.20	14.642	0.039	13.279	0.036	12.558	0.046	5.88	Disk	AAA
58	2MASS085854.39-472551.6	1.14	15.695	0.085	14.364	0.053	13.747	0.063	6.52	M STAR	AAA
59	2MASS085854.49-472429.4	0.24	13.834	0.026	12.418	0.025	11.85	0.026	7.84	GK STAR	AAA
60	2MASS085854.47-473159.7	0.38	15.599	—	15.205	0.157	13.99	0.142	—	—	UCB
62	2MASS085854.85-473433.3	0.30	15.066	—	13.574	0.046	12.369	—	—	—	UAU
63	2MASS085854.97-472658.6	0.33	16.308	0.112	14.427	0.045	13.741	0.045	13.33	GK STAR	BAA
66	2MASS085855.11-473500.1	0.07	13.957	0.025	12.829	0.025	12.377	0.028	4.79	GK STAR	AAA
67	2MASS085855.25-473150.3	0.89	14.354	—	15.166	0.106	14.131	0.147	—	—	UAB
68	2MASS085855.26-473120.4	0.15	16.665	0.178	15.005	0.067	14.692	0.111	13.26	GK STAR	CAB
71	2MASS085855.56-472745.2	0.66	15.921	0.102	13.933	0.044	12.623	0.031	9.8	—	AAA
72	2MASS085855.85-473251.2	0.44	17.441	—	14.797	0.063	13.844	0.046	—	—	UAA
73	2MASS085855.91-473150.1	0.15	16.616	—	15.375	0.118	13.466	0.095	—	—	UBE
74	2MASS085856.09-473520.9	0.20	15.639	0.079	14.311	0.039	13.925	0.06	8.08	GK STAR	AAA
75	2MASS085856.47-473223.2	0.28	15.592	—	14.571	—	14.57	0.168	—	—	UUC
77	2MASS085857.11-473238.5	0.70	17.368	—	15.754	0.144	13.978	0.056	—	—	UBA
79	2MASS085857.41-472730.1	0.80	16.026	—	15.312	0.096	14.434	0.105	—	—	UAA
81	2MASS085857.47-472744.2	0.77	16.83	—	15.313	—	14.612	0.119	—	—	UUB
82	2MASS085857.74-472918.8	0.12	19.621	3.036	14.987	0.067	13.98	0.075	—	—	DAA
85	VLT085857.88-473018.0	1.28	18	0.076	15.522	0.016	14.242	0.014	16.82	GK STAR	
86	VLT085857.92-473031.6	0.37	16.416	0.031	15.064	0.014	13.582	0.01	0	—	
87	2MASS085857.96-472733.7	0.58	15.775	0.084	14.575	0.07	13.854	0.074	6.14	M STAR	AAA
89	VLT085857.95-473122.1	0.28	18.835	0.096	16.419	0.023	14.803	0.016	13.27	Disk	
90	VLT085858.11-473144.9	0.21	—	—	—	—	14.945	—	—	—	FNT
92	2MASS085858.30-473257.9	0.13	15.651	0.121	14.027	0.057	13.049	0.056	10.03	M STAR	BAA
93	2MASS085858.31-472727.6	0.47	14.129	0.035	13.029	0.037	12.521	0.046	3.95	Disk	AAA
94	VLT085858.51-473059.1	0.22	—	—	17.283	—	14.768	—	—	—	FNT
96	VLT085858.59-473016.7	0.27	—	—	15.65	—	13.368	—	—	—	FNT
97	VLT085858.61-473110.3	0.62	15.299	0.018	13.98	0.008	13.417	0.009	6.54	GK STAR	
99	VLT085858.75-473144.2	0.35	—	—	15.654	—	14.424	—	—	—	FNT
100	2MASS085858.85-472725.0	0.07	15.82	—	14.841	0.07	13.98	0.075	—	—	UAA
101	VLT085858.91-473054.2	0.26	17.119	0.047	14.647	0.011	13.376	0.009	17.48	—	
104	2MASS085859.13-472809.0	0.20	15.225	—	14.36	0.075	13.66	0.104	—	—	UAA
106	2MASS085859.19-473232.9	0.34	17.471	—	16.371	—	13.947	0.068	—	—	UUA
107	2MASS085859.17-472658.1	0.48	12.215	0.019	10.989	0.025	10.319	0.018	9.99	Bright	AAA
109	VLT085859.43-473111.5	0.34	—	—	16.719	—	14.858	—	—	—	FNT
110	VLT085859.51-472952.4	0.32	15.566	0.019	13.769	0.007	12.627	0.006	11.88	M STAR	
111	2MASS085859.65-473228.6	0.37	17.52	—	14.389	—	14.143	0.138	—	—	UUB
112	2MASS085859.82-473222.8	0.76	14.443	0.028	11.175	0.023	9.407	0.025	25.47	Bright	AAA
114	VLT085859.87-473014.4	0.25	16.437	0.029	15.129	0.013	14.544	0.016	6.21	GK STAR	
115	2MASS085859.89-473552.2	0.73	15.347	0.053	13.882	0.041	13.092	0.041	6.74	—	AAA
116	VLT085859.92-472947.8	0.47	14.984	0.014	13.136	0.005	11.99	0.004	12.22	M STAR	
117	VLT085859.95-473104.2	0.3	19.946	—	19.132	—	17.303	—	—	—	FNT
119	VLT085900.05-473040.6	0.28	17.069	—	15.916	—	15.003	—	—	—	FNT

Table 10—Continued

SRC#	IR ID	offset	J	Jerr	H	Herr	K	Kerr	A_V	Model	flags
120	VLT085900.08-473007.0	0.17	15.334	0.017	14.011	0.008	13.23	0.008	7.21	M STAR	
122	2MASS085900.15-473311.1	0.19	15.928	0.092	14.348	0.044	13.775	0.071	10.07	GK STAR	AAA
124	2MASS085900.27-472758.4	0.24	17.556	—	15.215	0.075	14.211	0.068	—	—	UAA
125	VLT085900.31-473114.2	0.22	19.351	0.188	15.035	0.012	12.416	0.005	31.5	Disk	
126	VLT085900.31-472940.5	0.40	16.456	0.029	14.847	0.011	13.819	0.01	6.82	Disk	
127	2MASS085900.40-472559.1	0.84	14.395	0.034	12.081	0.027	10.597	0.021	16.74	M STAR	AAA
128	2MASS085900.64-472724.7	0.47	14.663	0.048	13.096	0.034	11.954	—	5.33	Disk	AAU
129	VLT085900.70-473050.8	0.59	16.165	0.045	13.996	0.01	12.92	0.012	14.18	GK STAR	
130	VLT085900.77-473046.8	0.04	14.214	0.012	12.994	0.005	12.511	0.008	5.81	GK STAR	
131	VLT085900.86-472942.4	0.38	—	—	17.19	—	15.954	—	—	—	FNT
132	2MASS085900.93-472819.3	0.28	16.087	0.124	14.486	0.052	14.005	0.055	11.1	—	BAA
133	VLT085901.00-473103.3	0.09	15.223	0.021	13.891	0.008	13.351	0.012	6.9	GK STAR	
134	VLT085901.09-473008.7	0.30	—	—	18.984	—	18.165	—	—	—	FNT
136	VLT085901.20-473131.5	0.58	17.809	0.055	15.385	0.015	14.255	0.013	17.27	—	
138	2MASS085901.51-472324.5	0.89	15.502	—	14.044	0.042	12.978	—	—	—	UAU
139	2MASS085901.49-472831.1	0.52	16.477	0.148	14.9	0.077	14.112	0.084	8.3	Disk	BAA
140	VLT085901.56-473109.9	0.23	14.041	0.009	12.365	0.004	11.449	0.004	8.65	Disk	
141	VLT085901.56-473119.5	0.13	15.774	—	13.991	—	12.963	—	—	—	FNT
142	2MASS085901.58-473210.8	0.60	16.511	0.169	14.832	0.134	13.163	0.098	2.65	—	CBA
143	VLT085901.67-473037.1	0.47	11.188	—	—	—	10.422	—	—	—	BRI
144	VLT085901.72-473046.0	0.25	15.469	0.019	14.015	0.008	13.322	0.009	7.36	Disk	
145	VLT085901.86-473056.7	0.27	14.733	0.013	13.367	0.006	12.784	0.007	7.03	GK STAR	
146	VLT085901.91-473035.0	0.83	16.24	0.035	14.912	0.014	14.295	0.02	6.23	Disk	
147	VLT085901.95-473114.8	0.19	14.418	0.011	12.567	0.004	11.488	0.004	9.76	Disk	
148	VLT085901.97-473102.0	0.48	12.328	0.004	11.453	0.002	10.971	0.003	7.35	Bright	
149	2MASS085902.07-473209.4	0.34	17.302	—	14.369	—	13.195	0.114	—	—	UUB
150	2MASS085902.24-472639.2	1.27	16.61	0.142	14.197	0.039	12.706	0.045	17.41	M STAR	CAA
151	VLT085902.15-473016.8	0.29	12.512	0.005	11.383	0.002	10.926	0.003	4.76	GK STAR	
152	VLT085902.35-472957.9	0.46	17.077	0.04	15.269	0.015	14.305	0.016	10.09	Disk	
153	VLT085902.40-473109.7	0.43	15.828	0.022	14.202	0.009	13.494	0.01	9.62	—	
154	VLT085902.42-472947.9	0.27	15.149	0.016	13.2	0.005	12.262	0.005	12.25	GK STAR	
155	VLT085902.48-473052.7	0.25	16.907	0.055	15.214	0.02	14.386	0.029	10.89	Bright	
156	VLT085902.47-473020.7	0.37	17.01	0.07	15.666	0.025	14.634	0.029	3.12	Disk	
158	VLT085902.53-473046.2	0.35	15.078	0.025	13.493	0.008	12.517	0.01	15.91	Bright	
159	2MASS085902.60-472846.4	0.13	17.009	0.214	15.006	0.07	13.818	0.089	—	—	DAA
161	VLT085902.90-473102.0	0.22	14.223	0.013	13.114	0.006	12.524	0.01	4.97	M STAR	
162	VLT085902.95-473039.8	0.26	15.542	0.02	14.126	0.009	13.526	0.013	7.58	GK STAR	
163	VLT085902.99-473035.6	0.40	15.024	0.028	13.243	0.007	12.238	0.009	9.38	Disk	
164	VLT085902.98-473044.4	0.09	16.208	0.031	13.755	0.007	11.775	0.004	10.86	Disk	
165	VLT085902.94-473051.7	0.97	—	—	15.279	—	13.669	—	0	—	FNT
166	VLT085903.08-472937.9	0.66	15.166	0.016	14.579	0.01	14.248	0.015	5.27	—	
167	2MASS085903.07-473008.7	0.45	16.541	0.045	14.838	0.015	13.943	0.018	9.19	Disk	
168	2MASS085903.35-472853.6	0.16	15.36	—	14.585	0.083	13.03	0.072	—	—	UAE
169	VLT085903.33-473045.4	0.42	16.781	0.049	15.364	0.023	14.621	0.031	10.6	Bright	
170	2MASS085903.47-472428.1	0.30	15.572	—	14.122	—	13.409	0.05	—	—	UUA
171	VLT085903.51-473058.0	0.35	13.81	0.009	12.293	0.004	11.645	0.005	8.6	GK STAR	
172	VLT085903.57-473032.3	0.14	16.591	0.051	15.078	0.032	13.776	0.023	3.29	Disk	
173	2MASS085903.70-473150.8	1.45	16.238	—	15.373	—	13.71	0.079	—	—	UUA
174	VLT085903.64-473040.1	0.23	—	—	14.724	—	12.958	—	12.49	—	FNT
176	VLT085903.74-473142.5	0.26	—	—	19.595	—	14.786	—	—	—	FNT
177	2MASS085903.83-472456.7	0.58	17.178	0.231	14.887	0.059	13.867	0.061	—	—	DAA
178	VLT085903.78-473004.6	0.58	17.041	0.073	15.621	0.025	14.54	0.023	3.78	Disk	
179	VLT085903.79-473048.2	0.35	14.63	0.014	13.273	0.007	12.605	0.034	6.92	—	
181	VLT085903.86-473108.8	0.66	17.568	0.073	15.348	0.017	13.997	0.014	12.68	Disk	
182	VLT085903.82-472954.4	0.74	16.941	0.062	15.289	0.021	14.274	0.027	10.37	M STAR	
183	VLT085903.88-473104.4	0.47	15.105	0.015	13.226	0.005	12.228	0.005	10.8	Disk	
184	VLT085903.96-473121.7	0.25	17.504	0.051	15.214	0.014	14.089	0.012	15.46	GK STAR	
185	VLT085904.02-473055.4	0.43	16.053	0.078	14.098	0.02	13.034	0.03	12.54	M STAR	
186	VLT085904.00-473052.9	0.32	15.509	0.038	13.635	0.012	12.435	0.016	12.64	M STAR	
187	VLT085904.02-473034.5	0.35	15.534	0.035	14.052	0.015	13.441	0.028	8.41	—	
189	VLT085904.08-473112.0	1.02	18.445	0.155	16.33	0.03	15.078	0.024	12.02	—	
190	2MASS085904.23-472321.9	0.14	16.108	0.11	13.785	—	12.515	—	18.6	Bright	BUU
191	VLT085904.26-473046.5	0.45	16.02	0.107	14.633	0.049	13.404	0.069	2.14	—	
192	VLT085904.31-473105.4	0.48	15.676	0.025	13.886	0.008	13.001	0.008	10.68	M STAR	
193	VLT085904.35-473130.5	0.52	19.717	0.194	18.27	0.074	16.285	0.053	0	—	
194	VLT085904.41-473055.9	0.43	13.488	0.007	11.753	0.003	10.942	0.003	10.3	GK STAR	
195	VLT085904.44-473120.4	0.24	—	—	16.448	—	14.746	—	—	—	FNT

Table 10—Continued

SRC#	IR ID	offset	J	Jerr	H	Herr	K	Kerr	A_V	Model	flags
196	VLT085904.45-473038.6	0.23	15.659	0.079	14.223	0.029	13.207	0.047	4.52	Disk	
197	VLT085904.56-473050.6	0.42	14.536	0.015	12.86	0.005	12.092	0.008	9.83	GK STAR	
198	VLT085904.63-473027.9	0.26	14.851	—	13.049	—	12.008	—	—	—	FNT
199	2MASS085904.69-472833.2	0.51	16.181	—	15.972	0.168	14.745	0.133	—	—	UCB
200	VLT085904.71-473036.6	0.27	14.719	0.016	13.09	0.006	12.058	0.009	7.07	Disk	
201	VLT085904.78-473031.3	0.58	15.561	0.023	13.934	0.01	13.263	0.012	9.93	GK STAR	
202	VLT085904.81-473054.1	0.83	16.736	0.06	14.67	0.014	13.836	0.019	14.7	GK STAR	
203	2MASS085904.92-473241.1	0.21	17.31	0.297	15.284	0.094	14.573	0.117	—	—	DAB
204	VLT085905.04-473126.2	0.50	19.039	0.132	17.112	0.038	15.677	0.034	7.95	M STAR	
205	VLT085905.00-473057.7	0.47	17.418	0.189	14.952	0.036	13.391	0.035	18.07	M STAR	
207	VLT085905.04-473047.2	0.44	15.675	0.025	13.944	0.008	13.154	0.009	10.42	GK STAR	
208	VLT085905.05-473053.1	0.45	17.452	0.083	15.316	0.021	14.007	0.023	11.86	—	
209	VLT085905.10-473101.0	0.67	15.407	0.018	13.665	0.007	12.849	0.008	10.36	GK STAR	
210	VLT085905.14-472953.1	0.21	17.587	—	15.682	—	14.718	—	19.16	—	FNT
211	VLT085905.20-473029.5	0.18	16.633	0.037	15.134	0.019	14.21	0.02	8.98	M STAR	
212	VLT085905.19-473017.2	0.55	17.433	0.076	15.717	0.025	14.961	0.038	10.48	GK STAR	
213	VLT085905.23-473032.6	0.57	15.949	0.038	14.584	0.017	13.525	0.014	8.73	M STAR	
214	VLT085905.23-473042.4	0.65	15.415	0.025	13.221	0.006	11.551	0.004	9.76	Disk	
217	VLT085905.39-473002.9	0.17	11.911	—	11.238	—	10.792	—	—	—	FNT
218	VLT085905.39-473047.9	0.46	16.607	0.044	14.819	0.016	13.943	0.019	10.52	GK STAR	
219	VLT085905.41-473030.2	0.31	13.441	0.007	11.993	0.003	11.444	0.004	8.44	GK STAR	
220	VLT085905.51-473036.0	0.41	12.217	0.004	11.104	0.002	10.516	0.002	8.53	Bright	
221	2MASS085905.64-473040.9	0.26	8.161	0.023	7.143	0.040	6.533	0.015	9.88	Bright	
223	VLT085905.63-473046.4	0.77	14.542	0.015	12.981	0.006	12.196	0.008	8.75	M STAR	
224	VLT085905.70-473050.1	0.63	16.107	0.03	14.253	0.01	13.397	0.012	11.59	GK STAR	
225	VLT085905.71-473009.0	0.57	15.598	0.023	13.855	0.008	13.138	0.01	11.17	GK STAR	
226	VLT085905.86-473030.7	0.33	14.473	0.012	12.887	0.005	12.194	0.006	9.19	GK STAR	
227	VLT085905.82-473036.4	0.58	16.878	0.134	14.989	0.038	13.966	0.023	10.73	Disk	
229	VLT085905.91-473042.3	0.59	15.683	0.044	14.197	0.013	13.409	0.013	7.04	Disk	
230	VLT085905.90-473054.5	0.72	16.689	0.037	14.719	0.012	13.691	0.012	11.81	Disk	
235	VLT085906.02-473020.7	0.61	16.71	0.043	14.706	0.011	13.607	0.01	11.71	Disk	
236	VLT085906.06-473101.1	0.58	18.194	0.1	15.796	0.021	14.228	0.018	17.66	M STAR	
238	VLT085906.14-473035.3	0.16	11.363	—	—	—	10.394	—	—	—	FNT
239	VLT085906.17-473044.4	0.30	13.908	—	12.707	—	11.922	—	—	—	FNT
240	VLT085906.17-473051.0	0.53	16.064	0.027	13.95	0.009	12.576	0.007	14.96	M STAR	
241	VLT085906.18-472958.6	0.57	17.336	0.189	15.102	0.037	14.03	0.043	15.11	GK STAR	
243	VLT085906.21-473025.7	0.84	15.762	0.024	14.115	0.008	13.399	0.01	9.85	Disk	
244	2MASS085906.38-472909.9	0.10	14.66	0.016	12.713	0.02	11.828	0.016	12.64	GK STAR	AAA
246	VLT085906.39-473037.3	0.49	15.01	0.017	13.53	0.007	12.801	0.009	7.43	GK STAR	
247	VLT085906.50-473126.4	0.22	17.178	—	15.108	—	13.534	—	17.05	—	FNT
248	VLT085906.53-473116.0	0.25	—	—	19.412	—	18.554	—	—	—	FNT
249	VLT085906.57-473059.6	0.67	18.985	0.179	17.144	0.057	15.436	0.056	4.57	Disk	
250	VLT085906.58-473018.2	0.64	17.071	0.052	14.981	0.015	13.813	0.017	12.35	—	
251	VLT085906.62-473021.9	0.23	—	—	16.41	—	14.901	—	—	—	FNT
252	VLT085906.67-472957.8	0.73	18.368	0.116	16.426	0.034	15.049	0.053	13.87	M STAR	
253	VLT085906.76-472941.4	0.52	19.533	0.179	15.612	0.017	13.205	0.009	27.74	Disk	
255	VLT085906.87-473102.0	0.64	19.709	0.18	16.297	0.024	13.886	0.014	20.66	Disk	
256	VLT085906.95-473032.5	0.45	18.158	0.181	16.892	0.049	15.446	0.07	0	Disk	
257	VLT085906.95-473137.3	0.81	17.443	0.045	15.778	0.017	14.849	0.016	8.39	Disk	
258	VLT085906.98-473054.2	0.60	17.69	0.055	15.905	0.019	14.692	0.017	12.12	M STAR	
259	VLT085907.18-472957.8	0.13	—	—	—	—	16.273	—	—	—	FNT
260	2MASS085907.31-472335.9	0.56	16.474	—	15.774	0.135	14.96	0.146	—	—	UBB
261	VLT085907.16-473117.9	0.53	—	—	17.963	—	15.612	—	—	—	FNT
263	2MASS085907.36-473305.3	0.09	13.151	0.02	11.736	0.023	11.137	0.018	7.58	GK STAR	AAA
264	VLT085907.32-473045.7	0.83	16.158	0.027	14.129	0.009	13.137	0.009	12.92	GK STAR	
267	VLT085907.66-473044.5	0.80	17.799	0.065	15.577	0.018	14.429	0.022	15.91	Bright	
270	VLT085907.84-473136.9	0.23	—	—	18.741	—	—	—	—	—	FNT
271	VLT085907.86-473100.2	0.70	16.202	0.036	14.125	0.013	13.005	0.018	16.23	Bright	
272	VLT085907.91-473025.6	0.63	17.17	0.073	14.685	0.016	13.387	0.016	18.15	Bright	
273	VLT085907.79-473122.2	2.02	19.001	0.102	18.163	0.056	17.214	0.054	0	M STAR	
274	VLT085908.05-473038.6	0.08	17.651	0.073	15.622	0.022	14.375	0.03	20.2	Bright	
275	VLT085907.98-473050.1	0.35	17.157	0.041	15.035	0.013	13.914	0.014	15.91	—	
276	VLT085908.02-473047.1	0.72	17.107	0.043	14.682	0.011	13.34	0.01	19.85	Bright	
278	VLT085908.22-472931.9	0.18	—	—	—	—	—	—	—	—	FNT
279	VLT085908.17-473051.2	1.00	17.729	0.056	15.614	0.017	14.37	0.018	19.45	Bright	
280	2MASS085908.25-473516.9	0.70	14.156	—	14.641	0.272	13.522	0.141	—	—	UDB
281	VLT085908.33-472954.7	0.68	16.821	0.035	15.709	0.019	15.062	0.03	5.25	M STAR	

Table 10—Continued

SRC#	IR ID	offset	J	Jerr	H	Herr	K	Kerr	A_V	Model	flags
282	VLT085908.50-473049.3	0.79	16.762	0.034	14.251	0.009	12.974	0.007	17.3	GK STAR	
283	VLT085908.70-473059.5	0.21	18.558	—	16.139	—	15.054	—	—	—	FNT
284	VLT085908.75-473026.8	0.10	—	—	—	—	17.135	—	—	—	FNT
285	VLT085908.70-473036.8	0.77	16.624	0.032	14.021	0.008	12.554	0.006	—	—	
287	VLT085909.00-473041.0	0.64	17.896	0.072	15.069	0.014	13.479	0.012	—	—	
288	2MASS085909.12-472916.8	0.20	14.672	—	12.959	—	12.516	0.016	—	—	UUA
289	2MASS085909.13-473405.2	0.21	14.944	0.035	13.671	0.029	13.379	0.025	8.08	GK STAR	AAE
290	VLT085909.29-472919.0	0.18	—	—	17.463	—	—	—	—	—	FNT
291	VLT085909.44-473019.9	0.16	—	—	16.207	—	13.542	—	—	—	FNT
293	VLT085909.56-473025.2	0.73	16.341	0.027	14.278	0.009	13.174	0.008	—	—	
294	2MASS085909.72-472845.4	0.19	18.016	—	15.537	0.105	13.989	0.067	—	—	UBA
295	VLT085909.68-473129.9	0.84	16.914	0.035	14.89	0.011	13.79	0.01	11.98	CC	
297	2MASS085909.87-473027.8	0.90	15.226	—	12.977	—	13.164	0.039	—	—	UUE
298	VLT085909.93-472940.8	0.71	16.596	0.031	14.751	0.011	13.734	0.01	10.17	—	
301	VLT085911.09-473123.6	0.14	—	—	18.865	—	15.613	—	—	—	FNT
303	2MASS085911.78-472943.2	1.03	16.618	—	14.852	—	14.992	0.17	—	—	UUC
305	2MASS085912.75-472959.9	0.16	17.059	—	16.584	—	14.851	0.14	—	—	UUB
309	2MASS085913.46-473247.3	0.43	14.336	0.031	13.066	0.034	12.405	0.035	9.4	—	AAA
311	2MASS085914.00-472856.5	0.14	17.648	—	14.941	0.059	11.51	0.02	—	—	UAA
316	2MASS085914.45-473050.6	0.19	15.826	—	14.525	0.082	13.022	0.069	—	—	UAA
317	2MASS085914.46-473118.9	0.04	16.78	—	14.578	0.054	13.651	0.051	—	—	UAA
319	2MASS085914.74-473147.4	0.37	18.271	—	17.211	—	14.928	0.139	—	—	UUB
320	2MASS085914.74-472931.7	0.10	15.473	—	13.647	0.04	12.756	0.041	—	—	UAA
323	2MASS085914.90-472927.9	0.11	15.964	—	15.001	0.074	14.001	0.063	—	—	UAA
327	2MASS085915.68-472608.9	0.09	16.448	—	15.496	0.101	15.123	—	—	—	UBU
330	2MASS085915.78-472701.2	0.35	18.473	—	15.696	0.132	13.196	0.052	—	—	UBA
331	2MASS085915.85-472852.9	0.31	16.782	0.167	14.795	0.068	13.562	0.047	13.51		CAA
332	2MASS085915.91-473257.5	0.24	12.325	0.018	11.197	0.021	10.617	0.02	8.19	Bright	AAA
335	2MASS085916.06-473313.1	0.60	16.499	0.14	14.869	0.08	13.587	—	5.07	—	BAU
342	2MASS085917.22-472756.8	0.16	16.189	—	14.77	0.065	13.589	0.058	—	—	UAA
343	2MASS085917.25-473011.1	0.15	18.422	—	15.142	0.081	13.715	0.05	—	—	UAA
344	2MASS085917.58-472748.1	0.38	16.278	0.117	14.744	0.066	14.069	0.061	8.61	—	BAA
345	2MASS085917.74-472851.4	0.13	15.555	—	14.257	0.06	13.462	0.069	—	—	UAA
349	2MASS085918.97-473224.9	0.11	16.509	0.137	14.747	0.062	13.688	0.056	11.28	M STAR	BAA
351	2MASS085919.33-472928.5	0.18	16.514	—	15.445	0.14	14.547	0.135	—	—	UBB
353	2MASS085919.80-472401.4	1.00	17.58	—	15.98	0.152	14.903	0.137	—	—	UCB
354	2MASS085919.92-473118.7	0.06	16.408	—	14.554	0.058	13.381	0.052	—	—	UAA
356	2MASS085920.23-472829.5	0.36	17.074	0.219	15.48	0.103	14.367	0.083	—	—	DBA
358	2MASS085920.70-472617.3	0.08	14.747	0.035	13.45	0.045	12.822	0.041	6.35	M STAR	AAA
360	2MASS085920.92-473119.3	0.60	16.577	—	14.931	0.075	13.726	0.056	—	—	UAA
362	2MASS085920.95-472914.1	0.02	15.46	0.058	14.162	0.031	13.562	0.033	5.95	Disk	AAA
364	2MASS085921.31-472555.6	0.27	15.561	0.071	14.035	0.056	13.247	0.051	7.6	Disk	AAA
366	2MASS085921.58-472928.9	0.00	14.283	0.031	12.41	0.03	11.505	0.031	11.69	Bright	AAA
367	2MASS085921.70-473234.5	0.44	17.686	—	16.491	—	15.023	0.145	—	—	UUB
368	2MASS085921.92-473038.3	0.12	13.209	0.023	12.381	0.028	11.897	0.031	7.77	Bright	AAA
371	2MASS085922.86-472633.6	0.09	16.311	0.114	14.772	0.075	13.853	0.07	6.73	Disk	BAA
372	2MASS085923.54-473551.7	0.09	15.461	0.065	13.752	0.036	12.922	0.037	10.82	Bright	AAA
373	2MASS085923.61-472650.0	0.25	15.784	0.083	14.594	0.055	14.026	0.064	4.72	Disk	AAA
374	2MASS085923.59-473750.8	0.66	12.878	0.019	11.227	0.025	10.005	0.023	5.85	M STAR	AAA
377	2MASS085924.35-473044.3	0.05	17.582	—	15.48	0.134	13.78	0.07	—	—	UBA
379	2MASS085924.73-473829.0	0.93	14.52	0.028	12.976	0.027	12.16	0.023	7.62	Disk	AAA
380	2MASS085924.70-473802.9	0.60	14.707	0.035	13.89	0.027	13.729	0.047	2.82	GK STAR	AAA
381	2MASS085925.13-473214.0	1.09	13.801	0.029	13.226	0.032	12.876	0.029	5.91	—	AAA
382	2MASS085925.06-472726.3	0.39	16.434	0.138	15.066	0.075	14.62	0.085	8.16	GK STAR	BAA
385	2MASS085925.95-472726.3	0.19	16.698	—	15.563	0.12	14.558	0.108	—	—	UBA
388	2MASS085926.26-472754.6	0.11	14.746	0.032	13.259	0.027	12.628	0.027	8.32	GK STAR	AAA
389	2MASS085926.55-473007.9	0.05	16.181	0.099	14.809	0.068	14.196	0.08	6.87	GK STAR	AAA
390	2MASS085926.70-473310.1	0.14	11.696	0.021	10.967	0.025	10.503	0.029	7.96	Bright	AAA
391	2MASS085927.84-472803.0	0.10	15.099	0.049	13.688	0.035	12.815	0.038	5.33	Disk	AAA
392	2MASS085928.17-472926.0	0.07	15.03	0.056	13.588	0.041	12.937	0.039	7.54	GK STAR	AAA
395	2MASS085928.61-472937.9	0.18	15.196	0.051	13.701	0.03	12.841	0.03	8.67	M STAR	AAA
396	2MASS085928.82-473221.7	0.52	10.621	0.021	9.287	0.025	8.484	0.021	12.93	Bright	AAA
398	2MASS085928.92-473140.5	0.13	16.01	0.09	14.571	0.066	13.849	0.063	9.83	Bright	AAA
400	2MASS085929.96-473149.9	0.13	15.763	—	14.151	0.045	13.127	0.043	—	—	UAA
401	2MASS085930.01-472633.9	0.00	17.077	0.232	15.115	0.085	14.698	0.119	—	—	DAB
402	2MASS085930.58-472759.8	0.49	17.185	0.295	15.389	0.108	14.887	0.118	—	—	DAB
403	2MASS085930.67-472449.7	0.79	14.343	0.029	13.422	0.034	12.999	0.032	5.32	—	AAA

Table 10—Continued

SRC#	IR ID	offset	J	Jerr	H	Herr	K	Kerr	A_V	Model	flags
405	2MASS085931.51-473350.4	0.37	16.834	0.199	15.598	0.121	14.986	0.13	8.27	—	CBB
408	2MASS085932.45-473235.8	0.23	16.771	0.178	15.704	0.129	15.039	0.139	2.24	Disk	CBB
409	2MASS085933.32-473253.7	0.11	15.683	—	14.565	—	14.286	0.103	—	—	UUA
414	2MASS085935.38-472723.4	0.23	13.758	0.023	12.734	0.024	12.346	0.024	3.86	GK STAR	AAA
415	2MASS085935.37-472818.2	0.41	14.66	—	14.93	0.374	14.51	0.188	—	—	UDC
416	2MASS085935.58-473137.2	0.08	16.34	0.121	14.655	0.055	14.022	0.065	11.04	GK STAR	BAA
418	2MASS085936.17-472558.0	0.72	15.415	0.071	14.189	0.046	13.954	—	7.88	Disk	AAU
419	2MASS085936.76-472921.8	0.22	16.735	—	15.652	0.14	14.718	0.105	—	—	UBB
420	2MASS085936.94-473304.7	0.04	13.97	0.026	12.811	0.027	12.211	0.019	5.34	M STAR	AAA
422	2MASS085937.45-473125.6	0.31	17.966	—	15.746	0.133	14.693	0.112	—	—	UBB
427	2MASS085941.57-473508.0	0.42	15.548	0.067	13.882	0.054	13.009	0.043	8.85	Disk	AAA
433	2MASS085946.73-473153.5	0.23	15.324	0.056	13.976	0.044	13.524	0.052	7.83	GK STAR	AAA
435	2MASS085948.36-472640.8	0.61	10.928	0.017	9.873	0.025	9.409	0.019	5.46	—	AAA
440	2MASS085950.41-472656.7	0.41	15.661	0.073	14.378	0.053	14.189	0.083	9.04	—	AAA
441	2MASS085951.38-473323.3	0.45	17.159	0.213	15.813	0.134	15.485	0.218	—	—	DBD
444	2MASS085953.64-472846.0	0.60	14.736	0.036	12.998	0.025	12.244	0.026	10.8	Disk	AAA
445	2MASS085953.90-472742.6	0.37	15.647	0.077	14.373	0.065	13.749	0.072	8.32	Bright	AAA
453	2MASS090004.84-472708.2	1.00	15.49	0.052	14.414	0.05	13.892	0.063	3.51	Disk	AAA
456	VLT085904.80-473028.5	0.04	14.355	0.012	12.738	0.005	12.073	0.006	9.84	Disk	
457	VLT085904.50-473034.9	0.18	11.482	—	11.061	—	10.51	—	—	—	FNT
459	VLT085906.25-473107.2	0.21	16.227	0.026	13.343	0.006	11.686	0.004	25.27	Bright	
460	VLT085906.27-473112.6	0.49	19.477	0.169	16.526	0.028	14.192	0.014	14.91	Disk	
461	VLT085900.88-473044.6	0.19	12.607	0.005	11.97	0.003	11.627	0.004	5.23	Bright	
462	VLT085903.02-473042.5	0.16	15.585	0.021	13.994	0.009	13.258	0.012	8.91	Disk	

Table 11. IR Photometry of X-ray Sources (non-members)

SRC#	IR ID	offset	J	Jerr	H	Herr	K	Kerr	A_V	Model	flags
1	2MASS085821.23-473107.9	0.73	15.154	0.045	14.123	0.032	13.879	0.049	5.12	GK STAR	AAA
2	2MASS085823.82-473001.6	0.52	16.171	0.12	14.048	0.065	12.772	0.048	11.94	GK STAR	BAA
3	2MASS085827.50-473008.8	0.99	16.532	0.121	14.926	0.047	14.095	0.053	11.64	Bright	BAA
6	2MASS085831.46-472807.9	0.52	14.047	0.031	13.389	0.032	13.253	0.038	0.82	GK STAR	AAA
10	2MASS085836.16-473135.8	0.60	17.356	—	15.527	0.116	14.504	0.085	—	—	UBA
12	2MASS085839.69-473127.1	1.03	17.169	—	15.011	0.057	13.754	0.042	—	—	UAA
13	2MASS085841.58-472835.0	0.34	15.577	0.071	14.273	0.043	13.743	0.051	6.6	GK STAR	AAA
15	2MASS085842.42-473041.6	1.34	12.376	0.023	11.98	0.02	11.922	0.026	0	GK STAR	AAA
17	2MASS085842.68-473015.5	0.30	14.083	0.029	13.446	0.028	13.35	0.048	0.85	GK STAR	AAA
18	2MASS085843.41-473251.3	0.43	15.915	0.099	14.51	0.055	13.842	0.071	0.00	–	AAA
32	2MASS085849.14-472917.2	0.45	15.898	—	15.419	0.12	13.98	—	—	—	UBU
34	2MASS085849.20-473115.1	0.16	11.887	0.02	11.5	0.025	11.433	0.023	0	GK STAR	AAA
39	2MASS085850.39-473319.5	0.13	9.516	0.02	9.076	0.025	8.922	0.023	0	GK STAR	AAA
42	2MASS085850.98-472924.0	0.08	15.47	0.058	14.786	0.051	14.613	0.106	0.89	GK STAR	AAA
44	2MASS085851.37-472722.2	0.34	15.69	0.076	14.045	0.03	13.053	0.031	7.61	GK STAR	AAA
54	2MASS085853.98-472620.1	0.08	13.859	0.035	13.134	0.041	13.006	0.051	1.81	GK STAR	AAA
64	2MASS085855.07-472502.1	0.25	11.362	0.017	11.007	0.024	10.881	0.018	0	—	AAA
80	2MASS085857.58-472426.1	0.96	14.355	0.034	13.119	0.034	12.331	0.036	3.59	GK STAR	AAA
83	2MASS085857.79- 472358.9	0.36	16.075	0.085	15.092	0.07	14.511	0.088	9.33	Bright	AAA
102	2MASS085858.97-473344.1	0.37	16.896	—	15.406	0.123	14.979	0.199	—	—	UBC
105	2MASS085859.07-473216.9	0.43	16.68	—	15.765	0.188	14.601	0.204	—	—	UCC
113	2MASS085859.97- 472244.5	0.96	13.265	0.023	12.714	0.028	12.442	0.035	3.88	Bright	AAA
137	VLT085901.38-473048.8	0.23	15.119	0.016	14.542	0.01	14.304	0.017	0	GK STAR	
175	2MASS085903.76-472759.5	0.29	15.337	0.055	14.406	0.047	14.095	0.085	3.19	GK STAR	AAA
206	2MASS085905.07-473307.5	0.10	15.742	0.085	14.947	0.082	14.403	0.123	0	—	AAB
245	VLT085906.34-473030.7	0.81	15.531	0.02	13.6	0.007	12.425	0.006	10.09	M Star	
262	VLT085907.33-473135.6	0.46	16.619	0.03	14.74	0.011	13.634	0.009	9.93	GK STAR	
277	2MASS085908.21-472406.8	0.92	15.294	—	14.833	—	14.307	0.095	—	—	UUA
286	2MASS085908.84-473637.8	0.59	11.637	0.018	11.387	0.025	11.34	0.025	0	GK STAR	AAA
300	2MASS085910.58-472349.4	0.57	15.51	0.054	14.519	0.06	13.961	0.063	4.07	M STAR	AAA
329	2MASS085915.74-472922.1	0.13	15.587	—	14.235	—	13.861	0.074	—	—	UUA
348	2MASS085918.60-472556.3	0.12	15.929	0.089	15.25	0.095	15.164	0.198	1.51	GK STAR	AAC
350	2MASS085919.26-472832.7	0.08	18.229	—	15.933	0.15	14.804	0.12	—	—	UCB
352	2MASS085919.58-473328.5	0.33	17.189	—	16.188	0.203	14.922	0.131	—	—	UCB
355	2MASS085919.88-472936.4	1.44	11.89	0.032	11.591	0.045	11.421	0.04	0	GK STAR	EEA
357	2MASS085920.30-473106.1	0.20	17.141	—	15.329	0.091	13.896	0.058	—	—	UAA
369	2MASS085922.23-472550.1	0.34	12.146	0.026	11.66	0.034	11.386	0.027	4.43	—	AAA
375	2MASS085923.67-472523.3	0.22	16.806	0.169	16.004	0.187	15.09	0.175	0	—	CCC
383	2MASS085925.72-473436.2	1.00	12.218	0.019	11.966	0.024	11.759	0.023	0	M STAR	AAA
397	2MASS085928.94-473217.2	0.55	13.761	0.07	10.712	—	9.901	—	—	—	AUU
404	2MASS085931.26-473330.4	0.18	13.066	0.048	12.42	0.054	12.197	0.05	0.34	M STAR	AAA

Table 11—Continued

SRC#	IR ID	offset	J	Jerr	H	Herr	K	Kerr	A_V	Model	flags
407	2MASS085931.70-472609.8	1.65	8.757	0.011	8.201	0.031	7.932	0.007	0	M Star	AAA
411	2MASS085934.46-472715.7	0.22	16.517	0.14	15.097	0.08	14.556	0.087	8.11	GK STAR	BAA
421	2MASS085937.41- 473435.2	0.39	15.848	0.096	14.706	0.068	14.202	0.077	5.93	Bright	AAA
426	2MASS085940.89-472526.5	0.04	15.424	0.054	14.818	0.059	14.635	0.095	0.93	—	AAA
428	2MASS085942.08-472419.8	0.58	16.127	0.1	15.009	0.087	14.556	0.096	4.64	GK STAR	AAA
432	2MASS085945.68-472841.8	0.60	15.435	0.054	14.687	0.055	14.651	0.111	2.87	M Star	AAB
434	2MASS085946.88-473804.4	1.20	15.209	0.044	14.178	0.042	13.808	0.057	4.1	GK STAR	AAA
437	2MASS085949.64-473116.8	0.48	15.829	0.063	14.615	0.059	14.014	0.073	4.78	—	AAA
438	2MASS085949.76-472527.6	1.01	15.272	—	14.422	0.051	14.331	—	—	—	UAU
442	2MASS085951.55-473309.1	0.78	15.99	0.122	14.84	0.096	14.229	0.085	5.33	M STAR	BAA
443	2MASS085952.59- 472736.3	1.10	13.742	0.021	13.059	0.03	12.838	0.029	1.42	Bright	AAA
447	2MASS085956.09- 473304.3	0.15	8.587	0.013	8.254	0.035	8.073	0.015	2.97	Bright	AAA
450	2MASS085957.89-472701.8	0.63	13.24	0.032	12.675	0.031	12.592	0.032	0	GK STAR	AAA
452	2MASS090004.38-472946.8	0.43	10.948	0.021	10.553	0.022	10.464	0.021	0	—	AAA
454	2MASS090006.68- 473032.4	0.54	15.172	0.056	13.988	0.039	13.311	0.038	10.51	Bright	AAA

Table 12. IR Photometry in the VLT field (Non–X–ray Sources)

IR ID	RA J2000.	DEC J2000.	J	Jerr	H	Herr	K	Kerr	A_V min.
VLT085911.02-472949.8	08:59:11.022	-47:29:49.81	19.537	0.148	17.724	0.048	16.190	0.038	5.58
VLT085910.86-473101.6	08:59:10.867	-47:31:01.67	16.763	0.033	16.097	0.020	15.586	0.023	0.00
VLT085910.79-473028.9	08:59:10.795	-47:30:28.94	18.031	0.068	16.531	0.025	14.550	0.015	0.00
VLT085910.72-473110.4	08:59:10.720	-47:31:10.40	19.667	0.149	17.745	0.046	16.176	0.034	6.81
VLT085910.59-472945.7	08:59:10.596	-47:29:45.70	18.288	0.068	16.753	0.027	15.356	0.021	2.84
VLT085910.40-472933.7	08:59:10.405	-47:29:33.72	18.673	0.087	17.420	0.038	16.060	0.032	0.00
VLT085910.38-472942.6	08:59:10.385	-47:29:42.61	17.808	0.054	15.600	0.016	13.753	0.010	8.54
VLT085910.08-473133.8	08:59:10.088	-47:31:33.87	17.889	0.056	16.588	0.025	15.528	0.023	2.30
VLT085910.07-473130.3	08:59:10.073	-47:31:30.35	18.173	0.068	16.885	0.031	15.652	0.026	0.74
VLT085910.00-472951.5	08:59:10.004	-47:29:51.50	18.399	0.075	16.508	0.024	15.135	0.019	7.95
VLT085909.95-473124.4	08:59:09.955	-47:31:24.40	18.770	0.092	17.486	0.040	15.951	0.030	0.00
VLT085909.67-473105.1	08:59:09.672	-47:31:05.16	19.403	0.174	17.753	0.066	16.420	0.095	4.94
VLT085909.67-473117.5	08:59:09.672	-47:31:17.57	18.613	0.082	17.455	0.039	16.167	0.031	0.00
VLT085909.64-473114.9	08:59:09.647	-47:31:14.91	19.296	0.121	17.196	0.034	15.597	0.025	9.03
VLT085909.36-472938.8	08:59:09.368	-47:29:38.80	17.672	0.052	16.507	0.024	15.457	0.023	0.50
VLT085909.26-472941.4	08:59:09.260	-47:29:41.43	18.370	0.072	16.885	0.030	15.576	0.026	2.85
VLT085909.23-473109.6	08:59:09.236	-47:31:09.69	18.428	0.077	16.619	0.027	15.097	0.023	5.62
VLT085909.16-472949.8	08:59:09.167	-47:29:49.86	17.535	0.050	15.153	0.013	13.648	0.010	13.69
VLT085908.94-472925.4	08:59:08.946	-47:29:25.47	19.017	0.114	17.409	0.038	15.351	0.021	0.00
VLT085908.89-473000.0	08:59:08.898	-47:30:00.00	17.395	0.047	16.584	0.028	16.059	0.039	0.00
VLT085908.89-472951.0	08:59:08.890	-47:29:51.02	18.594	0.109	17.415	0.060	16.374	0.084	0.77
VLT085908.88-472953.7	08:59:08.880	-47:29:53.74	18.346	0.095	16.370	0.028	14.780	0.024	7.39
VLT085908.79-473051.1	08:59:08.799	-47:30:51.10	14.477	0.011	13.970	0.008	13.739	0.011	0.00
VLT085908.72-473013.7	08:59:08.722	-47:30:13.77	18.139	0.066	16.598	0.026	15.492	0.025	5.25
VLT085908.44-473046.8	08:59:08.443	-47:30:46.87	19.122	0.176	16.935	0.046	15.400	0.038	10.75
VLT085908.42-473029.2	08:59:08.426	-47:30:29.24	16.701	0.040	15.952	0.029	15.338	0.060	0.00
VLT085908.37-473108.4	08:59:08.372	-47:31:08.42	18.981	0.127	16.984	0.045	15.314	0.072	7.04
VLT085908.36-473017.0	08:59:08.360	-47:30:17.02	18.513	0.085	16.765	0.029	15.587	0.025	7.54
VLT085908.34-473046.2	08:59:08.344	-47:30:46.26	18.734	0.120	16.165	0.025	14.388	0.016	14.09
VLT085908.15-473046.4	08:59:08.150	-47:30:46.40	18.422	0.094	16.094	0.025	14.440	0.019	11.74
VLT085908.13-472948.7	08:59:08.135	-47:29:48.77	19.273	0.178	17.610	0.051	16.250	0.053	4.90
VLT085908.03-473025.1	08:59:08.039	-47:30:25.12	17.978	0.120	15.660	0.029	14.401	0.032	14.77
VLT085907.96-473038.2	08:59:07.969	-47:30:38.21	17.440	0.062	15.046	0.014	13.755	0.015	15.57
VLT085907.92-473033.4	08:59:07.929	-47:30:33.41	16.098	0.028	13.394	0.006	11.670	0.005	16.38
VLT085907.80-473058.1	08:59:07.802	-47:30:58.11	17.158	0.068	15.647	0.031	14.284	0.041	2.78
VLT085907.79-473122.1	08:59:07.793	-47:31:22.16	19.001	0.102	18.163	0.056	17.214	0.054	0.00
VLT085907.77-473001.4	08:59:07.776	-47:30:01.43	17.635	0.054	15.653	0.017	14.234	0.017	8.84

Table 12—Continued

IR ID	RA J2000.	DEC J2000.	J	Jerr	H	Herr	K	Kerr	A_V min.
VLT085907.74-472950.2	08:59:07.742	-47:29:50.27	17.209	0.043	15.660	0.017	14.821	0.019	7.51
VLT085907.72-473003.6	08:59:07.722	-47:30:03.63	18.461	0.117	16.367	0.029	14.924	0.030	10.20
VLT085907.71-473043.7	08:59:07.717	-47:30:43.75	19.089	0.160	16.975	0.047	15.623	0.055	11.21
VLT085907.69-473118.0	08:59:07.696	-47:31:18.02	18.982	0.105	17.149	0.035	15.596	0.028	5.71
VLT085907.69-473053.7	08:59:07.693	-47:30:53.72	17.585	0.103	16.028	0.052	14.809	0.079	4.57
VLT085907.59-472926.4	08:59:07.591	-47:29:26.46	19.019	0.121	17.369	0.037	15.981	0.028	4.50
VLT085907.55-473046.1	08:59:07.555	-47:30:46.13	18.854	0.152	16.420	0.033	15.305	0.041	17.53
VLT085907.51-473115.5	08:59:07.510	-47:31:15.51	16.879	0.035	15.503	0.016	14.596	0.024	4.57
VLT085907.45-472948.1	08:59:07.451	-47:29:48.16	18.876	0.115	16.461	0.026	14.705	0.018	12.13
VLT085907.43-473040.6	08:59:07.439	-47:30:40.65	19.468	0.193	17.210	0.040	15.305	0.035	8.76
VLT085907.38-473054.3	08:59:07.382	-47:30:54.35	17.855	0.063	15.742	0.018	14.601	0.018	12.88
VLT085907.36-473057.7	08:59:07.366	-47:30:57.72	18.446	0.131	16.042	0.023	14.670	0.019	15.06
VLT085907.36-473037.0	08:59:07.362	-47:30:37.02	18.577	0.134	16.701	0.037	14.864	0.033	4.02
VLT085907.33-473043.5	08:59:07.339	-47:30:43.54	18.900	0.135	16.183	0.025	14.804	0.022	19.33
VLT085907.22-473014.8	08:59:07.222	-47:30:14.88	18.012	0.181	16.249	0.056	14.942	0.061	6.71
VLT085907.19-473052.6	08:59:07.193	-47:30:52.60	18.920	0.143	16.748	0.038	15.477	0.038	12.66
VLT085907.13-473036.5	08:59:07.137	-47:30:36.57	16.503	0.033	14.164	0.009	12.735	0.007	13.70
VLT085907.09-473047.8	08:59:07.092	-47:30:47.87	16.123	0.031	13.815	0.008	12.389	0.008	13.30
VLT085907.07-472949.5	08:59:07.075	-47:29:49.55	17.999	0.075	14.705	0.011	12.524	0.006	20.88
VLT085907.05-473039.1	08:59:07.059	-47:30:39.14	18.573	0.185	15.956	0.031	14.427	0.029	16.74
VLT085907.04-473127.4	08:59:07.049	-47:31:27.42	18.869	0.097	18.223	0.062	17.340	0.066	0.00
VLT085907.02-473017.0	08:59:07.022	-47:30:17.00	17.934	0.111	16.034	0.040	15.099	0.048	11.59
VLT085906.97-473010.4	08:59:06.975	-47:30:10.48	17.913	0.143	16.006	0.042	14.782	0.056	9.37
VLT085906.96-473023.2	08:59:06.960	-47:30:23.22	14.941	0.018	12.553	0.004	11.089	0.004	14.10
VLT085906.85-472936.3	08:59:06.858	-47:29:36.31	18.277	0.089	16.297	0.024	14.962	0.020	9.49
VLT085906.83-473025.0	08:59:06.837	-47:30:25.03	14.741	0.014	13.403	0.007	12.669	0.011	5.43
VLT085906.77-473040.1	08:59:06.772	-47:30:40.13	17.575	0.085	15.749	0.022	14.843	0.031	10.80
VLT085906.77-473019.9	08:59:06.770	-47:30:19.95	17.768	0.085	15.944	0.030	14.605	0.032	7.30
VLT085906.75-473120.9	08:59:06.756	-47:31:20.94	18.219	0.067	16.383	0.023	15.133	0.020	8.18
VLT085906.73-473124.0	08:59:06.730	-47:31:24.04	18.852	0.095	17.069	0.033	15.780	0.028	7.13
VLT085906.72-473005.5	08:59:06.728	-47:30:05.54	17.230	0.136	15.757	0.053	14.278	0.045	1.32
VLT085906.71-473054.9	08:59:06.716	-47:30:54.95	17.586	0.083	15.398	0.019	14.146	0.017	13.03
VLT085906.67-473111.1	08:59:06.673	-47:31:11.10	19.214	0.120	16.972	0.038	15.034	0.042	8.28
VLT085906.64-473041.0	08:59:06.642	-47:30:41.05	18.473	0.165	16.842	0.050	14.773	0.031	0.00
VLT085906.62-473036.2	08:59:06.627	-47:30:36.27	17.793	0.141	16.882	0.068	15.746	0.087	0.00
VLT085906.59-473035.6	08:59:06.597	-47:30:35.61	17.653	0.137	16.639	0.060	15.656	0.070	0.00
VLT085906.58-473054.2	08:59:06.587	-47:30:54.20	18.321	0.142	16.503	0.045	15.178	0.048	7.33

Table 12—Continued

IR ID	RA J2000.	DEC J2000.	J	Jerr	H	Herr	K	Kerr	A_V min.
VLT085906.53-473011.1	08:59:06.538	-47:30:11.14	18.453	0.178	16.161	0.041	15.143	0.071	16.35
VLT085906.49-473034.0	08:59:06.495	-47:30:34.04	16.706	0.056	14.991	0.015	14.164	0.028	9.90
VLT085906.47-473009.6	08:59:06.474	-47:30:09.64	17.738	0.117	15.447	0.029	14.096	0.034	13.66
VLT085906.46-473135.3	08:59:06.469	-47:31:35.36	17.236	0.041	15.960	0.019	15.209	0.020	4.44
VLT085906.46-473021.0	08:59:06.466	-47:30:21.00	17.568	0.075	15.112	0.015	13.574	0.012	14.44
VLT085906.40-473052.9	08:59:06.409	-47:30:52.90	14.983	0.016	13.634	0.007	12.857	0.009	5.24
VLT085906.40-473054.2	08:59:06.407	-47:30:54.22	17.393	0.082	15.392	0.023	14.243	0.024	11.27
VLT085906.40-473032.9	08:59:06.406	-47:30:32.90	17.897	0.138	16.086	0.049	14.465	0.031	4.86
VLT085906.39-473016.7	08:59:06.396	-47:30:16.75	18.414	0.146	16.308	0.038	15.250	0.050	13.45
VLT085906.39-473126.9	08:59:06.394	-47:31:26.90	17.330	0.043	15.155	0.013	13.670	0.010	10.98
VLT085906.37-473057.0	08:59:06.377	-47:30:57.02	17.496	0.128	15.961	0.044	14.889	0.054	5.44
VLT085906.35-473038.9	08:59:06.352	-47:30:38.91	17.455	0.087	15.466	0.023	14.370	0.030	11.53
VLT085906.34-473050.6	08:59:06.341	-47:30:50.64	18.282	0.181	16.236	0.052	14.706	0.040	8.84
VLT085906.33-473003.9	08:59:06.336	-47:30:03.95	15.885	0.049	13.857	0.011	12.855	0.017	12.82
VLT085906.32-472931.9	08:59:06.327	-47:29:31.90	18.464	0.101	17.062	0.036	15.690	0.033	1.20
VLT085906.23-473056.8	08:59:06.233	-47:30:56.85	17.167	0.087	14.809	0.017	13.134	0.012	11.99
VLT085906.20-472932.9	08:59:06.204	-47:29:32.95	17.358	0.045	15.931	0.019	14.932	0.020	4.54
VLT085906.17-473044.3	08:59:06.170	-47:30:44.36	13.949	0.009	12.759	0.005	12.024	0.005	3.38
VLT085906.13-473024.3	08:59:06.134	-47:30:24.37	18.954	0.193	17.501	0.088	15.811	0.083	0.00
VLT085906.09-473027.3	08:59:06.098	-47:30:27.30	18.636	0.190	17.139	0.064	15.787	0.076	2.67
VLT085906.09-473138.7	08:59:06.095	-47:31:38.79	18.011	0.059	15.986	0.019	14.672	0.015	10.28
VLT085906.09-473039.5	08:59:06.090	-47:30:39.59	17.971	0.116	16.276	0.040	15.218	0.052	7.77
VLT085906.08-473044.3	08:59:06.088	-47:30:44.34	15.196	0.020	13.820	0.008	12.936	0.008	4.75
VLT085906.05-473001.0	08:59:06.058	-47:30:01.00	17.777	0.121	16.136	0.031	14.898	0.032	5.58
VLT085906.01-473052.1	08:59:06.013	-47:30:52.17	16.941	0.076	14.962	0.021	13.934	0.030	11.94
VLT085905.98-472936.1	08:59:05.988	-47:29:36.16	17.790	0.065	16.354	0.026	15.365	0.028	4.74
VLT085905.97-473037.2	08:59:05.972	-47:30:37.24	17.199	0.192	15.382	0.040	14.535	0.045	11.15
VLT085905.96-473038.6	08:59:05.960	-47:30:38.61	16.508	0.105	14.585	0.019	13.384	0.013	9.78
VLT085905.90-473032.5	08:59:05.900	-47:30:32.58	16.317	0.036	14.611	0.017	13.053	0.010	3.91
VLT085905.89-473026.6	08:59:05.897	-47:30:26.63	17.882	0.101	16.849	0.057	15.836	0.095	0.00
VLT085905.86-473039.9	08:59:05.863	-47:30:39.93	15.792	0.094	14.767	0.051	13.536	0.032	0.00
VLT085905.86-473112.3	08:59:05.861	-47:31:12.30	19.175	0.122	17.841	0.057	16.515	0.084	0.63
VLT085905.84-473050.1	08:59:05.842	-47:30:50.10	17.647	0.100	15.868	0.033	14.573	0.039	7.03
VLT085905.82-473047.0	08:59:05.821	-47:30:47.04	15.868	0.035	14.165	0.012	13.136	0.015	8.11
VLT085905.79-473017.8	08:59:05.799	-47:30:17.86	17.432	0.071	15.291	0.017	13.974	0.014	11.86
VLT085905.77-473024.9	08:59:05.772	-47:30:24.93	18.125	0.129	16.700	0.042	15.623	0.066	3.88
VLT085905.72-473044.6	08:59:05.725	-47:30:44.62	15.385	0.061	13.589	0.016	12.702	0.017	10.54

Table 12—Continued

IR ID	RA J2000.	DEC J2000.	J	Jerr	H	Herr	K	Kerr	A_V min.
VLT085905.72-473028.6	08:59:05.724	-47:30:28.63	16.645	0.051	15.087	0.019	14.397	0.035	8.83
VLT085905.70-473052.6	08:59:05.703	-47:30:52.60	17.106	0.073	14.957	0.018	13.963	0.023	14.56
VLT085905.63-473054.1	08:59:05.632	-47:30:54.18	17.033	0.055	14.842	0.014	13.616	0.014	13.28
VLT085905.60-473043.6	08:59:05.606	-47:30:43.64	15.711	0.097	14.013	0.033	13.246	0.033	10.15
VLT085905.56-473048.7	08:59:05.560	-47:30:48.77	17.995	0.146	16.046	0.043	15.009	0.047	11.45
VLT085905.53-473016.3	08:59:05.539	-47:30:16.39	17.238	0.067	15.661	0.021	14.568	0.022	5.86
VLT085905.47-473113.1	08:59:05.479	-47:31:13.17	18.341	0.120	15.879	0.027	13.952	0.022	11.41
VLT085905.47-473050.0	08:59:05.472	-47:30:50.04	18.658	0.173	17.029	0.055	15.867	0.057	6.02
VLT085905.45-473034.4	08:59:05.451	-47:30:34.48	13.788	0.009	12.635	0.004	11.982	0.005	3.52
VLT085905.44-473045.2	08:59:05.447	-47:30:45.29	12.347	0.005	11.155	0.002	10.470	0.002	3.80
VLT085905.43-473031.9	08:59:05.438	-47:30:31.96	15.701	0.027	14.537	0.016	13.223	0.013	0.00
VLT085905.43-473130.3	08:59:05.436	-47:31:30.38	18.927	0.155	17.120	0.046	15.849	0.062	7.61
VLT085905.41-473021.4	08:59:05.415	-47:30:21.42	17.579	0.074	16.078	0.032	14.942	0.038	4.46
VLT085905.41-473004.9	08:59:05.412	-47:30:04.96	17.433	0.135	16.344	0.070	15.255	0.078	0.00
VLT085905.39-473110.0	08:59:05.395	-47:31:10.09	17.949	0.069	15.737	0.020	14.611	0.030	14.37
VLT085905.39-473038.1	08:59:05.395	-47:30:38.13	15.730	0.079	14.176	0.027	13.223	0.021	6.66
VLT085905.38-473016.4	08:59:05.384	-47:30:16.44	17.596	0.090	15.963	0.028	15.142	0.040	8.81
VLT085905.38-473033.2	08:59:05.381	-47:30:33.22	16.422	0.063	14.980	0.026	14.084	0.026	5.57
VLT085905.37-473054.8	08:59:05.378	-47:30:54.81	14.820	0.017	13.696	0.009	13.028	0.017	3.00
VLT085905.36-473031.6	08:59:05.363	-47:30:31.63	17.069	0.068	16.157	0.057	14.855	0.042	0.00
VLT085905.35-473100.2	08:59:05.354	-47:31:00.29	18.280	0.158	16.420	0.058	15.461	0.091	10.85
VLT085905.35-473053.2	08:59:05.353	-47:30:53.28	16.336	0.044	14.468	0.012	13.538	0.014	11.19
VLT085905.29-473057.0	08:59:05.295	-47:30:57.01	17.363	0.145	15.758	0.047	14.757	0.071	6.98
VLT085905.29-473003.1	08:59:05.291	-47:30:03.12	15.451	0.028	13.794	0.011	12.802	0.016	7.77
VLT085905.27-473105.8	08:59:05.278	-47:31:05.80	18.743	0.119	16.537	0.032	15.367	0.050	13.94
VLT085905.25-473112.4	08:59:05.259	-47:31:12.49	17.701	0.062	15.579	0.018	14.004	0.017	9.53
VLT085905.24-473052.4	08:59:05.248	-47:30:52.47	17.535	0.122	15.523	0.036	14.367	0.057	11.37
VLT085905.24-473000.0	08:59:05.246	-47:30:00.03	17.488	0.162	15.657	0.045	14.647	0.061	10.04
VLT085905.24-473112.3	08:59:05.243	-47:31:12.36	17.701	0.062	15.573	0.018	13.992	0.016	9.56
VLT085905.20-473036.2	08:59:05.208	-47:30:36.29	18.256	0.187	17.093	0.073	16.021	0.055	0.30
VLT085905.20-472954.8	08:59:05.200	-47:29:54.87	17.430	0.126	15.933	0.050	14.553	0.055	2.45
VLT085905.18-473008.3	08:59:05.189	-47:30:08.30	16.931	0.057	15.136	0.018	14.168	0.024	9.87
VLT085905.16-473121.2	08:59:05.160	-47:31:21.26	18.684	0.107	17.716	0.060	16.775	0.088	0.00
VLT085905.10-473110.0	08:59:05.108	-47:31:10.01	18.458	0.088	16.008	0.021	14.679	0.020	16.04
VLT085905.10-473041.5	08:59:05.107	-47:30:41.56	17.812	0.092	16.328	0.040	15.423	0.073	6.08
VLT085905.10-473033.4	08:59:05.102	-47:30:33.45	15.927	0.029	14.418	0.012	13.581	0.012	6.97
VLT085905.09-473140.3	08:59:05.091	-47:31:40.39	15.451	0.018	14.864	0.011	14.611	0.015	0.00

Table 12—Continued

IR ID	RA J2000.	DEC J2000.	J	Jerr	H	Herr	K	Kerr	A_V min.
VLT085905.06-473030.5	08:59:05.061	-47:30:30.59	16.343	0.037	14.524	0.015	13.419	0.010	9.11
VLT085905.05-473059.4	08:59:05.053	-47:30:59.45	17.369	0.049	15.299	0.020	14.048	0.029	11.41
VLT085905.04-473019.2	08:59:05.041	-47:30:19.23	18.136	0.133	16.582	0.050	15.491	0.066	5.55
VLT085905.02-473026.0	08:59:05.026	-47:30:26.05	16.590	0.040	14.915	0.015	14.168	0.020	9.99
VLT085905.00-473057.7	08:59:05.001	-47:30:57.75	17.418	0.189	14.952	0.036	13.391	0.035	11.51
VLT085904.95-473034.9	08:59:04.957	-47:30:34.94	17.456	0.099	15.862	0.027	14.592	0.029	4.67
VLT085904.95-473126.3	08:59:04.957	-47:31:26.36	17.845	0.061	15.459	0.015	14.140	0.013	15.23
VLT085904.94-473027.7	08:59:04.944	-47:30:27.76	17.550	0.108	15.832	0.035	14.972	0.050	9.68
VLT085904.88-473121.1	08:59:04.885	-47:31:21.11	17.977	0.071	15.962	0.020	14.824	0.020	11.55
VLT085904.88-473112.8	08:59:04.882	-47:31:12.86	19.532	0.184	16.794	0.037	14.985	0.027	16.17
VLT085904.87-473112.1	08:59:04.871	-47:31:12.13	19.386	0.154	16.911	0.039	15.244	0.034	13.67
VLT085904.85-473048.6	08:59:04.858	-47:30:48.67	15.850	0.044	14.155	0.016	13.239	0.029	8.91
VLT085904.85-473047.6	08:59:04.857	-47:30:47.64	15.237	0.031	13.268	0.010	12.103	0.013	10.70
VLT085904.84-473035.0	08:59:04.843	-47:30:35.08	15.956	0.026	14.578	0.011	13.792	0.021	5.57
VLT085904.83-473037.1	08:59:04.839	-47:30:37.16	17.358	0.100	16.022	0.037	14.920	0.054	2.45
VLT085904.83-473101.2	08:59:04.837	-47:31:01.22	17.995	0.067	16.110	0.027	15.072	0.042	10.56
VLT085904.79-472954.4	08:59:04.798	-47:29:54.41	17.836	0.099	16.110	0.035	15.142	0.056	8.92
VLT085904.77-473020.8	08:59:04.778	-47:30:20.84	16.283	0.038	14.638	0.014	13.789	0.019	8.75
VLT085904.71-473040.8	08:59:04.719	-47:30:40.83	15.753	0.033	14.982	0.024	14.538	0.055	0.00
VLT085904.68-473048.7	08:59:04.682	-47:30:48.72	15.728	0.041	13.994	0.014	12.872	0.019	7.80
VLT085904.65-473010.5	08:59:04.655	-47:30:10.59	17.359	0.095	15.383	0.024	14.327	0.034	11.67
VLT085904.61-473027.8	08:59:04.610	-47:30:27.89	14.846	0.023	13.032	0.007	12.053	0.010	10.05
VLT085904.60-473048.0	08:59:04.602	-47:30:48.09	16.424	0.079	14.644	0.025	13.416	0.032	7.58
VLT085904.59-473109.2	08:59:04.596	-47:31:09.23	19.699	0.177	17.330	0.055	15.469	0.041	10.65
VLT085904.59-473016.2	08:59:04.596	-47:30:16.26	16.933	0.061	15.388	0.024	14.608	0.042	7.92
VLT085904.58-472953.7	08:59:04.581	-47:29:53.76	18.019	0.115	16.386	0.038	15.254	0.035	6.32
VLT085904.57-473040.4	08:59:04.577	-47:30:40.40	15.602	0.077	13.906	0.025	12.868	0.039	7.94
VLT085904.56-473033.9	08:59:04.564	-47:30:33.92	15.632	0.078	14.583	0.036	13.621	0.049	0.00
VLT085904.44-473038.6	08:59:04.447	-47:30:38.61	15.659	0.079	14.223	0.029	13.207	0.047	0.93
VLT085904.40-473013.0	08:59:04.407	-47:30:13.05	16.255	0.037	14.494	0.012	13.753	0.017	11.23
VLT085904.39-473112.7	08:59:04.391	-47:31:12.75	19.084	0.131	17.202	0.046	16.015	0.063	9.32
VLT085904.37-473059.4	08:59:04.376	-47:30:59.43	17.164	0.056	15.424	0.019	14.611	0.025	10.36
VLT085904.31-473129.7	08:59:04.318	-47:31:29.79	19.736	0.195	17.342	0.041	15.449	0.029	10.74
VLT085904.29-473047.4	08:59:04.291	-47:30:47.40	16.359	0.135	15.027	0.058	13.779	0.082	1.22
VLT085904.28-473034.8	08:59:04.284	-47:30:34.80	16.202	0.117	14.941	0.046	13.848	0.061	1.49
VLT085904.27-473113.9	08:59:04.272	-47:31:13.91	18.681	0.123	16.082	0.024	14.806	0.023	18.52
VLT085904.23-473040.7	08:59:04.234	-47:30:40.79	17.103	0.135	15.085	0.037	14.101	0.061	12.83

Table 12—Continued

IR ID	RA J2000.	DEC J2000.	J	Jerr	H	Herr	K	Kerr	A_V min.
VLT085904.22-473122.0	08:59:04.229	-47:31:22.08	17.226	0.052	15.009	0.014	13.769	0.012	13.53
VLT085904.22-473013.4	08:59:04.220	-47:30:13.48	17.362	0.083	16.042	0.038	15.089	0.055	3.42
VLT085904.21-473012.1	08:59:04.216	-47:30:12.17	17.964	0.184	16.232	0.054	15.387	0.084	9.99
VLT085904.20-473059.9	08:59:04.205	-47:30:59.94	16.292	0.029	14.446	0.010	13.406	0.012	10.00
VLT085904.18-473051.5	08:59:04.188	-47:30:51.50	15.246	0.044	14.274	0.026	12.938	0.031	0.00
VLT085904.17-473051.1	08:59:04.177	-47:30:51.17	15.291	0.047	14.272	0.026	13.033	0.040	0.00
VLT085904.15-473028.8	08:59:04.155	-47:30:28.83	17.600	0.160	16.350	0.078	14.776	0.073	0.00
VLT085904.14-473001.8	08:59:04.145	-47:30:01.87	14.298	0.011	13.121	0.005	12.447	0.007	3.69
VLT085904.13-473010.1	08:59:04.137	-47:30:10.10	17.313	0.114	15.768	0.040	14.555	0.049	4.45
VLT085904.09-473059.2	08:59:04.095	-47:30:59.21	17.524	0.091	16.148	0.040	15.020	0.052	2.80
VLT085904.02-473110.9	08:59:04.029	-47:31:10.99	18.135	0.117	15.967	0.022	14.642	0.017	12.17
VLT085903.98-473057.1	08:59:03.987	-47:30:57.15	16.412	0.069	15.018	0.034	13.670	0.037	1.28
VLT085903.92-473056.4	08:59:03.928	-47:30:56.44	16.838	0.107	15.734	0.061	14.508	0.083	0.00
VLT085903.90-473040.2	08:59:03.903	-47:30:40.25	17.816	0.176	15.675	0.114	13.957	0.098	8.64
VLT085903.89-473110.0	08:59:03.897	-47:31:10.07	17.304	0.050	15.190	0.014	14.208	0.015	14.17
VLT085903.87-473111.1	08:59:03.872	-47:31:11.18	18.297	0.087	16.489	0.031	15.360	0.036	8.76
VLT085903.84-472945.5	08:59:03.842	-47:29:45.51	18.725	0.116	16.647	0.030	15.575	0.034	12.95
VLT085903.77-473136.2	08:59:03.770	-47:31:36.24	17.641	0.050	16.279	0.022	15.392	0.022	4.54
VLT085903.75-473108.5	08:59:03.750	-47:31:08.50	17.077	0.051	15.070	0.015	14.115	0.016	12.91
VLT085903.69-473040.2	08:59:03.698	-47:30:40.24	15.335	0.096	13.755	0.033	12.767	0.052	6.74
VLT085903.69-473039.2	08:59:03.692	-47:30:39.21	15.907	0.120	14.597	0.048	13.256	0.055	0.17
VLT085903.67-473119.7	08:59:03.673	-47:31:19.78	17.547	0.067	15.698	0.018	14.805	0.018	11.22
VLT085903.66-473052.3	08:59:03.667	-47:30:52.37	17.356	0.128	15.877	0.093	14.399	0.086	1.41
VLT085903.62-473056.2	08:59:03.623	-47:30:56.27	15.417	0.036	13.565	0.013	12.467	0.015	9.62
VLT085903.61-473017.3	08:59:03.610	-47:30:17.32	16.800	0.051	15.443	0.024	14.614	0.034	4.93
VLT085903.58-473053.3	08:59:03.589	-47:30:53.36	17.574	0.071	16.328	0.064	15.185	0.098	0.88
VLT085903.56-473030.3	08:59:03.565	-47:30:30.39	16.978	0.071	15.390	0.046	14.752	0.044	9.66
VLT085903.54-473101.9	08:59:03.543	-47:31:01.94	17.215	0.101	15.526	0.030	14.533	0.038	8.21
VLT085903.51-473108.0	08:59:03.517	-47:31:08.05	17.651	0.096	15.939	0.028	15.061	0.042	9.45
VLT085903.46-473140.1	08:59:03.464	-47:31:40.14	15.146	0.015	14.646	0.010	14.408	0.014	0.00
VLT085903.42-473050.6	08:59:03.428	-47:30:50.69	16.493	0.035	14.766	0.013	13.891	0.024	9.68
VLT085903.38-473059.0	08:59:03.380	-47:30:59.07	17.065	0.106	15.227	0.032	14.457	0.054	12.06
VLT085903.37-473059.0	08:59:03.379	-47:30:59.07	17.065	0.106	15.226	0.032	14.447	0.054	12.00
VLT085903.32-473049.0	08:59:03.327	-47:30:49.08	17.275	0.055	15.854	0.024	15.073	0.036	6.20
VLT085903.29-473118.8	08:59:03.298	-47:31:18.84	18.007	0.105	16.402	0.046	15.223	0.070	5.55
VLT085903.28-473113.6	08:59:03.289	-47:31:13.62	17.997	0.110	15.820	0.027	14.618	0.034	13.28
VLT085903.27-473049.0	08:59:03.275	-47:30:49.06	17.560	0.066	16.276	0.030	15.278	0.036	2.57

Table 12—Continued

IR ID	RA J2000.	DEC J2000.	J	Jerr	H	Herr	K	Kerr	A_V min.
VLT085903.27-473059.8	08:59:03.270	-47:30:59.87	17.825	0.190	16.065	0.057	15.024	0.089	8.80
VLT085903.16-473048.3	08:59:03.162	-47:30:48.36	17.733	0.074	15.973	0.024	15.167	0.028	10.69
VLT085903.13-473011.1	08:59:03.139	-47:30:11.17	18.067	0.161	16.131	0.041	15.013	0.047	10.62
VLT085903.11-473119.4	08:59:03.119	-47:31:19.46	18.784	0.128	16.788	0.032	15.890	0.045	13.22
VLT085903.11-473122.8	08:59:03.116	-47:31:22.85	16.992	0.054	15.022	0.014	14.047	0.014	12.24
VLT085903.04-473034.4	08:59:03.046	-47:30:34.48	17.180	0.126	15.617	0.044	14.888	0.073	8.58
VLT085903.01-473032.8	08:59:03.016	-47:30:32.89	17.304	0.091	15.916	0.058	14.441	0.041	0.18
VLT085903.01-473142.3	08:59:03.015	-47:31:42.37	19.828	0.179	18.969	0.087	18.030	0.081	0.00
VLT085903.01-473103.7	08:59:03.014	-47:31:03.79	15.920	0.034	14.158	0.010	13.169	0.012	9.25
VLT085902.96-473122.8	08:59:02.965	-47:31:22.87	18.171	0.146	16.667	0.043	15.571	0.045	4.82
VLT085902.88-473030.7	08:59:02.884	-47:30:30.72	16.748	0.058	15.062	0.033	13.932	0.021	7.07
VLT085902.87-473121.0	08:59:02.870	-47:31:21.03	17.799	0.078	15.860	0.022	14.625	0.021	9.72
VLT085902.75-473046.8	08:59:02.755	-47:30:46.85	15.149	0.040	13.837	0.015	13.223	0.028	6.03
VLT085902.73-473111.6	08:59:02.736	-47:31:11.69	17.753	0.088	16.135	0.035	15.211	0.063	7.78
VLT085902.66-473108.2	08:59:02.667	-47:31:08.29	17.760	0.071	16.131	0.027	15.074	0.036	6.86
VLT085902.63-473042.3	08:59:02.635	-47:30:42.33	16.662	0.106	15.107	0.027	14.190	0.039	6.96
VLT085902.62-472933.2	08:59:02.625	-47:29:33.23	17.225	0.047	15.843	0.019	15.035	0.021	5.45
VLT085902.60-473028.6	08:59:02.607	-47:30:28.67	18.034	0.192	16.352	0.058	15.436	0.089	8.73
VLT085902.60-473113.1	08:59:02.606	-47:31:13.17	16.398	0.032	14.498	0.010	13.025	0.008	7.28
VLT085902.59-473035.2	08:59:02.596	-47:30:35.25	15.779	0.058	14.499	0.019	13.579	0.031	3.14
VLT085902.59-473131.5	08:59:02.594	-47:31:31.57	18.671	0.125	17.464	0.056	16.417	0.080	1.11
VLT085902.55-473053.4	08:59:02.552	-47:30:53.49	16.357	0.048	14.648	0.015	13.707	0.020	8.90
VLT085902.52-473127.7	08:59:02.527	-47:31:27.71	18.073	0.091	16.251	0.028	15.212	0.034	9.68
VLT085902.49-473059.5	08:59:02.491	-47:30:59.51	17.711	0.110	16.322	0.032	15.340	0.036	4.15
VLT085902.46-473123.0	08:59:02.461	-47:31:23.01	16.686	0.034	14.802	0.012	13.983	0.014	12.30
VLT085902.45-473112.2	08:59:02.454	-47:31:12.28	19.139	0.193	17.829	0.065	16.652	0.054	1.49
VLT085902.40-473103.0	08:59:02.406	-47:31:03.02	18.055	0.159	16.205	0.039	15.249	0.047	10.73
VLT085902.39-473005.4	08:59:02.392	-47:30:05.40	19.217	0.191	17.535	0.073	15.731	0.051	1.60
VLT085902.38-473034.0	08:59:02.389	-47:30:34.06	15.975	0.068	14.867	0.027	14.296	0.074	3.56
VLT085902.35-473003.0	08:59:02.355	-47:30:03.00	18.774	0.165	17.282	0.062	16.072	0.066	3.74
VLT085902.33-473107.8	08:59:02.334	-47:31:07.82	16.635	0.033	14.623	0.010	13.002	0.007	7.64
VLT085902.33-473035.1	08:59:02.331	-47:30:35.11	16.038	0.043	14.771	0.018	13.968	0.029	3.90
VLT085902.29-473041.3	08:59:02.298	-47:30:41.35	17.768	0.190	16.494	0.064	15.262	0.067	0.55
VLT085902.29-473118.7	08:59:02.291	-47:31:18.74	17.718	0.056	15.747	0.019	14.583	0.019	10.74
VLT085902.26-473050.1	08:59:02.265	-47:30:50.10	18.425	0.134	17.321	0.071	16.130	0.098	0.00
VLT085902.23-473054.2	08:59:02.230	-47:30:54.23	18.136	0.128	16.529	0.047	15.144	0.052	3.93
VLT085902.22-473116.2	08:59:02.222	-47:31:16.25	17.919	0.102	15.946	0.032	15.036	0.037	12.80

Table 12—Continued

IR ID	RA J2000.	DEC J2000.	J	Jerr	H	Herr	K	Kerr	A_V min.
VLT085902.22-473056.8	08:59:02.222	-47:30:56.86	18.143	0.123	16.291	0.036	15.125	0.042	9.07
VLT085902.21-473031.8	08:59:02.216	-47:30:31.86	16.256	0.046	15.386	0.042	14.244	0.025	0.00
VLT085902.21-473105.8	08:59:02.215	-47:31:05.88	19.424	0.198	17.255	0.045	16.146	0.046	13.92
VLT085902.20-473103.3	08:59:02.205	-47:31:03.30	16.208	0.038	14.431	0.012	13.377	0.012	8.94
VLT085902.17-472953.3	08:59:02.176	-47:29:53.35	18.416	0.127	16.927	0.049	15.747	0.056	3.94
VLT085902.11-473026.7	08:59:02.114	-47:30:26.72	15.305	0.019	13.866	0.008	13.165	0.011	7.09
VLT085902.09-473115.5	08:59:02.095	-47:31:15.51	17.786	0.105	16.096	0.039	14.826	0.034	6.00
VLT085902.09-473022.5	08:59:02.092	-47:30:22.59	17.624	0.117	16.680	0.090	15.249	0.077	0.00
VLT085902.09-472951.9	08:59:02.090	-47:29:51.99	19.000	0.191	17.421	0.067	15.919	0.058	2.60
VLT085902.06-473100.8	08:59:02.067	-47:31:00.84	16.611	0.043	15.392	0.020	14.634	0.023	3.59
VLT085902.04-473113.4	08:59:02.048	-47:31:13.40	18.077	0.079	16.281	0.023	15.184	0.023	8.85
VLT085902.03-472931.4	08:59:02.038	-47:29:31.41	19.387	0.141	17.306	0.039	15.984	0.036	10.99
VLT085902.02-473020.8	08:59:02.028	-47:30:20.86	16.847	0.049	15.237	0.017	14.243	0.017	7.11
VLT085902.00-473037.3	08:59:02.003	-47:30:37.31	16.643	0.050	15.377	0.019	14.710	0.025	4.97
VLT085901.98-473059.4	08:59:01.982	-47:30:59.49	16.735	0.053	15.143	0.020	14.223	0.023	7.45
VLT085901.90-473028.3	08:59:01.900	-47:30:28.35	14.917	0.018	13.384	0.007	12.547	0.008	7.30
VLT085901.84-473105.9	08:59:01.843	-47:31:05.95	18.346	0.176	16.710	0.050	15.687	0.050	7.23
VLT085901.83-473037.4	08:59:01.838	-47:30:37.43	15.636	0.024	14.451	0.011	13.631	0.011	2.62
VLT085901.82-473055.1	08:59:01.829	-47:30:55.11	18.064	0.114	15.971	0.024	14.444	0.017	9.51
VLT085901.75-473119.0	08:59:01.755	-47:31:19.06	19.730	0.179	18.012	0.073	16.807	0.061	6.91
VLT085901.69-473115.6	08:59:01.691	-47:31:15.65	17.265	0.051	14.926	0.012	13.346	0.009	12.49
VLT085901.66-473127.3	08:59:01.665	-47:31:27.36	17.182	0.044	16.466	0.028	15.990	0.035	0.00
VLT085901.60-473119.1	08:59:01.607	-47:31:19.18	15.799	0.021	14.062	0.008	13.073	0.007	8.90
VLT085901.50-473115.6	08:59:01.507	-47:31:15.67	18.407	0.082	16.635	0.030	15.509	0.028	8.29
VLT085901.47-473003.4	08:59:01.475	-47:30:03.49	14.194	0.010	13.187	0.005	12.644	0.007	2.38
VLT085901.44-473121.9	08:59:01.446	-47:31:21.99	17.717	0.067	15.377	0.015	14.001	0.012	14.14
VLT085901.42-473020.9	08:59:01.424	-47:30:20.99	17.310	0.110	16.243	0.056	15.434	0.079	1.08
VLT085901.40-473057.5	08:59:01.402	-47:30:57.56	18.134	0.122	16.646	0.051	15.861	0.070	7.10
VLT085901.34-472951.7	08:59:01.344	-47:29:51.71	18.911	0.111	17.571	0.043	16.335	0.043	1.43
VLT085901.27-473002.7	08:59:01.275	-47:30:02.75	18.084	0.092	16.193	0.025	14.892	0.022	8.53
VLT085901.24-473003.8	08:59:01.249	-47:30:03.87	18.685	0.166	16.426	0.029	14.841	0.022	11.34
VLT085901.21-473109.0	08:59:01.210	-47:31:09.07	17.097	0.058	15.820	0.028	15.017	0.039	4.03
VLT085901.15-473031.8	08:59:01.150	-47:30:31.87	16.099	0.026	15.054	0.019	13.893	0.016	0.00
VLT085901.13-473117.2	08:59:01.134	-47:31:17.28	18.657	0.095	16.721	0.028	15.634	0.028	10.87
VLT085901.13-472935.2	08:59:01.132	-47:29:35.26	18.692	0.093	17.754	0.047	17.085	0.049	0.42
VLT085901.10-473033.3	08:59:01.107	-47:30:33.39	17.962	0.076	16.768	0.041	15.954	0.047	2.80
VLT085901.09-473122.1	08:59:01.098	-47:31:22.13	18.821	0.162	16.576	0.031	15.277	0.024	13.44

Table 12—Continued

IR ID	RA J2000.	DEC J2000.	J	Jerr	H	Herr	K	Kerr	A_V min.
VLT085901.05-473110.8	08:59:01.054	-47:31:10.82	17.936	0.132	16.521	0.057	15.452	0.092	3.81
VLT085900.98-473031.1	08:59:00.984	-47:30:31.12	16.979	0.068	15.123	0.026	13.987	0.021	9.37
VLT085900.92-473014.1	08:59:00.928	-47:30:14.19	17.091	0.041	15.470	0.016	14.551	0.015	7.86
VLT085900.91-473139.7	08:59:00.918	-47:31:39.76	17.406	0.046	16.169	0.021	15.406	0.025	3.80
VLT085900.87-472933.4	08:59:00.870	-47:29:33.47	17.480	0.048	15.387	0.014	14.028	0.011	10.86
VLT085900.85-472922.1	08:59:00.859	-47:29:22.19	18.234	0.071	17.191	0.034	16.259	0.037	0.00
VLT085900.82-473055.5	08:59:00.824	-47:30:55.54	17.010	0.108	16.110	0.054	15.193	0.086	0.00
VLT085900.67-473042.4	08:59:00.677	-47:30:42.42	17.133	0.089	15.823	0.032	14.952	0.034	3.94
VLT085900.63-473013.3	08:59:00.638	-47:30:13.36	19.107	0.168	17.790	0.082	16.457	0.071	0.34
VLT085900.63-473046.9	08:59:00.635	-47:30:46.98	16.135	0.052	15.009	0.020	14.355	0.038	3.14
VLT085900.56-473100.7	08:59:00.569	-47:31:00.71	18.067	0.153	15.714	0.032	13.681	0.019	9.05
VLT085900.47-473004.6	08:59:00.470	-47:30:04.61	16.877	0.045	15.215	0.014	14.356	0.015	8.91
VLT085900.45-473048.4	08:59:00.454	-47:30:48.46	16.508	0.101	14.941	0.031	13.747	0.032	4.91
VLT085900.39-473117.8	08:59:00.397	-47:31:17.88	19.362	0.180	17.712	0.067	16.078	0.070	2.53
VLT085900.38-472941.0	08:59:00.381	-47:29:41.08	17.621	0.052	16.241	0.022	15.416	0.022	5.28
VLT085900.33-473022.1	08:59:00.334	-47:30:22.11	18.585	0.147	16.515	0.033	15.300	0.031	11.70
VLT085900.26-472922.9	08:59:00.262	-47:29:22.92	16.989	0.043	15.808	0.019	15.306	0.027	5.12
VLT085900.20-472949.5	08:59:00.209	-47:29:49.58	18.256	0.080	16.701	0.028	15.491	0.025	4.61
VLT085900.19-473023.0	08:59:00.195	-47:30:23.05	18.077	0.079	16.988	0.035	16.077	0.040	0.57
VLT085900.17-473115.6	08:59:00.178	-47:31:15.69	18.545	0.099	17.378	0.046	16.519	0.069	2.06
VLT085900.17-473040.6	08:59:00.170	-47:30:40.67	16.913	0.135	15.930	0.053	15.008	0.068	0.00
VLT085900.15-472940.8	08:59:00.152	-47:29:40.82	16.842	0.035	15.122	0.013	13.940	0.011	7.12
VLT085900.14-473027.2	08:59:00.149	-47:30:27.23	18.259	0.149	16.143	0.029	14.594	0.021	9.65
VLT085900.11-473114.3	08:59:00.117	-47:31:14.34	19.556	0.182	16.496	0.026	14.380	0.015	18.16
VLT085900.04-473045.4	08:59:00.046	-47:30:45.48	16.953	0.056	15.624	0.022	14.634	0.025	3.25
VLT085900.03-473113.8	08:59:00.039	-47:31:13.89	18.857	0.103	15.756	0.017	14.060	0.013	22.10
VLT085900.03-472957.4	08:59:00.032	-47:29:57.49	17.347	0.044	15.241	0.013	13.701	0.010	9.59
VLT085900.02-473004.9	08:59:00.024	-47:30:04.98	18.141	0.093	16.824	0.033	15.938	0.035	3.92
VLT085859.99-473106.4	08:58:59.996	-47:31:06.40	17.142	0.040	15.718	0.018	14.913	0.021	6.05
VLT085859.94-473000.5	08:58:59.946	-47:30:00.53	18.826	0.121	17.103	0.035	15.632	0.026	4.84
VLT085859.94-473030.1	08:58:59.940	-47:30:30.19	17.328	0.074	15.798	0.025	14.764	0.026	5.68
VLT085859.87-473111.1	08:58:59.878	-47:31:11.10	18.836	0.151	16.841	0.032	15.024	0.022	5.83
VLT085859.85-473002.6	08:58:59.853	-47:30:02.66	17.840	0.078	16.222	0.023	15.365	0.023	8.32
VLT085859.83-473050.2	08:58:59.836	-47:30:50.25	18.706	0.148	17.265	0.063	16.311	0.057	5.09
VLT085859.71-473024.2	08:58:59.714	-47:30:24.23	17.903	0.152	15.246	0.020	13.665	0.014	16.88
VLT085859.67-473012.0	08:58:59.678	-47:30:12.00	18.916	0.109	17.821	0.054	16.973	0.070	1.16
VLT085859.62-472954.6	08:58:59.620	-47:29:54.66	17.800	0.058	16.254	0.022	15.127	0.019	5.15

Table 12—Continued

IR ID	RA J2000.	DEC J2000.	J	Jerr	H	Herr	K	Kerr	A_V min.
VLT085859.60-473127.5	08:58:59.602	-47:31:27.56	16.208	0.026	14.375	0.009	13.433	0.009	10.61
VLT085859.50-473028.3	08:58:59.500	-47:30:28.37	18.067	0.110	17.029	0.056	15.996	0.063	0.00
VLT085859.48-473036.2	08:58:59.488	-47:30:36.24	17.247	0.045	16.677	0.031	16.333	0.049	0.00
VLT085859.45-472956.2	08:58:59.454	-47:29:56.22	19.061	0.145	17.758	0.052	16.576	0.046	1.35
VLT085859.10-473100.8	08:58:59.101	-47:31:00.88	17.362	0.045	16.039	0.020	15.292	0.022	5.12
VLT085859.07-473123.0	08:58:59.078	-47:31:23.00	16.875	0.035	15.943	0.019	15.403	0.025	1.37
VLT085859.06-473059.1	08:58:59.069	-47:30:59.17	19.056	0.126	17.489	0.042	16.371	0.040	5.52
VLT085859.02-473138.1	08:58:59.029	-47:31:38.15	17.143	0.039	16.544	0.025	16.015	0.034	0.00
VLT085858.66-473010.9	08:58:58.664	-47:30:10.94	17.543	0.049	16.290	0.022	15.491	0.023	3.73
VLT085858.47-473143.6	08:58:58.473	-47:31:43.66	18.197	0.067	15.744	0.017	14.147	0.012	13.93
VLT085858.45-472926.6	08:58:58.451	-47:29:26.60	17.377	0.044	16.218	0.021	15.476	0.024	2.89
VLT085858.32-473108.1	08:58:58.328	-47:31:08.10	18.857	0.144	16.886	0.036	15.179	0.025	6.38
VLT085858.31-473045.0	08:58:58.316	-47:30:45.07	16.884	0.035	15.805	0.018	15.168	0.021	2.63
VLT085858.28-472926.0	08:58:58.287	-47:29:26.03	18.147	0.073	17.536	0.046	17.028	0.065	0.00
VLT085858.15-472950.1	08:58:58.157	-47:29:50.15	19.041	0.115	16.599	0.026	14.705	0.016	11.39
VLT085858.10-473009.5	08:58:58.107	-47:30:09.58	18.639	0.152	16.752	0.035	15.574	0.032	9.46
VLT085858.08-473022.6	08:58:58.088	-47:30:22.69	17.351	0.050	16.044	0.021	14.730	0.017	0.35
VLT085858.02-473017.6	08:58:58.023	-47:30:17.66	18.625	0.131	16.168	0.024	14.726	0.018	15.23
VLT085857.99-472951.6	08:58:57.993	-47:29:51.66	19.355	0.136	17.683	0.044	16.186	0.034	3.93
VLT085857.79-473138.8	08:58:57.791	-47:31:38.87	15.584	0.019	15.143	0.013	14.882	0.017	0.00
VLT085857.77-472940.2	08:58:57.773	-47:29:40.25	19.557	0.196	17.646	0.051	15.992	0.035	5.98
VLT085857.63-473059.6	08:58:57.639	-47:30:59.68	14.085	0.009	13.854	0.007	13.802	0.010	0.00
VLT085857.56-472924.5	08:58:57.561	-47:29:24.55	15.817	0.021	14.758	0.011	14.314	0.013	3.90
VLT085857.41-473002.9	08:58:57.416	-47:30:02.91	18.118	0.086	17.637	0.048	17.357	0.076	0.00
VLT085857.35-473014.6	08:58:57.356	-47:30:14.66	17.713	0.071	15.813	0.019	14.696	0.018	10.13
VLT085857.18-473136.3	08:58:57.180	-47:31:36.33	17.952	0.059	15.987	0.019	14.567	0.015	8.60
VLT085857.11-473045.2	08:58:57.116	-47:30:45.22	17.960	0.067	17.148	0.034	16.338	0.035	0.00
VLT085857.04-473143.2	08:58:57.049	-47:31:43.23	16.998	0.037	15.648	0.016	14.914	0.018	5.60
VLT085856.86-472945.8	08:58:56.862	-47:29:45.87	15.348	0.018	12.927	0.005	11.841	0.004	17.59
VLT085856.84-473019.1	08:58:56.847	-47:30:19.13	19.468	0.174	17.195	0.039	15.878	0.028	13.69
VLT085856.76-472952.1	08:58:56.763	-47:29:52.19	17.490	0.050	15.209	0.013	13.813	0.011	13.16

Table 13. Candidate OB stars in RCW 38

SRC #	RA (J2000.0)	DEC (J2000.0)	off–axis (angle) (arcsec)	A_V (From IR) (mag)	A_V (From N_H) (mag)	Abs. K	L_{bol} (log $L_\odot$)	L_X/L_{bol} (log)
21	8:58:43.87	-47:28:57.1	236.1	1.1	4.5	-0.51	3.09	-5.32
53	8:58:50.37	-47:33:19.4	108.9	8.9	8.9	-1.81	3.62	-5.48
107	8:58:59.20	-47:26:57.9	232.7	4.4	12.2	-1.31	3.42	-6.02
112	8:58:59.79	-47:32:23.5	111.0	23.9	26.9	-4.35	4.64	-7.71
125	8:59:00.33	-47:31:14.3	53.1	31.5	31.2	-2.17	3.76	-6.32
127	8:59:00.39	-47:25:58.3	288.9	13	17.0	-1.97	3.68	-6.34
140	8:59:01.56	-47:31:10.2	40.7	8.7	14.9	-0.65	3.15	-5.50
143	8:59:01.64	-47:30:37.5	31.0	2.7	5.8	-1.02	3.30	-5.96
147	8:59:01.95	-47:31:15.0	41.3	9.8	8.3	-0.73	3.18	-5.61
151	8:59:02.17	-47:30:16.6	37.1	4.8	10.0	-0.75	3.19	-4.86
164	8:59:02.98	-47:30:44.4	16.8	10.9	9.8	-0.56	3.12	-5.99
171	8:59:03.53	-47:30:58.3	18.2	8.6	9.3	-0.44	3.07	-5.05
194	8:59:04.45	-47:30:56.2	12.4	10.3	11.5	-1.33	3.42	-5.75
214	8:59:05.30	-47:30:42.5	6.8	9.8	4.3	-0.67	3.16	-5.37
217	8:59:05.41	-47:30:02.9	41.8	7.8	17.7	-1.21	3.38	-6.18
219	8:59:05.44	-47:30:30.1	16.1	8.5	7.7	-0.63	3.14	-5.61
220	8:59:05.55	-47:30:35.8	12.3	3.5	9.5	-1.02	3.30	-4.99
221	8:59:05.66	-47:30:40.9	10.8	9.9	11.5	-5.69	5.90	-6.80
238	8:59:06.16	-47:30:35.3	17.7	11.2	10.0	-1.98	3.68	-5.85
244	8:59:06.38	-47:29:10.0	95.7	12.7	14.2	-0.71	3.17	-6.12
251	8:59:06.64	-47:30:21.9	30.0	–	115.2	–	4.70	-6.93
253	8:59:06.82	-47:29:41.4	66.4	27.8	26.1	-0.98	3.28	-6.08
263	8:59:07.37	-47:33:05.2	143.9	7.6	7.5	-0.84	3.23	-5.52
285	8:59:08.78	-47:30:37.0	42.5	17.1	19.0	-0.46	3.07	-5.34
332	8:59:15.90	-47:32:57.3	171.3	3.8	19.4	-0.95	3.27	-6.52
366	8:59:21.58	-47:29:28.9	187.4	11.5	12.9	-0.90	3.25	-5.47
374	8:59:23.66	-47:37:50.8	468.3	5.9	11.7	-1.79	3.61	-6.48
396	8:59:28.79	-47:32:22.1	263.5	4.9	10.1	-3.20	4.17	-7.06
457	8:59:04.50	-47:30:35.1	9.0	0	18.7	-0.64	3.15	-6.24
VLT232	8:59:06.96	-47:30:23.2	21.9	14.1	–	-1.60	3.53	<-7.12
VLT453	8:59:05.45	-47:30:45.3	5.6	3.8	–	-1.09	3.30	<-5.89

This figure "fig1a.jpg" is available in "jpg" format from:

http://arXiv.org/ps/astro-ph/0605096v1

This figure "fig1b.jpg" is available in "jpg" format from:

http://arXiv.org/ps/astro-ph/0605096v1

This figure "fig2.jpg" is available in "jpg" format from:

http://arXiv.org/ps/astro-ph/0605096v1


This figure "fig5a.jpg" is available in "jpg" format from:
http://arXiv.org/ps/astro-ph/0605096v1

This figure "fig5b.jpg" is available in "jpg" format from:

http://arXiv.org/ps/astro-ph/0605096v1


This figure "fig12_color.jpg" is available in "jpg" format from:
http://arXiv.org/ps/astro-ph/0605096v1


This figure "fig18.jpg" is available in "jpg" format from:
http://arXiv.org/ps/astro-ph/0605096v1


This figure "fig21.jpg" is available in "jpg" format from:
http://arXiv.org/ps/astro-ph/0605096v1

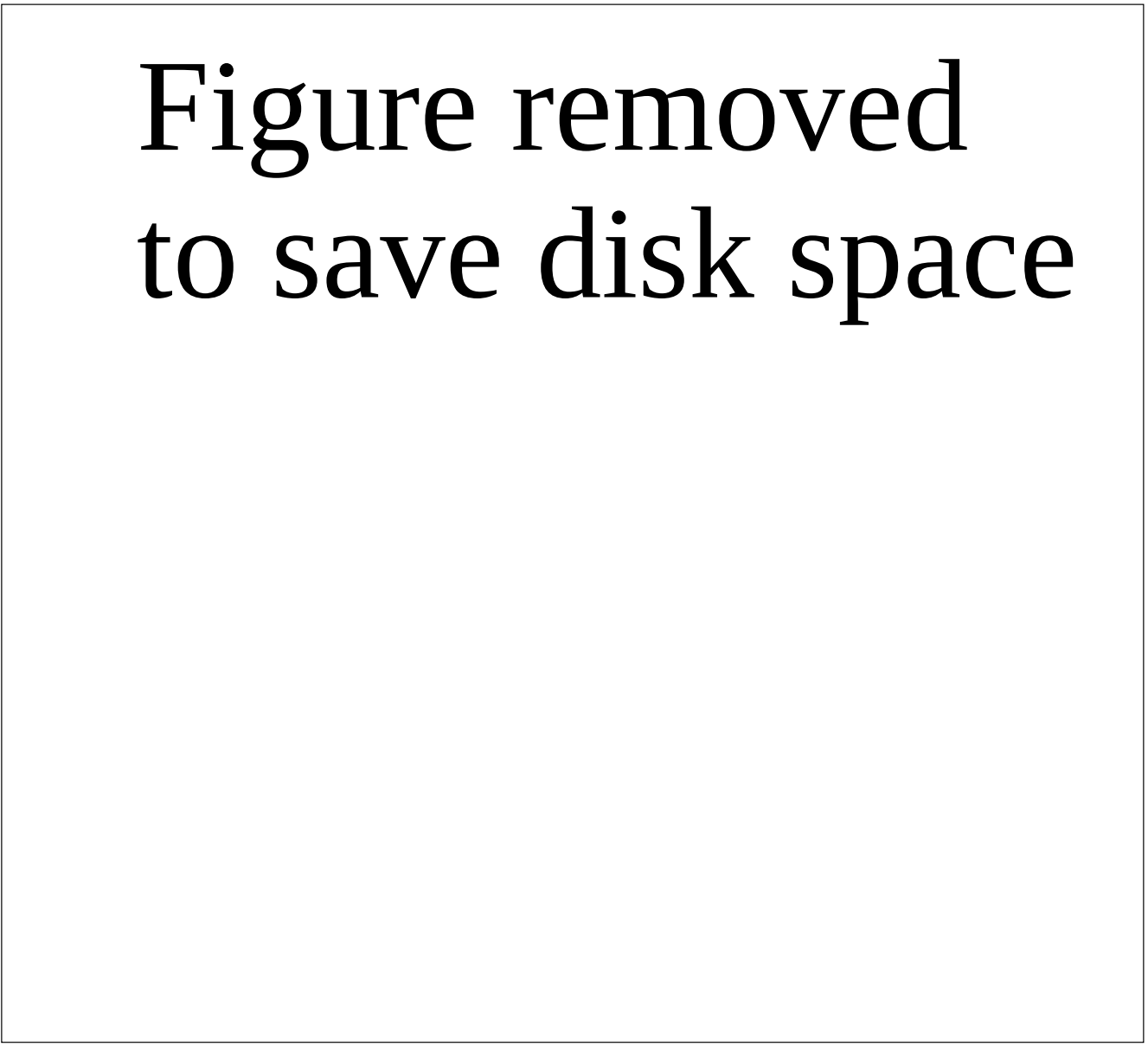
Figure removed
to save disk space